ISTANBUL TECHNICAL UNIVERSITY ★ GRADUATE SCHOOL

SYNTHESIS, CHARACTERIZATION AND BIOCOMPATIBILITY TESTS OF MAGNETIC NANOPARTICLES

M.Sc. THESIS

AYSA AZMOUDEH

Department of Metallurgical and Materials Engineering

Material Engineering Programme

AUGUST 2023

ISTANBUL TECHNICAL UNIVERSITY ★ GRADUATE SCHOOL

SYNTHESIS, CHARACTERIZATION AND BIOCOMPATIBILITY TESTS OF MAGNETIC NANOPARTICLES

M.Sc. THESIS

Aysa AZMOUDEH
(506191434)

Department of Metallurgical and Materials Engineering

Material Engineering Programme

Thesis Advisor: Assoc. Prof. Dr. Duygu AĞAOĞULLARI

AUGUST 2023

İSTANBUL TEKNİK ÜNİVERSİTESİ ★ LİSANSÜSTÜ EĞİTİM ENSTİTÜSÜ

MANYETİK NANOPARTİKÜLLERİN SENTEZLENMESİ, KARAKTERİZASYONU VE BİYOUYUMLULUK TESTLERİNİN GERÇEKLEŞTİRİLMESİ

YÜKSEK LİSANS TEZİ

Aysa AZMOUDEH
(506191434)

Metalurji ve Malzeme Mühendisliği Anabilim Dalı

Malzeme Mühendisliği Programı

Tez Danışmanı: Doç. Dr. Duygu AĞAOĞULLARI

AĞUSTOS 2023

Aysa AZMOUDEH, a M.Sc. student of ITU Graduate School student ID 506191434 successfully defended the thesis entitled “SYNTHESIS, CHARACTERIZATION AND BIOCOMPATIBILITY TESTS OF MAGNETIC NANOPARTICLES”, which she prepared after fulfilling the requirements specified in the associated legislations, before the jury whose signatures are below.

Thesis Advisor : **Assoc. Prof. Dr. Duygu AĞAOĞULLARI** .....
Istanbul Technical University

Jury Members : **Assoc. Prof. Dr. Muhammet Übeydullah KAHVECİ**.....
Istanbul Technical University

Assoc. Prof. Dr. Özge BALCI-ÇAĞIRAN .....
Koç University

Date of Submission : 02 August 2023
Date of Defense : 10 August 2023

To my incredibly patient family,

FOREWORD

It is with great pleasure and a sense of accomplishment that I present my Master's thesis. This work represents the culmination of months of dedicated research, rigorous analysis, and deep exploration. Undertaking this endeavor would not have been possible without the support and guidance of numerous individuals, to whom I would like to express my heartfelt gratitude.

First and foremost, I am immensely grateful to my supervisor, Assoc. Prof. Dr. Duygu AĞAOĞULLARI, for her invaluable mentorship, expertise, and unwavering commitment throughout this research journey. Her guidance, constructive feedback, and insightful discussions have been instrumental in shaping and refining my ideas. I am grateful for the experience of working in the ITU Particulate Materials Laboratory (PML). I want to thank Prof. Dr. M. Lütfi ÖVEÇOĞLU, who has generously shared his knowledge and expertise during my work.

I would thank Assoc. Prof. Dr. Muhammet Übeydullah KAHVECİ and M.Sc. Şeyma SARI for their help in designing polymers and guiding me through my research. I would thank Prof. Gizem Dinler DOĞANAY and M.Sc. Miray TÜRK for their help with cytotoxicity tests to show the potential of nanoparticles for possible biomedical applications. I would be grateful to the Sencer MORAL and Res. Assist. Dr. Sıddıka MERTDİNÇ, and for their help during my research. I would also be thankful to lab mates from Particulate Materials Laboratories, Res. Asst. İlayda SÜZER, Dr. Hasan GÖKÇE, M.Sc. Ammar ALKRAIDI, M.Sc. Amir AKBARI, and M.Sc. Burçak BOZTEMUR, for giving me a joyful laboratory life with their precious friendships.

This study was supported by Istanbul Technical University Scientific Research Projects (ITU BAP, M.Sc. Thesis Projects) with the project number MYL-2022-44189.

My deep gratitude goes to my mom, dad, and my brother for their unwavering support, understanding, and love throughout my academic journey. Their belief in me has been an immense source of strength and inspiration.

August 2023

Aysa AZMOUDEH
(Biomedical Engineer)

TABLE OF CONTENTS

Page

ABBREVIATIONS

BCC : Base Centered Cubic
CVD : Chemical Vapor Deposition
EDS : Energy Dispersive X-Ray Spectroscope
FCC : Face Centered Cubic
FTIR : Fourier Transform Infrared Spectroscopy
HCl : Hydrochloric Acid
HF : Hydrofloric Acid
ITU : Istanbul Technical University
MA : Mechanical Alloying
MHT : Magnetic Hyperthermia
MLG : Multi Layer Graphene
MNP : Magnetic Nanoparticle
MRI : Magnetic Resonance Imaging
MTT : Thiazolyl Blue Tetrazolium Bromide
PM : Powder Metallurgy
SEM : Scanning Electron Microscope
TEM : Transmission Electron Microscope
VSM : Vibrating Sample Magnetometer
XRD : X-Ray Diffractometer

SYMBOLS

Å	**:** Ångstrom
emu	**:** Electromagnetic unit
eV	**:** Electron volt
g	**:** Gram
h	**:** Hour
H_c	**:** Coercivity
M	**:** Molarity
mbar	**:** Milibar
min	**:** Minute
mL	**:** Mililiter
M_r	**:** Remenant magnetisation
M_s	**:** Magnetic saturation
nm	**:** Nanometer
Oe	**:** Oersted
Pa	**:** Pascal
rpm	**:** Rotation per minute
µg	**:** Microgram
µl	**:** Microliter
µm	**:** Micrometer

LIST OF TABLES

Page

LIST OF FIGURES

Page

SYNTHESIS, CHARACTERIZATION AND BIOCOMPATIBILITY TESTS OF MAGNETIC NANOPARTICLES

SUMMARY

Nanotechnology advancements have surged recently in numerous fields, particularly in energy, environmental, electronic, and biological applications. Magnetic nanoparticles (MNPs) are one of the improvements that nanotechnology has brought to these application fields. MNPs are employed in biological, electrical, soil, or water filtration and catalytic applications. MNPs are one of them and are essential for the diagnosis and treatment of cancer. In research such as magnetic resonance imaging (MRI) for cancer diagnosis, like hyperthermia, magnetic nanoparticles are used as contrast agents.

Particle sizes, shape, surface characteristics, biocompatibility, magnetic properties, and thermal and chemical stabilities are crucial for using nanomaterials in biomedical applications. Using magnetic nanoparticles will improve the surface area on which the medicine is carried and released because surface area increases as particle size decreases. Additionally, unless encased in protective layers, several iron oxide nanoparticles lose their chemical stability in bodily fluids. The efficiency of imaging applications could suffer from them becoming oxidized and having lower magnetization values. The concept of coating nanoparticles with protective layers has arisen to stop the degradation of magnetic nanoparticles in body fluids and to stop them from losing their magnetic capabilities. These types of materials are referred to as core/shell materials. Different inert materials are coated on the magnetic core to ensure its stability in biological settings. There have been studies on how to surround a metal with its noble metal or oxide to form a passivation layer. Silica and carbon-based (graphene, graphene oxide, etc.) shell materials are frequently chosen coating materials.

MNPs and their encapsulations have been created using a variety of production techniques. Solvothermal synthesis could be used to create magnetic nanoparticles like Fe_3O_4. On the other hand, biocompatible surfaces can be created by encapsulating magnetic nanoparticles in various substances, including graphene. Although too many techniques were explored to encapsulate MNPs in graphene, chemical vapor deposition is one of the more effective ones.

In this research, Fe_3O_4 and Fe_3O_4@rGO nanoparticles are synthesized by the solvothermal method, and for having high crystallinity and removal of organic compounds, the calcination process is applied by argon gases. Furthermore, encapsulation studies were carried out by feeding these substrates to the chemical vapor deposition (CVD) system and using methane (CH_4) and hydrogen (H_2) gases. The temperature (950°C), holding times (1 h), system pressures (50 mbar), and gas flow rates (100 mL/min) were investigated as variables. Leaching steps using HF and HCl acid solutions ensure the synthesis of pure powders free of uncoated Fe_3O_4 and demonstrate the chemical stability of synthesized nanoparticles. According to the magnetic saturation and coercivity values obtained from VSM tests, synthesized

Fe_3O_4@rGO@graphene nanoparticles have soft ferromagnetic properties that demonstrate potential for biomedical and environmental applications. Magnetic saturation and coercivity values of Fe_3O_4@rGO@graphene were determined as approximately 139 emu/g and 402 Oe.

Second, they are functionalized by coating Fe_3O_4@rGO@graphene core-shell nanoparticles with PMA-POEGMA polymer via Atom Transfer Radical Polymerization (ATRP). Cytotoxicity tests were carried out to demonstrate the usage of these nanoparticles in biomedicine. These nanoparticles were tested for biocompatibility (biocompatibility on MCF7 cancer cells for up to 48 h).

In conclusion, Fe_3O_4 and Fe_3O_4@rGO nanoparticles were made via solvothermal synthesis. The calcination procedure is carried out using argon gases to achieve high crystallinity and the elimination of organic contaminants. These substrates were fed into the chemical vapor deposition (CVD) system together with methane (CH_4) and hydrogen (H_2) gases to conduct encapsulation tests. After leaching by HF and HCl acid solutions, Fe_3O_4@rGO@graphene nanoparticles are coated with PMA-POEGMA polymer. Then biocompatibilities were carried out to evaluate the materials' potential for biomedical applications (biocompatible up to 48 h on MCF7 cancer cells). The graphene encapsulation investigations are another thesis goal that optimization experiments on multilayer graphene-encapsulated magnetic nanoparticles (Fe_3O_4@rGO) in the CVD system.

This work offers a novel contribution to the literature in terms of analyzing the biocompatibility of the encapsulated products made possible by optimizing the chemical vapor deposition technique. These magnetic nanomaterials, created in core/shell structures under optimal conditions and whose biocompatibility has been demonstrated by cytotoxicity testing, are candidates for biomedical applications.

MANYETİK NANOPARTİKÜLLERİN SENTEZLENMESİ, KARAKTERİZASYONU VE BİYOUYUMLULUK TESTLERİNİN GERÇEKLEŞTİRİLMESİ

ÖZET

Nanoteknoloji alanındaki gelişmeler son yıllarda artış göstermektedir. Özellikle enerji, çevresel, elektronik ve biyolojik uygulamalarda nanoteknolojinin kullanımı oldukça yaygındır. Manyetik nanopartiküller (MNP'ler) de, farklı nanoteknolojik uygulamalar için geliştirilen malzemelerden biridir. MNP'ler biyolojik uygulamalarda, elektronik cihazlarda, toprak veya su filtrasyonunda ve katalitik uygulamalarda kullanılmaktadırlar. Geniş uygulama alanlarından dolayı MNP'lerin geliştirilmesi üzerine son yıllarda yapılmış pek çok çalışma bulunmaktadır. Bu uygulama alanları arasında MNP'lerin biyolojik uygulamaları üzerine yapılan çalışmalar da bulunmaktadır. Kanser teşhisi (X-ışını kontrast maddeleri, manyetik rezonans görüntüleme ajanları), kanser tedavisi (hipertermi, radyasyon tedavisi), ilaçların ve genlerin taşınımı, biyosensörler, antibakteriyel ajanlar, doku mühendisliği vb. manyetik nanopartiküllerin kullanıldığı biyolojik uygulamalardan bazılarıdır.

MNP'ler, hücreler, virüsler, genler veya proteinler ile benzer veya daha küçük boyutlara sahip olduğundan biyolojik ortama kolayca eklenebilir. Sadece karşılaştırılabilir boyutları değil, aynı zamanda biyouyumluluk, yapısal ve manyetik özellikleri de MNP'lerin biyolojik uygulamalar için uygunluklarının göstergesidir. Bu özelliklerinden dolayı MNP'ler pek çok farklı biyomedikal uygulamalar için uygundur. Demir, demir oksitler (hematit (γ-Fe_2O_3) ve manyetit (Fe_3O_4)), manganez, nikel ve/veya kobalt katkılı demir oksitler, bimetalikler (FeCo, FeNi, CuNi ve FePt), biyomedikal tedaviler için kullanılan bazı MNP örnekleridir.

Partikül boyutu, morfoloji, yüzey özellikleri, biyouyumluluk, manyetik özellikler ve termal/ kimyasal kararlılık, nanomalzemelerin biyomedikal uygulamalarda kullanımı için çok önemli değişkenlerdir. Manyetik nanopartiküller kullanılarak, ilaç taşınımı veya salınımı yapılan yüzey geliştirilebilir çünkü partikül boyutu küçüldükçe yüzey alanı artmaktadır. Ayrıca, herhangi bir koruyucu tabaka ile kaplanmadıkları sürece, demir oksit nanopartikülleri vücut sıvılarında kimyasal kararlılıklarını kaybederler. Herhangibir koruyu tabaka ile kaplanmamış manyetik nanopartiküller oksitlenebildiklerinden dolayı düşük manyetizasyon değerlerine sahip olup görüntüleme uygulamalarında verimliliği düşürmektedirler. Manyetik nanopartiküllerin vücut sıvılarında bozunmasını önlemek ve manyetik özelliklerini kaybetmelerini engellemek için nanopartiküllerin koruyucu tabakalarla kaplanması kavramı ortaya çıkmıştır. Bu tür malzemelere çekirdek/kabuk tipi malzemeler adı verilmektedir. Biyolojik ortamlarda kararlığını sağlamak için manyetik çekirdeğin üzerine farklı inert malzemeler kaplanmaktadır. Pasivasyon tabakası oluşturmak için bir metalin soy metal veya metal oksitler ile kaplandığına dair çalışmalar yapılmıştır. Bunların yanısıra silika ve karbon bazlı (grafen, grafen oksit vb.) kabuk malzemeleri de sıklıkla tercih edilen kaplama malzemeleridir.

Manyetik nanopartiküllerin grafen ile kaplanmasında farklı hammaddelerden hareketle pek çok farklı yöntem kullanılmaktadır. Bu yöntemlerden bazıları, karbon ark deşarj metodu, doğrudan katı-hal reaksiyonları, mekanik alaşımlama destekli ısıl işlem, hidrotermal sentezleme, kimyasal ayrıştırma/indirgeme, plazma ile tavlama, sprey piroliz, otoklavda sentezleme ve kimyasal buhar biriktirme olarak sıralanabilir. Bu yöntemler arasında kimyasal buhar biriktirme sıklıkla kullanılan bir tekniktir. Karbon kaynağı olarak metan, asetilen gibi gazlar kullanılarak grafen ile kapsülasyon çalışmaları yapılmaktadır. Metan gazı dekompozisyonu sonucu carbon manyetik nanopartiküllerin üzerini kaplayarak çekirdek/kabuk yapısındaki partiküller elde edilmiş olur. Bir diğer yöntem olan solvotermal sentez de, Fe_3O_4 gibi manyetik nanopartiküller oluşturmak için kullanılabilir. Tüm bu yöntemlerde, manyetik nanoparçacıkların grafen gibi çeşitli maddeler ile kapsüllenmesiyle biyouyumlu yüzeyler oluşturulabilir. Böylece sentezlenen grafen ile enkapsüllenmiş manyetik nanopartiküller kanser teşhis ve tedavisi başta olmak üzere çeşitli biyomedikal uygulamalarda kullanılabilmektedirler. Enkapsülasyon sonrası nanopartiküllerin kimyasal kararlılıkları arttırılmış ve korozyon dirençleri iyileştirilmiştir.

Bu tez çalışmasında da, Fe_3O_4 and Fe_3O_4@rGO nanopartiküllerinin solvotermal yöntemle sentezlenmesi ve yüksek kristalliğe sahip olmaları ve organik bileşikleri uzaklaştırabilmeleri için argon gazları ile kalsinasyon işlemi uygulamaları gerçekleştirilmiştir. Ayrıca bu malzemelerin kimyasal buhar biriktirme (CVD) sistemine beslenmesi ve metan (CH_4) ve hidrojen (H_2) gazları kullanılarak grafen ile enkapsülasyon çalışmaları yapılmıştır. Enkapsülasyon sıcaklığı (950°C), bu sıcaklıkta bekleme süresi (1 saat), gaz basınçları (50 mbar) ve gaz akış hızları (100 mL/dak) değişken olarak incelenmiştir. CVD çalışmaları tamamlandıktan sonra tozlar saflaştırılmıştır. HF ve HCl asit çözeltilerinin kullanıldığı liç adımları, kaplanmamış Fe_3O_4 içermeyen saf tozların sentezini sağlar ve sentezlenen nanoparçacıkların kimyasal kararlılığını göstermektedir. Sırasıyla HF ve HCl çözeltilerine eklenen tozlar öncelikle ultrasonik banyoda karıştırılmış, sonra santrifüjlenerek saf su ile yıkamıştır. Tekrarlı yıkama işleminin ardından saf tozlar elde edilmiştir. VSM testlerinden elde edilen manyetik doygunluk ve koersivite değerlerine göre, sentezlenen Fe_3O_4@rGO@graphene nanoparçacıkları, biyomedikal ve çevresel uygulamalar için potansiyel gösteren yumuşak ferromanyetik özelliklere sahiptir. Fe_3O_4@rGO@graphene manyetik doygunluk ve koersivite değerleri yaklaşık olarak 139 emu/g and 402 Oe olarak belirlenmiştir.

Bir diğer yöntemde ise, Atom Transfer Radikal Polimerizasyonu (ATRP) yoluyla Fe_3O_4@rGO@graphene çekirdek-kabuk nanopartiküllerini PMA-POEGMA polimeri ile kaplayarak işlevselleştirilirler. Bu nanopartiküllerin biyotıpta kullanımını göstermek için sitotoksisite testleri yapılmıştır. Bu nanoparçacıklar biyouyumluluk (48 saate kadar MCF7 kanser hücreleri üzerinde biyouyumluluk) açısından test edilmiştir.

Sonuç olarak, solvotermal sentezleme yoluyla Fe_3O_4 and Fe_3O_4@rGO nanoparçacıkları saf bir şekilde sentezlenmiştir. Kalsinasyon prosedürü ile yüksek kristallik elde edilmiştir ve organik kirleticileri ortadan kaldırmak için argon gazları kullanılarak gerçekleştirilmiştir. Bu malzemeler, enkapsülasyon çalışmaları yapmak için metan (CH_4) ve hidrojen (H_2) gazlarıyla birlikte kimyasal buhar biriktirme (CVD) sistemine beslenmiştir. HF ve HCl asit çözeltileri ile liç sonrası, Fe_3O_4@rGO@grafen nanoparçacıkları, PMA-POEGMA polimeri ile kaplanmıştır. Ardından, malzemelerin biyomedikal uygulamalarda kullanım potansiyelini değerlendirmek için biyouyumluluklar gerçekleştirilmiştir (MCF7 kanser hücrelerinde 48 saate kadar biyouyumlu). Grafen kapsülleme araştırmaları ise sunulan tezin bir başka amacıdır.

CVD sisteminde çok katmanlı grafen kapsüllü manyetik nanopartiküller (Fe_3O_4@rGO) üzerinde optimizasyon deneyleri gerçekleştirilmiştir.

Kimyasal buhar biriktirme tekniğinin optimize edilmesiyle mümkün kılınan kapsüllenmiş ürünlerin biyouyumluluğunun analizi açısından bu çalışma, literatüre yeni bir katkı sunmaktadır. Optimum koşullar altında çekirdek/kabuk yapılarında oluşturulan ve biyouyumluluğu sitotoksisite testleri ile kanıtlanmış olan bu manyetik nanomalzemeler, biyomedikal uygulamalarda kullanılmaya adaydır.

1. INTRODUCTION

Nanotechnology is an interdisciplinary field that combines various branches of science in various ways, including materials science, chemistry, physics, electronics, and medicine. In recent years, scientists have been more eager to research nanotechnology by utilizing cutting-edge and advantageous manufacturing techniques. Due to their small sizes (1-100 nm) and extraordinary magnetic capabilities, magnetic nanoparticles (MNPs) have been researched for their potential uses in various fields involving biomedicine, electronics, agriculture, and the environment.

Researchers have been attempting to expand the type of magnetic nanoparticles (MNPs) in various scientific domains, as nanotechnology in biomedicine and early cancer diagnosis and therapy has gained momentum over the past 20 years. Particularly, attention is being drawn to the idea of using MNPs as an efficient tool in magnetic resonance imaging for the diagnosis and treatment of cancer, the development of nano vectors for the transport of anti-cancer drugs to target organs and imaging contrast agents and applications for hyperthermia. Science, engineering, and medicine are all incorporated into the transdisciplinary study of cancer, including numerous applications for molecular-level imaging, diagnostics, and targeted therapy. Among the cutting-edge projects in progress are studied for the early detection of cancerous cells, tissue disturbances, and malignant lesions in biological fluids. By supplying the crucial components required in the global fight against cancer, these nanostructures are thought to have the potential to change science and medicine. MNPs could be focused and directed at tumor tissues using magnetic fields or radio waves, allowing the detection of cancerous regions. MNPs are employed for therapeutic applications, such as hyperthermia and cancer diagnostics. In a hyperthermia application, magnetic nanoparticles targeted toward cancerous cells transform electromagnetic energy into heat, increasing the temperature of the MNPs and diseased tissues to between 41 and 47 °C, killing the cancerous cells in the targeted cancerous region. This application is predicated on the notion that the pharmaceuticals (medications) loaded on MNPs are released or delivered to the specific cancerous

tissue after being guided by a magnetic field to the target site. Drug release is thereby restricted to cancerous tissues that are of interest.

Prior research on cancer diagnosis and treatment nanostructures focused on semi-noble or metallic nobles (such as Cu, Ag, and Au). The production of Fe, the element with the highest saturation magnetization, and nanoparticles (Fe_2O_3, Fe_3O_4, Fe-Pt, Fe-Co, Fe-Au, Fe-Pt-Au, etc.) in numerous different compositions containing Fe was then studied, and its potential for use in biological applications has started to be investigated. On the other hand, the concept of coating their outer surfaces with a high-specification material or a protective layer has emerged to ensure that the magnetic iron-based nanoparticles do not undergo any change in biological fluids; that is the saturation magnetization value has not changed., and to isolate the nanoparticles from one another magnetically. Additionally, efforts were made to coat or encapsulate iron-based nanoparticle surfaces with noble metals like Au and Pt or to passivate the surfaces of the particles with their oxides. However, it was shown in these tests that the nanoparticle's saturation magnetization diminished after a week. As protective encapsulation materials, SiO_2, BN, and organic polymers (polyethylene glycol) have also been used in studies. However, these materials' biocompatibility, ease of bonding with functional groups, and thermal and chemical stability have not yielded positive results. The literature has noted that encapsulation layers with different properties are created using very different techniques, and these studies are still ongoing. Encapsulation experiments with carbon, graphite, or graphene layers with very high chemical stability have begun in the following processes.

As an alternative to Fe and Fe oxide-based nanoparticles used in MRI, targeted delivery/distribution of anti-cancer drugs and imaging contrast agents, hyperthermia applications, and saturation magnetization values and chemical stability degrade over time with environmental effects. Fe_3O_4-based core/shell-type nanoparticles are synthesized from various raw materials under various processing circumstances, and then their outer surfaces are coated with multilayer graphene while using cutting-edge characterization methods. the characteristics of the goods produced using various methods (nanocapsule particle size distribution, graphene formation, thickness of the graphene layers, stability, structural stability, thermal stability, chemical stability, and magnetic properties), as well as assessing their potential for use in the biomedical industry.

The current dissertation study is highly inventive in connecting a synergy between powder/gas metallurgy and graphene/silica metallurgy. This dissertation's interdisciplinary research studies have demonstrated the possibility of encapsulated MNPsto being used as biomedicines. Additionally, by utilizing the characteristics of MNPs and exploring their scientific and technological potentials, this dissertation is significant in that it contributes significantly to the national and international scientific literature. It also makes finding new methods, thorough optimization studies, and applications possible.

The primary goal of this dissertation is to create core-shell type Fe_3O_4-based MNPs for prospective biomedical applications. There are four sections to this dissertation paper. The first two sections discuss how Fe_3O_4 and Fe_3O_4@rGO nanoparticles were made. The remaining two parts also deal with Fe_3O_4-based nanoparticles that are multilayer graphene-encapsulated and polymer-functionalized. Finally, cytotoxicity studies were run to demonstrate the potential biomedical uses of particular nanoparticles.

Iron oxide (Fe_3O_4) and carbon-encapsulated iron oxide (Fe_3O_4@rGO) powders were produced in the first section using solvothermal synthesis techniques. This process might take up to 26 h.

In the second section, solvothermal synthesis successfully created iron oxide (Fe_3O_4) and carbon-encapsulated iron oxide (Fe_3O_4@rGO) nanoparticles. The calcination procedure was then used to improve crystallinity and remove organic contaminants. Numerous factors, including various temperatures and times of day, were thoroughly explored to optimize the synthesis conditions.

The third section describes the synthesis, enhancement, and characterization of Fe_3O_4@rGO@graphene core-shell nanoparticles enclosed by multi-layer graphene (MLG). CVD experiments were conducted using low vacuum and CH_4/H_2 gas fluxes in a tube furnace to determine how Fe_3O_4@rGO@graphene core-shell nanoparticle production was affected by gas fluxes, temperature, pressure, and holding time. The ideal CVD parameters were 950°C, 50 mbar, 60 min, and CH_4/H_2:1/1. We started synthesizing PMA-POEGMA using Atom Transfer Radical Polymerization (ATRP) to disperse graphene-encapsulated iron oxide nanoparticles. After polymerization, the solution was purified by dialyzing it for 48 h against H_2O in a dialysis membrane

(MWCO 1 kDa). Moreover, we functionalized Fe_3O_4@rGO@graphene core-shell nanoparticles by covering them with PMA-POEGMA.

The possible biomedical applications of a few chosen synthesized nanoparticles were examined in the final section. For the first time, the cytotoxicity of the optimized nanoparticles on cancer cell lines was examined about their potential for biomedical applications. To synthesize soft ferromagnetic multi-layer graphene (MLG) encapsulated nanoparticles, this study defines the best CVD conditions and shows how harmful they are to cells.

2. LITERATURE REVIEW

2.1 Magnetic Nanoparticles

The ferromagnetic materials with size were predicted in 1930, and they understood that net magnetization resulted from a particle below a crucial limit that would be able to the distinct magnetic region where unbound electrons' magnetic moments line up parallel. After that, studying magnetism at the nanoscale has been devoted to incredible research works. As a result, decreasing the size of ferromagnetic materials can change their multi-domain behaviors to single-domain behaviors with higher coercivity (H_c) [1]. In the 1950s, research on the actions of magnetic nanoparticles (MNPs) was published, and this was done just after the magnetic behavior of magnetic nanoparticles was worked by Néel's pioneering. Particularly since the beginning of the new millennium, magnetic nanoparticles (from 1 to 100 nm) have become necessary materials for technology and science [1,2]. The properties of nano entities, such as magnetic characteristics that depend on the size and a high surface-to-volume ratio, vary from those of their bulk materials, making them remarkably versatile, strong, and reactive [2].

The material properties of magnetic nanoparticles result from the particle-particle interactions and the intrinsic properties of the particles. Mostly believed that there is an ordinary difference between ionic compounds and metals. Ferromagnetic metals have itinerant moments, and the band structure details influence the magnitude of the moment. Due to band narrowing that is occurred by reducing coordination at the surface, Co, Ni, and Fe nanoparticles produce larger than-bulk moments [3,4]. Furthermore, nanoparticles in the magnetic ground state can be severely changed because of having the same basic spin, single magnetic domains, moments, and orientation found in bulk materials. As a result, microstructural details and the finite size of both the core and surface influence the ground state strongly.

In addition, magnetic excitation spectra of bulk materials are different from nanoparticles [3]. One of the nanoparticles' magnetic properties is size-dependent.

When a magnetic NP's size falls below a specific critical size, the NP behaves as a single-domain because of ferromagnetic coupling in one direction. The predetermination of nanostructured materials has distinctive chemical, magnetic, structural, and electrical properties [2], so MNPs have gotten substantial interest in a greater variety of application domains due to such characteristics, such as gyroscopic devices, environmental tools, magnetic fluids, spintronics, data/energy, magnetic inks, storage/harvesting, catalysis, and imaging [2,4]. High saturation magnetization (M_s) materials such as ferrites ($Mn0.6Zn0.4Fe_2O_4$ and $CoFe_2O_4$), alloys (FeCo, Alnico, and Permalloy), and pure metals (Fe, Co, and Ni) are usually chosen for biomedical applications to produce MNPs [4]. Due to their ability to selectively attach to functional molecules, endow the target with magnetic properties, and enable Under the control of an electromagnet or permanent magnet's magnetic field, manipulation and transportation to a desired place, nanoparticles with magnetic properties have significant advantages [3].

Iron oxide nanoparticles, or ferrite nanoparticles (a magnetite-like crystal structure), are the magnetic nanoparticles that have received the most attention to date. Superparamagnetic less than 128 nm size ferrite particles prevent them from only exhibiting their magnetic activity when an external magnetic field is applied, resulting in self-agglomeration [5]. It is possible to significantly boost the magnetic moment of ferrite nanoparticles by carefully assembling many superparamagnetic nanoparticles to form clusters of superparamagnetic nanoparticles, like magnetic nanobeads [5]. When the external magnetic field is eliminated, the remanence equals zero. Ferrite nanoparticles frequently change their surface using surfactants, silica, silicones, or phosphoric acid derivatives to boost their stability in solutions. Due to their relatively inert surface, maghemite or magnetite magnetic nanoparticles often do not permit covalent solid contact with functionalization molecules. On the other hand, the MNPs' reactivity can be raised by coating their surface with silica [6].

Nanoparticles, such as metallic, may be helpful for some applications as technological applications due to their more excellent magnetic moments, whereas oxides (maghemite, magnetite) may be helpful for biological applications. As a result, these nanoparticles can be made simultaneously smaller than their oxide counterparts, Metallic nanoparticles. However, suffer significantly from being pyrophoric and having different degrees of reactivity to oxidizing agents. Due to their increased

difficulty in handling and propensity for unanticipated side effects, they are less appropriate for use in biological applications. Additionally, metallic particle colloids are far more challenging to produce [5,6]. Surfactants, polymers, precious metals, and light oxidation can all be used to passivate the metallic cores of magnetic nanoparticles. When exposed to oxygen on their surface, co-nanoparticles create an anti-ferromagnetic CoO layer. Recently, it has been possible to create magnetically-cored nanoparticles comprised of either elemental iron or cobalt and a nonreactive graphene shell. Contrasting the benefits with those of ferrite or elemental nanoparticles [6,7].

2.2 Synthesis Methods of Magnetic Nanoparticles

There are several different phases and compositions to synthesize magnetic nanoparticles, for example, pure metals, such as Fe and Co, iron oxides, such as Fe_3O_4 and g-Fe_2O_3, spinel-type ferromagnets, such as $MgFe_3O_4$, $MnFe_3O_4$, $CoFe_3O_4$, alloys, such as $CoPt_3$ and FePt. Some methods include thermal decomposition, co-precipitation, solvothermal synthesis, hydrothermal synthesis, and laser pyrolysis techniques which are helped to obtain high-quality magnetic nanoparticles [8].

2.2.1 Thermal decomposition

Organometallic complex precursor thermolysis in high-boiling-point organic solvents with surfactants is used in thermal breakdown methods to create nanoparticles of diverse materials. To regulate the size and shape of the resultant nanoparticles, it is usual practice to change the quantities of the precursors, surfactants, solvents, and experimental factors, including heating rate, heating temperature, and heating time [9]. The most frequent organometallic building blocks for producing magnetic nanomaterials are metal acetylacetonates, metal-oleate complexes, and metal carbonyls. The most popular surfactant is oleic acid. There are two ways that you can include precursors in the reaction. Precursors and surfactants can be combined using one approach at room temperature before being heated according to the planned protocol. Metal complexes with acetylacetonates and oleates are frequently broken down during this process. The second approach uses a hot injection that causes the precursors to be injected into a hot solution with surfactants, which causes the nanoparticles to form and develop [10]. This technique was typically used to

decompose metal carbonyl precursors. The ability to produce MNPs with excellent crystallinity, controlled shape, and a high yield with a limited size dispersion is one of the key benefits of thermal decomposition methods [11,12].

2.2.2 Co-precipitation

Coprecipitation is a well-known and simple technique for producing iron oxide nanoparticles. In this process, Fe^{2+} and Fe^{3+} salts are precipitated from aqueous solutions such as NaOH, chlorides, sulfates, and nitrates. Examples of experimental parameters that can be utilized to control the size, shape, and composition of the nanoparticles as they form include the kind of precursors, the precursor ratio, the surface ligand, the reaction temperature, and the pH [13]. For stabilizing purposes during precipitation to enhance the size distribution of the as-prepared nanoparticles, a variety of surface ligands, including surfactants, inorganic compounds, and polymers, have been utilized. High yields of water-soluble nanoparticles can be produced using this technology directly through a simple procedure, which is one of its main advantages [14]. Feridex, Resovist, and Combidex are a few examples of the several iron oxide nanoparticle-based MRI contrast agents produced by this approach, as shown in Figure 2.1. However, because the water's evaporation point constrains the reaction temperature, products prepared using this method can have poor crystallinity [15].

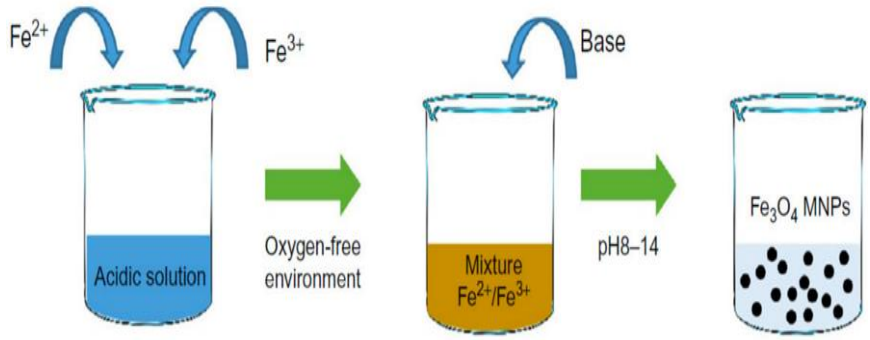

Figure 2.1: Illustrates the co-precipitation process for synthesizing iron oxide magnetic nanoparticles [16].

2.2.3 Hydrothermal synthesis

The heterogeneous reactions in aqueous fluids at pressures and temperatures above ambient to produce inorganic compounds are known as "hydrothermal synthesis." In this procedure, to dramatically increase the pressure within the autoclave for the

reaction over atmospheric pressure, the boiling point of water is reached by heating an aqueous mixture of precursors in a stainless-steel container tightly sealed [17]. Without using post-annealing techniques, high temperature and pressure operate in concert to create incredibly crystalline materials in a single process. Hydrothermal processes can now create a wide range of nanomaterials, including magnetic nanoparticles. The parameters for the reaction, such as the solvent, stabilizing agents, temperature and reaction duration, and a description of the precursors' type and concentration, substantially impact the results [18]. Hydrothermal synthesis, as opposed to methods for "low-temperature" coprecipitation, which often produce poorly crystalline nanoparticles, produced magnetic nanomaterials with extraordinarily high crystallinity because of the conditions for reactions at high temperatures and pressures, as shown in Figure 2.2. The yield of products from hydrothermal methods is generally lower than that of coprecipitation processes [11,17].

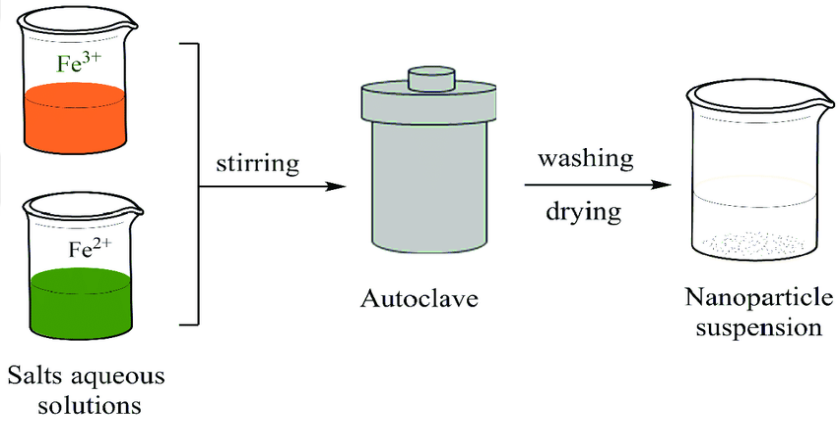

Figure 2.2: Hydrothermal synthesis of IONPs [19].

2.2.4 Solvothermal synthesis

Like the hydrothermal method, the solvothermal approach uses organic solvents during the synthesis process rather than water. If alcohols are utilized as the reaction media, the reactions are referred to as alcohothermal. Creating NCs with good crystalline characteristics depends on these synthetic techniques [20]. By enclosing the reaction mixture in a sealed vessel, a solvothermal technique allows the chemical reaction to proceed in the solvent at a temperature above its typical boiling point (e.g., bomb or autoclave). These circumstances enhance the solvent's capacity to dissolve solids and quicken chemical reactions involving different solid species. In a typical technique, the precursors and other reagents, including the solvent, are loaded into an

autoclave in the proper ratios and heated in an oven at a specific temperature for a predetermined time [21]. Before getting the finished product, the sample must first be cleaned with water and alcohol to eliminate any contaminants, as shown in Figure 2.3. The fundamental advantage of this strategy is its capacity to dissolve nearly increasing the temperature as well as the pressure will dissolve any substance in the solvent to the necessary levels. Most NCs in the groundbreaking work need more size and form control [22].

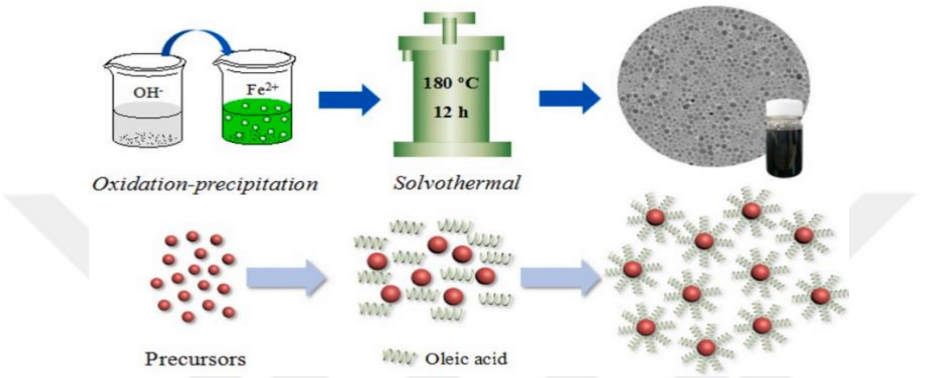

Figure 2.3: Iron Oxıde NPs synthesizing procedure by solvothermal method [23].

2.2.5 Laser pyrolysis

To create nanoparticles, one of the techniques created is laser pyrolysis. During laser pyrolysis, the precursors in the gaseous phase are transferred by argon to a chamber where they come into contact with the laser beam. The 2400 W high-power laser beam produces heightened localized temperatures that cause nanoparticles to form and develop. After that, a filter-equipped catcher gathers the nanoparticles [24]. Although laser pyrolysis is known as a gaseous-phase process, liquid reactants are still permitted. When using liquid reactants, they can either be evaporated or condensed into tiny droplets (for example, using an ultrasonication process) and then added to the reaction chamber [25,26].

2.2.6 Flame spray synthesis

Thermal spray methods like flame spray synthesis turn diverse materials into coatings and powders. It entails the employment of a high-temperature flame to melt and atomize a feedstock material into tiny particles that are subsequently sprayed onto a substrate [27]. The combustion of a fuel gas and oxygen mixture typically produces this flame, as shown in Figure 2.4. The feedstock material is often delivered into the

flame as a powder or wire, where it is quickly heated and melted. Following melting, the material is sprayed onto a substrate, which can be made of metals, ceramics, polymers, or composites [28,29].

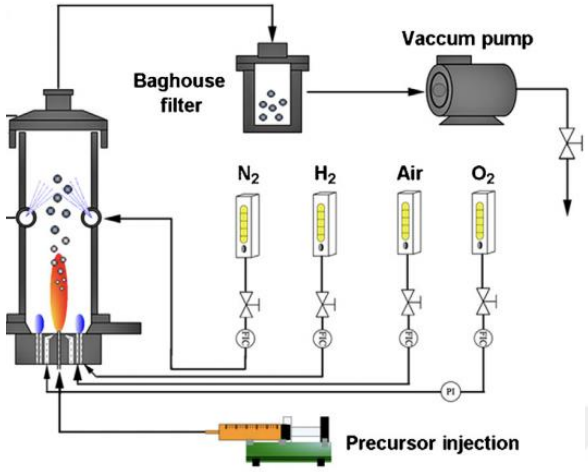

Figure 2.4: Schematic of magnetic nanoparticles' FSP synthesis setup [30].

2.2.7 Microemulsion

A form of colloidal dispersion known as a microemulsion is created when a surfactant stabilizes the mixture of two immiscible liquids, typically water and oil. To maintain the oil droplets suspended in the continuous phase, the surfactant molecules organize themselves in a layer around the droplets of the dispersed phase (water). The resulting combination has a low viscosity and seems translucent. The small droplet size of microemulsions, typically between 10 and 100 nanometers, gives them a significant amount of interfacial area and improves their stability [31]. The droplet size can be managed by altering the microemulsion's composition, including the concentration of the surfactant and cosurfactant, which illustrates the example in Figure 2.5. Due to their unique qualities, such as high solubilization capacity, higher bioavailability, and increased stability of active substances, microemulsions are widely emicroemumployed in various industries, including the pharmaceutical, cosmetic, and food industries. They are also employed in oil recovery, polymerization, catalysis, and as templates for the creation of nanoparticles [32].

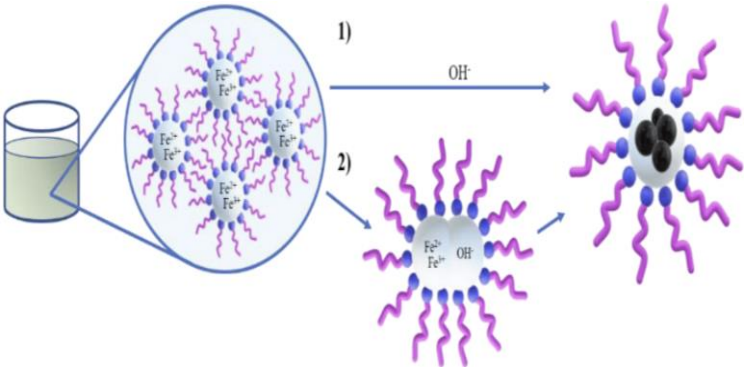

Figure 2.5: Diagram showing the fabrication of the investigated magnetic nanoparticles. Water-based solutions of the iron precursors are utilized to create a microemulsion in the oil phase [33].

2.3 Biomedical Applications of Magnetic Nanoparticles

Scientists may manufacture unusual NPs with sizes, morphologies, and compositions that can be controlled for various applications. Of the several types of NPs, magnetic NPs are a potential nanoscale tool in the biomedical field. For instance, their usage as contrast agents in magnetic resonance imaging (MRI) procedures results from NPs' ability to create magnetic fields and affect their local surroundings [2,8]. Additionally, they are desirable candidates for application in cell separation/purification, cell monitoring [34], and medicine delivery because an external magnetic field can manipulate them. They are also suitable as anticancer due to their capacity to produce heat when subjected to alternating magnetic field therapies [2,3]. Pure metals are not appropriate for usage in vivo because of their extreme toxicity and oxidative qualities (despite having higher M_s). Due to their excellent chemical/colloidal stability and biocompatibility, iron oxides became the most common materials. They were being researched for use in magnetic hyperthermia [34–36], Magnetic resonance imaging [34,37], MRI contrast agents [34], and targeted drug delivery systems [38]. It is possible to improve biocompatibility, suspension characteristics, or colloidal stability. Therefore, a coating made of ceramics, polymers, or molecules that are sterically hindered or strongly charged is typically used to shield magnetic nanoparticles [2,4].

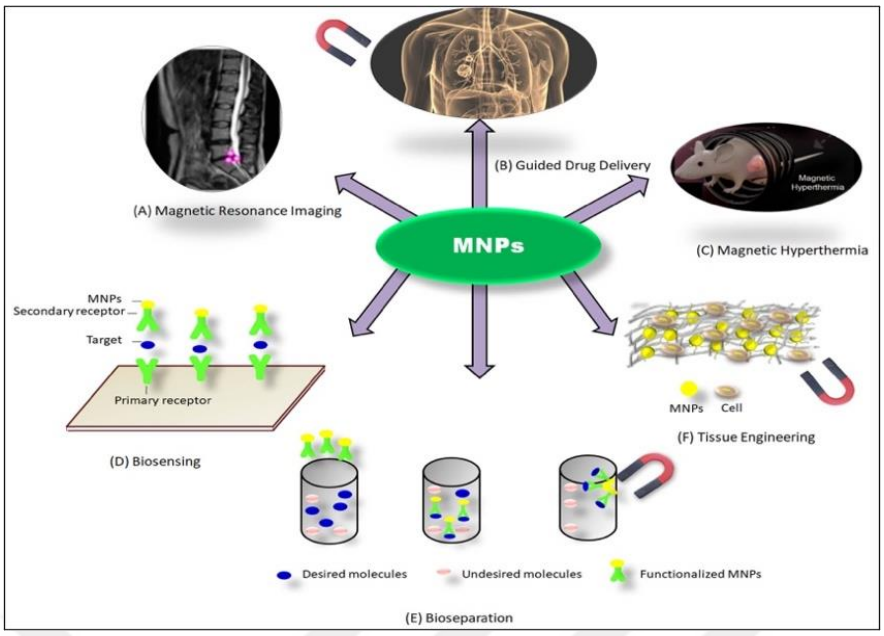

Figure 2.6: Different MNP applications are shown schematically [39].

2.3.1 Magnetic hyperthermia

For treating cancer tumors, hyperthermia is a useful therapeutic strategy. Theoretically, concentrated nanoscale heaters that destroy malignant cells from the inside out might be utilized instead of traditional medications to treat cancer without medication usage. [34,35]. The most critical choices for effective therapy are magnetic materials with Curie temperatures between 42 and 60°C since they serve as in vivo temperature control switches, which prevent overheating. There have been approaches for intracellular hyperthermia using MNPs created because it is widely known that tumor cells are more sensitive to increases in temperature than healthy cells. These methods involve concentrating the particles at the tumor site and remotely heating them to the necessary hyperthermic temperatures (42–45°C) using an applied magnetic field [36]. Due to the disorganized vasculature (as previously mentioned), MNPs tend to accumulate in tumors after being injected into organs with tumors, which causes the tumor to heat up instead of the neighboring healthy tissue. Direct injection into solid tumors, along with exposure to an alternating magnetic field, has been shown to result in tumor regression, as shown in Figure 2.7. In human cancer models like breast cancer, recent research has demonstrated the usefulness of heating 10–30 nm iron oxide particles with MNPs. However, it is noted that more research is required to optimize the delivery and regulate heat dispersion. Thus, hyperthermia has been

proposed as a non-invasive and non-toxic approach to initiating gene expression locally [34].

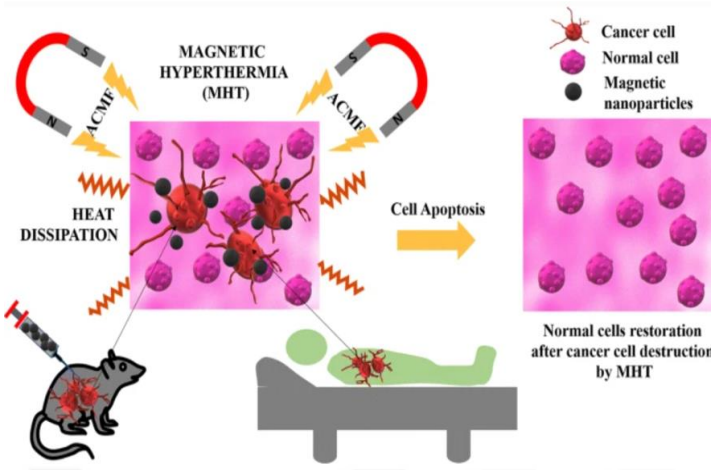

Figure 2.7: Schematic presentation of magnetic hyperthermia of MNPs [40].

2.3.2 Magnetic resonance imaging

Because of its non-invasiveness, MRI has exceptional spatial resolution, tomographic capabilities, and an effective imaging method. Over the past ten years, MRI applications have progressively grown because of the benefit of great spatial resolution of contrast fluctuations across tissues. agents with nanoparticles for contrast provide improved cellular uptake and delayed removal from the cancer site compared to conventional gadolinium chelates. Iron oxide cores, also known as Superparamagnetic iron oxides (SPIOs), which have dimensions of greater than 50 nm, and ultrasmall SPIOs (USPIOs), which are commonly employed in MRIs as "T2 contrast agents," are two different types which are currently under investigation and offer exciting new possibilities for imaging, diagnosis, and treatment. In the coming years, it is reasonable to anticipate that MRI will grow substantially more sensitive [37]. When the sensitivity of MRI molecular imaging approaches and possibly exceeds that of fluorochromes (fluorescent chemicals used to label biological material), the necessity for nanoparticles may become less important. Contrarily, theranostics is a separate factor that will make nanoparticles important even in MRI versions that are more sensitive. The nanoparticle's cargo may include signal-generating chemicals and medicinal compounds, as shown in Figure 2.8. With this combination, molecular imaging and therapy can be integrated since the nanoparticle can be positioned inside the living patient while also releasing medications into a target region. This "treatment" plus

"diagnostics" or "theranostics" has the potential to track the efficacy of therapy while also providing it in the future [34,37].

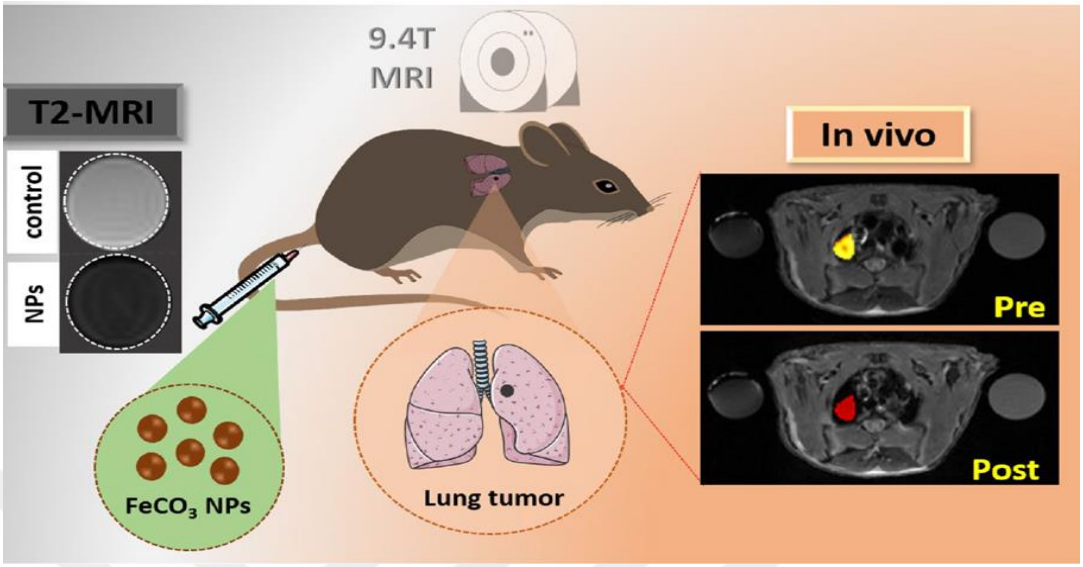

Figure 2.8: Lung tumor in vivo MR imaging on $FeCO_3$ NPs shown schematically. [41].

2.3.3 Magnetic biosensors

In biosensors, magnetic nanoparticles can be utilized as sensing components, enabling the detection of specific biomolecules or analytes. A magnetic sensor can detect changes in the nanoparticles' magnetic characteristics when they are functionalized with particular receptors or ligands that bind to the target of interest. Compared to non-MNP-based techniques, MNP-based sensing techniques offer benefits regarding analytical figures of merit, including improved sensitivity, a low limit of detection (LOD), a high signal-to-noise ratio, and a quicker analysis time. [34,42]. MNPs are used in sensing applications by directly attaching tagged supports to the sensor, incorporating them into the transducer components, dispersing them throughout the sample, and then attracting them with an external magnetic field to the active sensing surface of the biosensor [43].

2.3.4 Drug delivery

There are some benefits from the potential of drug delivery systems based on the use of nano and microparticle stems, similar to the capacity to target particular body areas. The amount of drug required to achieve a specific concentration close to the target is reduced, and the attention of the medication at nontarget sites is decreased, reducing

harmful side effects [44]. Magnetic nanoparticles (NPs) can target tumors either passively or actively. The extravasation of the NPs at the sick site (tumor), where the microvasculature is hyperpermeable and leaky, is what causes passive targeting. The primary restriction is instead related to how long NPs stay in the blood. As a result, only cancers in organs with the mononuclear phagocyte system (MPS) would be treated with traditional NPs for drug delivery via passive targeting (liver, spleen, and bone marrow). Active targeting is based on both particular physical traits and the over- or exclusive expression of certain receptors or epitopes in tumor cells. As a result, drug-conjugated vectors responsive to physical stimuli (such as temperature, pH, electric charge, light, sound, and magnetism) have been produced [45].

Instead, active targeting may be based on overexpressed species such as polysaccharides (hyaluronic acid), polyunsaturated fatty acids, DNA, low molecular weight ligands (folic acid, thiamine, sugars), peptides (RGD, LHRD), proteins (transferrin, antibodies, lectins), peptides, and lectins. A medication or therapeutic radionuclide is coupled to a magnetic substance for magnetic targeting, injected into the body, and then concentrated in the desired location using an externally applied field of magnetism or an internal permanent magnet. The particles subsequently release the medicine or provide a local effect, depending on the use (Radiation from radioactive microspheres or magnetic NP-induced hyperthermia). The drug-conjugated magnetic NPs can be used to stimulate drug release magnetically. It can happen through pathways requiring enzyme activity or alterations in physiological parameters like osmolality, pH, or temperature. Drug release can also happen through simple diffusion [38,45].

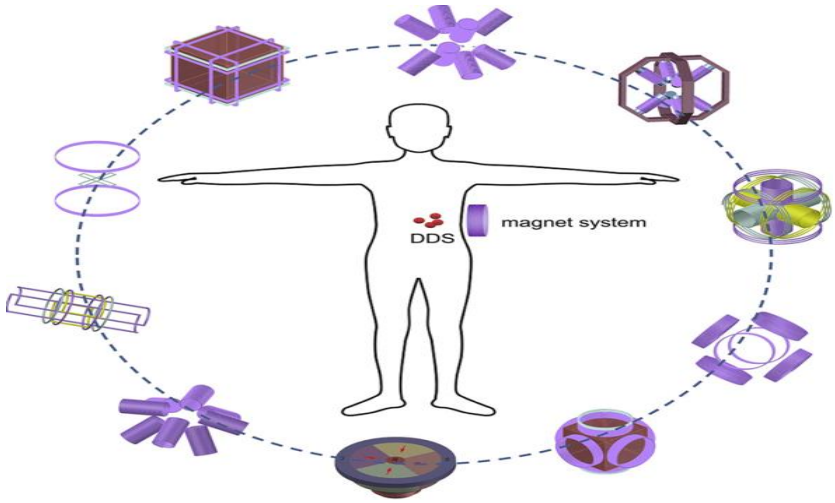

Figure 2.9: Schematic illustration of magnetic drug targeting [46].

2.4 Encapsulation of Magnetic Nanoparticles

Nanomaterials are employed in many industries, such as biotechnology, electronics, and sensors. This is partly because nanomaterials stand out from individual atoms and the bulk phase due to their distinctive characteristics. The growing interest in magnetic nanostructure materials has been sparked by the unique features and possible applications of magnetic nanoparticles like magnetite, maghemite, nickel, and cobalt, particularly in biomedicine and bioengineering such as magnetically assisted drug delivery, cell isolation, etc. Most of these applications ask for embedding magnetic nanoparticles in a nonmagnetic matrix to prevent aggregation and sedimentation of magnetic nanoparticles and to provide them with special surface qualities for certain purposes [47]. The study of the surface chemistry of magnetic nanoparticles (MNPs), which are used in various technical applications, including micro/nano-electronics, catalysis, chemical sensing, information storage, and medical diagnostics, is becoming increasingly important. Examples include enhancing contrast in magnetic resonance imaging, controlled drug delivery, tissue regeneration, removing biological fluids from the body, immunoassay, and biological targeting or separation. An important problem in numerous applications is the synthesis of MNPs with controlled size, content, and surface properties. This topic has attracted a growing amount of interdisciplinary study [48]. Significant progress has been achieved in the bottom-up production of MNPs, including transition metals, alloys, and metal oxides, using chemical processes, including breakdown, reduction, or oxidation reactions in both aqueous and organic media. Since MNPs are required for proper biocompatibility and interfacial reactivity,

the capacity to customize surface characteristics is essential in many biological application domains. The surfaces of MNPs can be altered or functionalized using polymers, organic monolayers, oxides, and metals in various ways, such as by conjugating them to proteins, enzymes, or antibodies or by designing anticancer drug delivery systems [49].

2.5 Coating Methods

Different types of coating are used mostly in biomedical applications, such as liquid phase coating, solid phase coating, and gas phase coating.

2.5.1 Physical vapor deposition (PVD) coating

Applications for the PVD process span from aesthetic items to industrial parts, and it is well recognized for offering materials exposed to caustic media corrosion and wear resistance as well as thin protective layers on their surface. This method makes it possible to alter the coating layers' mechanical, corrosion, and aesthetic properties as necessary. Most of the time, PVD is a high vacuum procedure that transforms solid/liquid materials into a vapor phase, followed by a metal vapor condensation that creates a solid, dense coating. The two most well-known PVD processes are sputtering and evaporation. Due to the thinness of PVD coating layers, multiple coatings are always necessary, and material selection should be carefully thought out [50]. In addition to serving as aesthetic components, many PVD-coated parts have significant wear rates that cause an abrasion on the surface and wear away the coating layer as illustrated in Figure 2.10. As a result of this process, the parts are less able to withstand corrosion and are more vulnerable to corrosive fluids. Different supply units, such as electron beams, heating wires, laser beams, molecular beams, etc., may provide the thermal energy required for evaporation. This thermal energy heats the atoms of the source material, which may be solid or liquid, to the point of evaporation. The vaporized particles travel a long way through the vacuum before depositing on the substrate. The base material of the coating has a considerable impact on the corrosion qualities of the coated parts, according to several research that looked at the material composition of PVD coatings [51].

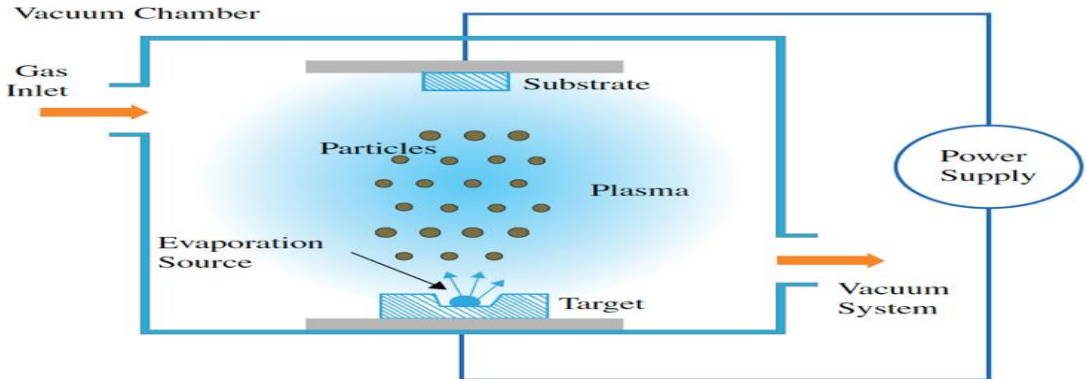

Figure 2.10: Process of physical vapor deposition (PVD) shown schematically [50].

2.5.2 Chemical vapor deposition (CVD) coating

An alternative type of vapor deposition is CVD. The semiconductor industry extensively uses this technique, which employs a high vacuum to produce a solid, high-quality, high-resistance coating layer on any substrate. CVD can be used on mechanical parts that are frequently in contact and need to be protected from corrosion and wear. In this procedure, a wafer-shaped substrate is exposed to a mixture of volatile material precursors, where a chemical reaction causes a layer to be deposited on the material's surface. However, some of the byproducts of these chemical activities, which are removed by the vacuum pump's constant input, can still be present in the chamber [52]. The heaters maintain a high temperature to support the chemical interaction between the substrate and the vaporized CVD ingredients as they are pumped from the right side. With the use of the CVD approach, a variety of materials with various compositions and forms are available, including Carbides, nitrides, oxynitrides, diamond, polymers, graphene, fibers/nanofibers/nanotubes, titanium, and W are examples of materials. Amorphous, polycrystalline, and monocrystalline microstructures are just a few additional options for these materials' microstructures [53].

The three categories of the CVD process are the three pressures are air, low pressure, and ultra-high vacuum, with the last two being the most common. Various CVD process classifications depend on substrate heating, material characteristics, and the kinds of plasma used to vaporize the components Figure 2.11. This list of used categories frequently includes photo-assisted CVD, plasma-enhanced CVD, microwave-plasma-assisted CVD, direct liquid injection CVD, aerosol-assisted CVD, and CVD with direct fluid injection. Depending on the uses, there are arguments for

and against CVD over PVD. The substrate in the CVD process is heated to 900 °C, which precludes the utilization of temperature-sensitive materials. PVD offers a remedy for these kinds of materials. Yet, there is minimal material waste since CVD may only be applied to the heated region. The computer-controlled lasers could enhance this capability to selectively heat the desired areas [51,54].

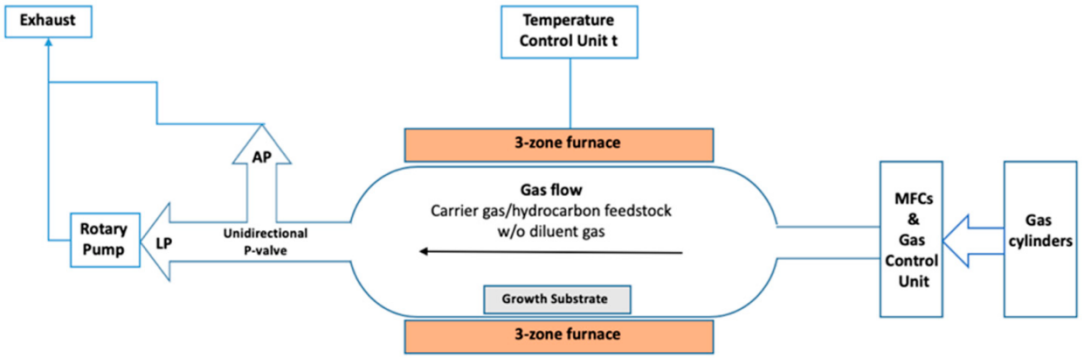

Figure 2.11: Chemical vapor deposition system [55].

2.5.3 Electrodeposition coating

By putting metallic ions on a substrate, materials are supposed to be safeguarded through electrodeposition. During this stage, ions transfer in the unit cell due to the difference in potential between the anode and cathode poles. The submerged sample eventually forms a coating layer by slowly absorbing ions from the other electrode [56]. Numerous studies have been conducted on common electrodeposition materials. The results of the tests demonstrate a significant improvement in the corrosion properties of the substrate due to the electrodeposited coatings. Aside from that, it has been proven that this technique works well to make polymeric coverings that are highly hydrophobic, such as polythiophene. Electrolytic deposition (ELD) and electrophoretic deposition (EPD) are two methods that are generally used in electrodeposition [51,56].

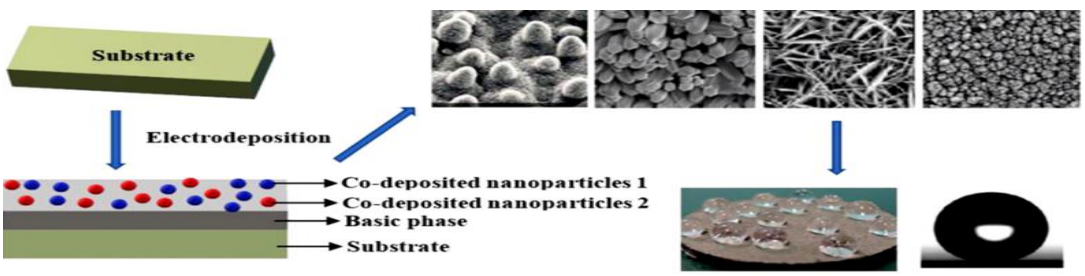

Figure 2.12: The electrodeposition coating process is depicted schematically [56].

2.5.4 Sol-gel coating

The sol-gel coating is one of the most efficient coating techniques for biomedical equipment. The variety of studies on this technique and its applications might make it easier to set up and conduct experiments while maintaining the validity of the results. Conversely, Sol-gel can improve pre-existing coating layers regarding corrosion and ion release. Sol-gel can quickly seal porosity-coating structures or damaged layers because of its liquid-permeating nature [57]. The "Sol" solution is created by dissolving in ethanol or distilled water, and there are precursors of calcium phosphorous (CaP). To extract a gel phase from the resulting mixture, it is heated at various temperatures, the aqueous portion of the mix must be enabled, and the viscosity must be raised to the required level. During this phase, sol-gel changes from a liquid phase to a gel phase. After being prepared, the components or gadgets are slowly and steadily dipped into the sol-gel medium. This procedure may be repeated to create a multilayered or thicker coating of the same substance. Applying a sol-gel coating in several ways, including dipping, spraying, and spinning. The requirement for dipping and withdrawing at a constant rate to maintain a uniform coating thickness across the substrate surface may be a drawback of this method. In multilayered coating structures, failure is always possible during heat treatment [51,57].

2.5.5 Thermal spray coating

A set of processes known as "thermal spray coating" involve melting a specified assortment of planned materials using a plasma, electric, or chemical combustion heat source and then spraying the molten components onto a surface to form a protective layer. These types of wear- and corrosion-resistant coatings are reliable. The components are heated to a molten or semi-solid phase and then sprayed onto the substrate using a high-speed jet. Chemical combustion, or the most frequent type of heat source, is plasma discharge [58]. It significantly improves compared to the thickness provided by PVD, CVD, or electroplating techniques since the thickness obtained with the thickness of thermal spray coatings can range from 20 m to a few millimeters. Different materials, such as refractory metals and metallic alloys, ceramics, polymers, and composites, can easily cover a substrate's reasonably large surface area with a thermal spray coating, as an example illustrated in Figure 2.13. Thermal spray coatings are classified into several groups based on their characteristics

and manufacturing needs. The most prominent categories include flame, wire arc spraying, High-velocity air fuel (HVAF), high-velocity oxyfuel (HVOF), warm/cold, plasma, detonation, and fusion [51,58].

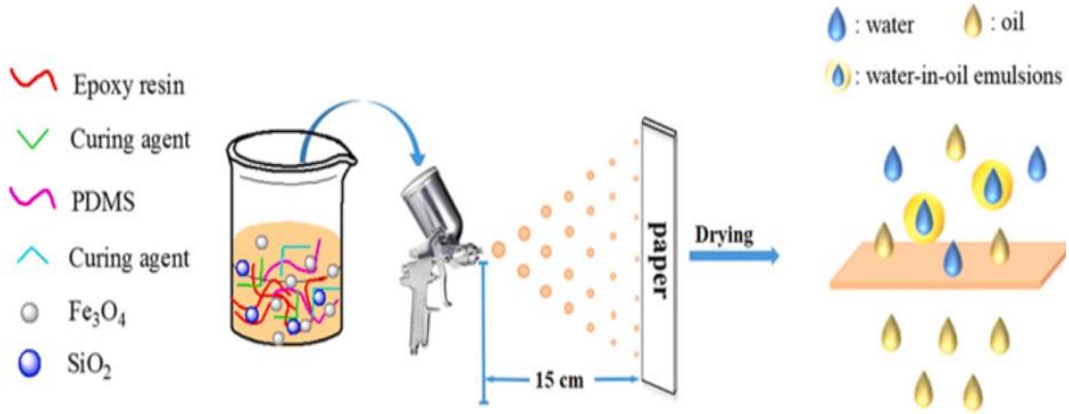

Figure 2.13: Thermal spray coating method is shown schematically [58].

2.6 Coating Materials

The most often used materials for coating nanoparticles in biomedical applications include gold, metal oxide, silica, and carbon-based coatings.

2.6.1 Silica coatings

Coating magnetic nanoparticles with silica is emerging as a potential and significant strategy in fundamental research and technological application. A magnetic dipolar attraction between magnetic nanoparticles could be screened in the first place by the silica that forms on their surfaces. This promotes the scattering of magnetic nanoparticles in a liquid medium and guards against leaching in an acidic setting. Second, due to the silica layer's abundant silanol groups, silica-coated magnetic nanoparticles might be easily activated to add a range of functional groups to the surface [59]. The silica layer offers magnetic nanoparticles in biological systems a chemically inert surface, which is the most significant factor. Silica-coated magnetic nanoparticles can be prepared using one of four primary techniques. The first technique, the sol-gel process, utilizes silicon alkoxides as a source of silica matrix. In this procedure, colloidal magnetic nanoparticles are coated with silica phase in a straightforward alcohol/water combination.

The second approach uses metal compounds as the source of the magnetic phase under specified conditions (such as salts, complexes, or alkoxides) to create magnetic nanoparticles inside the pores of pre-synthesized silica [60]. The third technique, known as aerosol pyrolysis, involved creating silica-coated magnetic nanoparticles in a flame environment by aerosol pyrolyzing a precursor combination of silicon alkoxides and metal compounds. The W/O microemulsion approach, the fourth technique, is the most recent one to be published for producing silica-coated magnetic nanoparticles. In this procedure, an inverse microemulsion was made using non-ionic surfactants to generate or suspend magnetic nanoparticles, and tetraethyl orthosilicate was hydrolyzed and condensed to form silica surrounding the magnetic nanoparticles (TEOS). For making silica-coated magnetic nanoparticles, the sol-gel approach has been used more frequently than the others due to its benefits, such as its low cost and lack of surfactants as well as its comparatively mild reaction conditions [59,61].

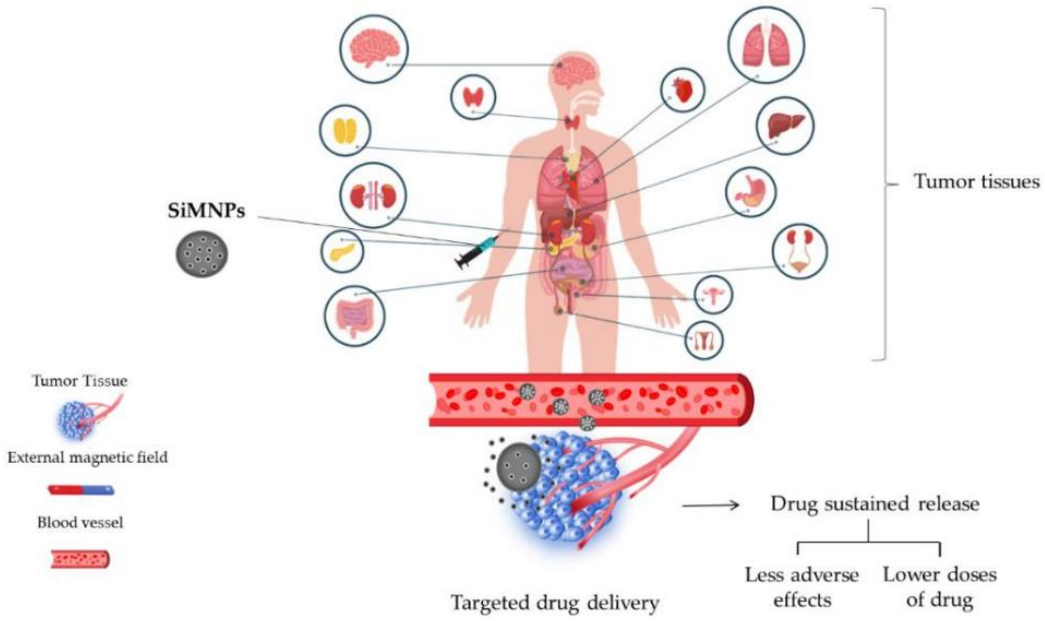

Figure 2.14: Schematic of silica-based magnetic nanoparticle usage on drug delivery [61].

2.6.2 Gold coatings

Magnetic nanoparticles with gold shells are one of the most promising systems. Such core@shell nanoparticles, for instance, MNPs@Au, offer improved stability, allow for fine-tuning of surface biocompatibility, and, more significantly, give the surfaces the proper interfacial chemical, biological, or catalytic reactivities. The required size and composition of MNPs@Au can be challenging to synthesize and characterize.

Numerous examples have been reported on the synthesis of MNPs@Au [62]. For instance, gold was deposited onto iron oxide nanoparticles (9 nm) through hydroxylamine, making gold-coated iron oxide by introducing seeds into an aqueous solution (Fe_2O_3 or partially oxidized Fe_3O_4) nanoparticles (60 nm). Using a reverse micelle technique, gold-coated magnetite and gold-coated iron nanoparticles have also been created. The creation of gold-coated Fe_3O_4 nanoparticles was demonstrated using a similar technique, which entailed attaching gold nanoparticles (2–3 nm) through 3-aminopropyl triethyl silane onto 10 nm-sized Fe_3O_4 nanoparticles [63]. Wet chemical reduction, layer-by-layer electrostatic deposition, x-ray radiation, laser ablation, sonochemical reactions, layer-by-layer electrostatic deposition, and photochemical reduction are a few additional methods that have been reported for the synthesis of gold-coated magnetic core@shell particles. There are several more varieties of gold-coated magnetic nanoparticles, including FePt nanoparticles with an Au shell, cobalt nanoparticles with a gold shell, iron oxide core (Fe_3O_4/-Fe_2O_3) with a thick silica shell, and Au nanoparticles with a shell made of gold [49,62].

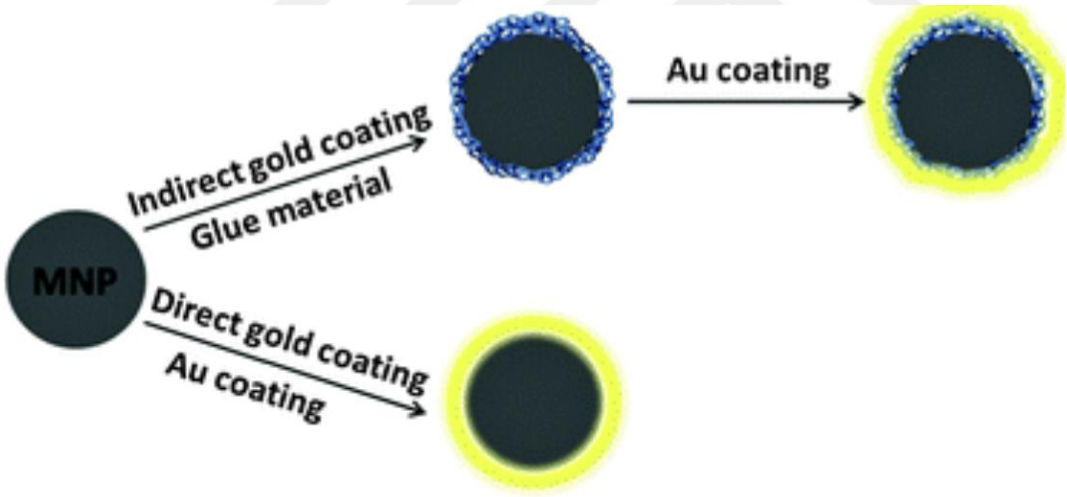

Figure 2.15: The two methods for gold plating are shown schematically [64].

2.6.3 Metal oxide coatings

A metal product's surface may be coated with a thin layer of metal oxide in a process known as metal oxide coating. Electrical insulation, corrosion protection, ornamental enhancement, and use as a foundation for other protective goods, including varnishes, paints, and grease paints, are just a few of the many uses for this coating [65]. Metal oxide coatings are commonly produced using various techniques, including electrochemical processes like anodizing, chemical oxidation in the air or liquid media,

and chemical oxidation using alkalis or acids [65,66]. By acting as a barrier against corrosion, metal oxide coatings are frequently employed to increase the tenacity and lifetime of metallic constructions. For instance, creating a passive chromium oxide layer on the stainless-steel surface confers corrosion resistance. Depending on the exact oxidizing conditions and the alloy composition, these coatings can range in thickness from a few hundred microns to several hundred microns [66]. It is important to remember that metal oxide coatings might have various properties and applications depending on the particular type of metal oxide employed. For instance, anodizing is a specific metal oxide coating frequently applied to aluminum and other metals, in which an electrochemical process creates an oxide surface layer on the metal item, enhancing its durability, corrosion resistance, and aesthetic appeal [67].

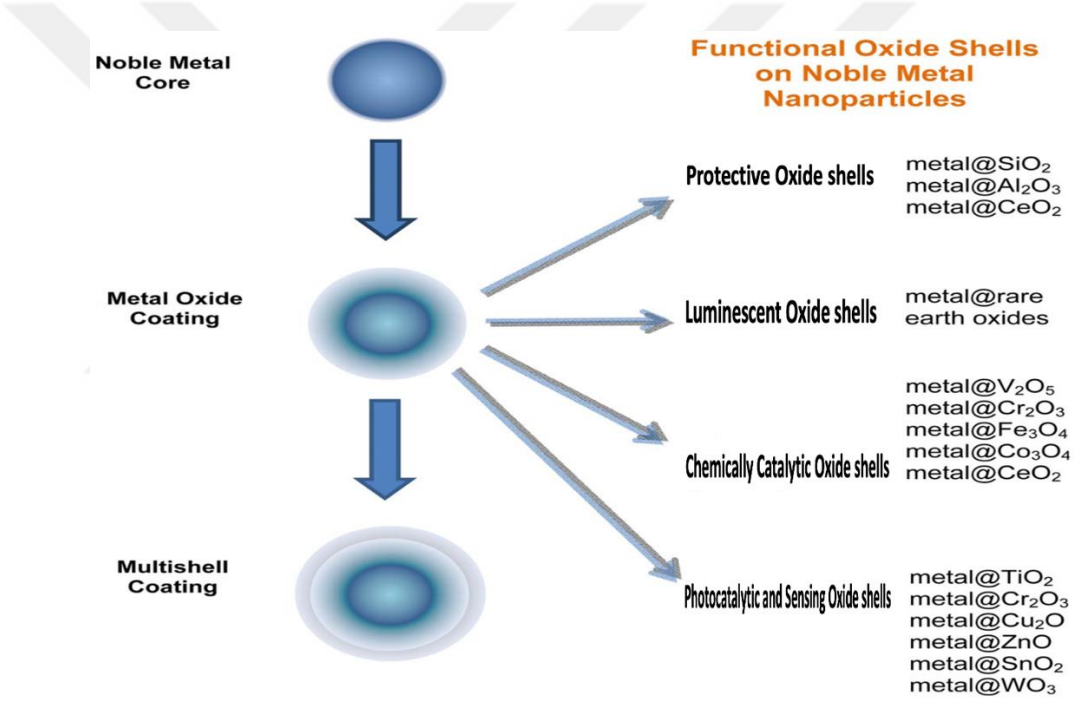

Figure 2.16: Noble metal nanoparticles with a functional metal-oxide coating (metal@oxides) can be used as protective, luminous, catalytic, photocatalytic, and sensing oxide shells [68].

2.6.4 Carbon-based coatings

2.6.4.1 Graphene coatings

An allotrope of carbon called graphene comprises a single layer of atoms organized in a hexagonal lattice. It is derived from graphite, and "graphene" refers to the number of double bonds found in graphite. A valence band covers the whole surface of a graphene sheet because each atom is joined to its three closest neighbors by sigma bonds and a

delocalized π bond. The best explanations for graphene's extraordinary features come from ideas for massless relativistic particles. It is considered a semimetal with distinctive electronic properties [69].

The fascinating features of graphene make it an attractive material for research and various uses. High strength and flexibility are two of its mechanical characteristics, and it has a tensile strength that is about 100 times larger than steel. The thermal and electrical conductivity of graphene is also quite good, with electron mobility as high as 200,000 cm^2/Vs [70]. It also exhibits high specific surface area and exceptional optical transparency. A wide variety of new potential applications have been made possible by discovering graphene. It has applications in the sciences of materials, electronics, energy, and medicine. For instance, graphene's unique qualities make it attractive for use in electronics for applications that speed up information processing, such as neuromorphic computing, which tries to mimic neural cells' actions and memory capabilities. Because of its excellent electrical conductivity and transparency, graphene can be used in solar cells, flexible displays, and touchscreens. Due to its enormous surface area and strong electrical conductivity, it also has promise for use in energy storage systems like supercapacitors. Medical applications for graphene-based materials include tissue engineering, biosensing, and drug delivery systems [71].

Due to their outstanding thermal stability and unique optical properties, graphene-coated nanoparticles have attracted much attention lately. There is a lot of potential for using graphene, one of the most crucial carbon nanomaterials, in biomedical applications. Graphene, which was first discovered in 2004, is a single sheet or several layers of carbon atoms joined together by sp^2 bonds. This material is unique in both its physical and chemical properties. However, the first graphene-based biomedical uses debuted in 2008. Graphene nanoparticles work well as NIR light absorbers. These nanoparticles, as opposed to carbon nanotubes, are a better option for PTT applications due to their vast surface-to-volume ratio, minimal toxicity, and excellent penetrance in malignant tumors. Additionally, functionalized graphene is extremely durable and soluble in bodily fluids [72].

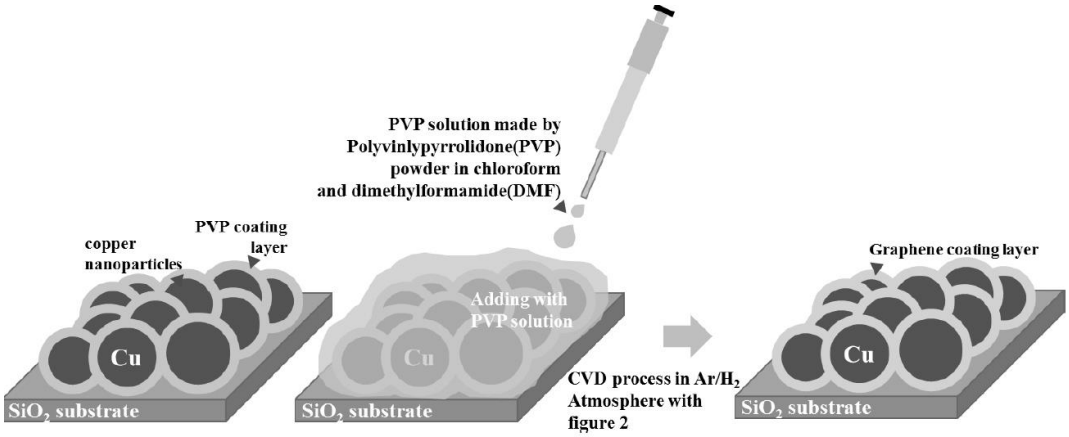

Figure 2.17: Schematic illustrating the method of copper nanoparticle coating with graphene [73].

2.6.4.2 Graphene oxide coatings

The oxidized version of graphene, an allotrope of carbon with a single sheet of atoms organized in a hexagonal lattice, is known as graphene oxide. Two-dimensional graphene has exceptional electrical conductivity and mechanical strength [74]. By subjecting graphene to powerful oxidizing agents and acids, oxygen-containing functional groups are eventually added to the graphene lattice, yielding graphene oxide. Graphene undergoes oxidation to become a substance that is water-sand other solvents, making it simpler to treat. The layered structure of graphite is preserved in graphene oxide, but there is a broader and more erratic gap between the layers. Graphene oxide, a monomolecular sheet that resembles graphene but has different characteristics, can be formed from it [75].

The graphene oxide's functional groups enable chemical alterations and the incorporation of graphene oxide into composites or films. It has been used as a base for optical applications to make robust paper-like materials, sensors, and energy storage devices. Due to their distinctive characteristics and future uses, magnetic nanoparticles (NPs) coated with graphene oxide (GO) have attracted interest in a number of disciplines. Increased stability, better dispersibility, and more surface area for functionalization and interaction with other molecules or materials are benefits of combining magnetic NPs with GO [75,76].

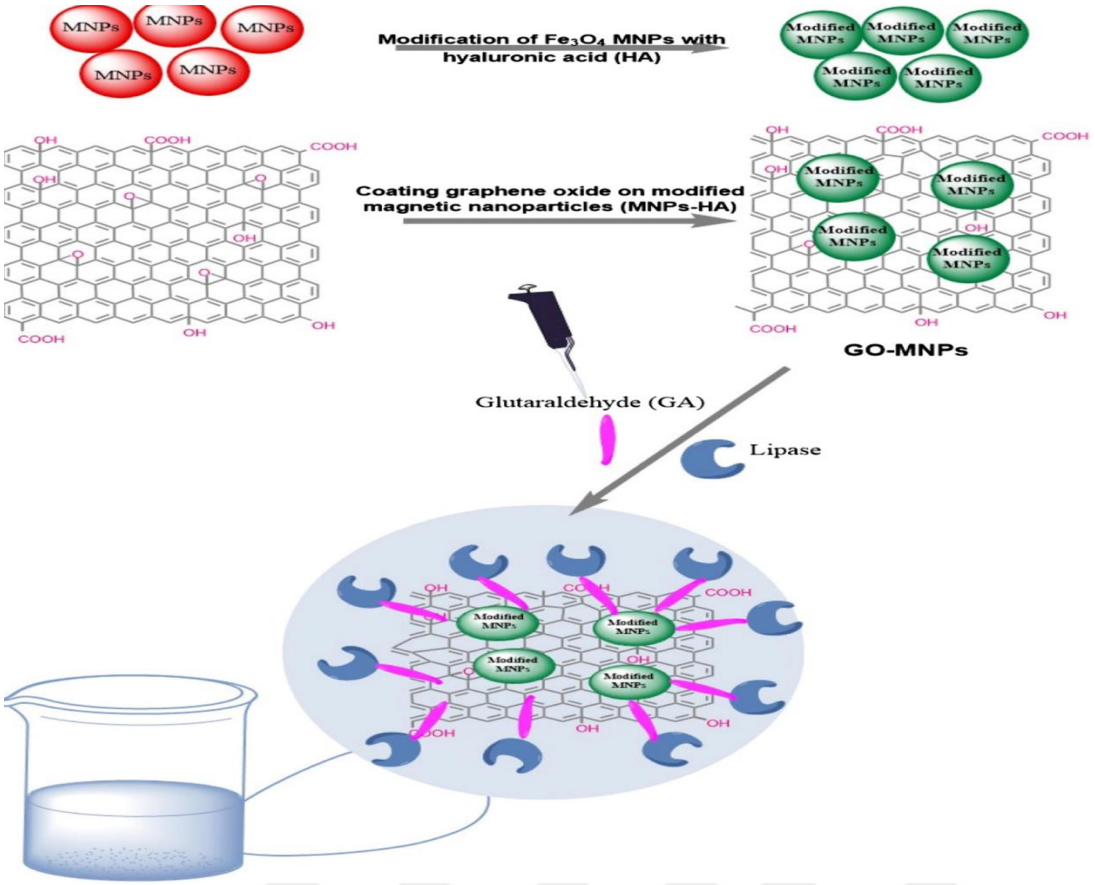

Figure 2.18: The assembly technique for lipase-GO-MNPs-CLEAs is shown in the diagram [77].

2.6.4.3 Reduced graphene oxide coatings

A reduction technique was utilized to eliminate the oxygen-containing functional groups from reduced graphene oxide (rGO), a graphene oxide derivative (GO). Reducing graphene oxide to yield rGO is a crucial step in the study and use of graphene. It seeks to repair the graphene's sp^2 carbon network, producing a substance with enhanced electrical, thermal, and mechanical properties [78]. Chemical reduction, thermal reduction, and electrochemical reduction are a few techniques for reducing graphene oxide. The conjugated pi-electron graphene system is restored by removing or substituting oxygen-containing groups in these reduction techniques [79]. It is possible to manipulate the reduction of graphene oxide to create rGO with various oxygen contents and characteristics. A reduction's intensity and the attributes of rGO can be adjusted to particular applications by changing the reduction conditions, such as temperature, reaction time, and reducing agents. Due to its distinctive features and simplicity of manufacture, reduced graphene oxide has drawn interest in several industries, including electronics, energy storage, sensors, and composites [80].

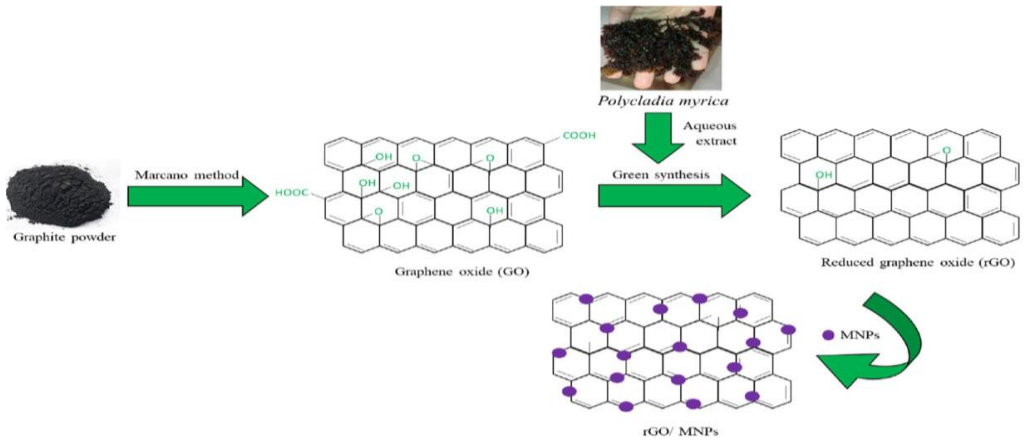

Figure 2.19: Schematic of the graphene oxide-based nanocomposite's production process [81].

2.6.4.4 Amorphous carbon coatings

A carbon compound with no crystalline structure and an amorphous state is called amorphous carbon coating. Free, reactive carbon that lacks a crystalline form is called amorphous carbon. It displays short-range order and is defined by a haphazard arrangement of carbon atoms. "Amorphous carbon" is a word used in mineralogy to refer to impure forms of carbon that are neither graphite nor diamond. Coal, carbon generated from carbides, and other carbon compounds are examples of these amorphous carbon types [82,83].

Numerous characteristics and uses can be found for amorphous carbon. Due to its unique properties, it can be used in coatings, films, electrodes, and energy storage devices. The ratio of sp^2 to sp^3 hybridized bonds, formation processes, and environmental factors impact the properties of amorphous carbon, including hardness, friction, and thermal stability [84,85].

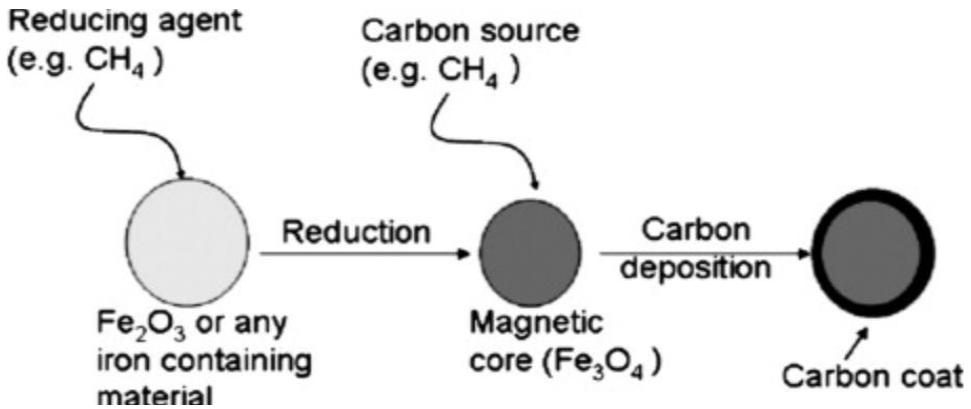

Figure 2.20: Thin layer coated MNPs with amorphous carbon [86].

Table 2.1: Representative microstructures of some encapsulated NPs [87–91].

Sample	Production Parameters and Microstructure
(FeCo@Silica) Hydrothermal Method	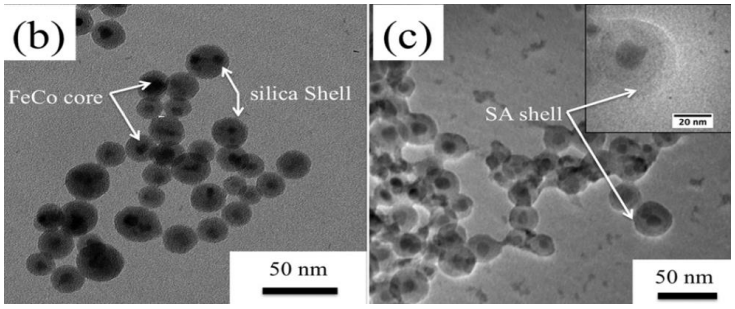
(Fe_3O_4@Au) Hydrothermal Method	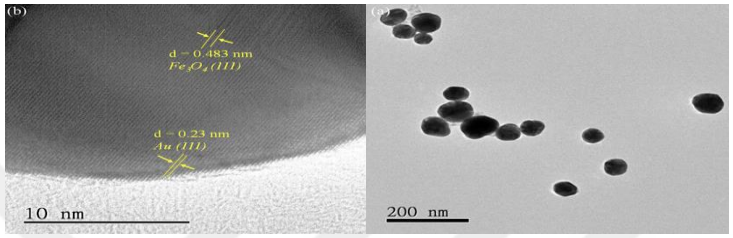
(Fe_3O_4@rGo) Hydrothermal Method	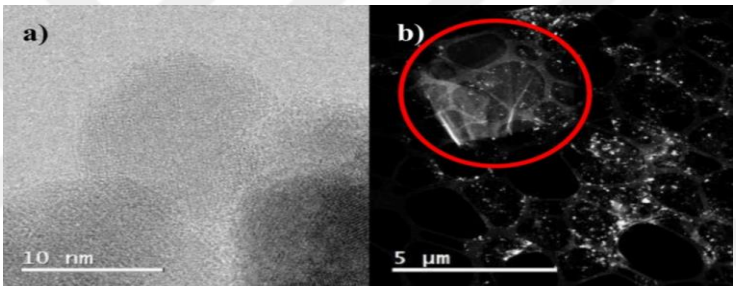
(Fe_3O_4@nGO) Hydrothermal Method	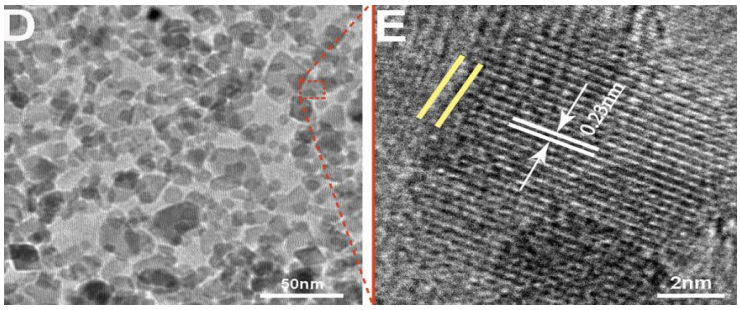
(Fe@Graphene) CVD Technique	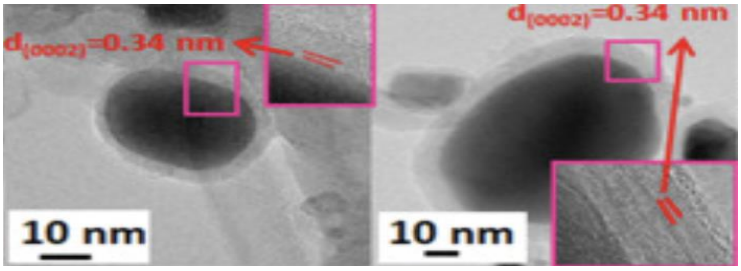

2.7 Methods for Functionalization of Magnetic Nanoparticles

Some methods used for functionalization are listed in the following titles.

2.7.1 Covalent functionalization

In this technique, the functional group or molecule and the surface of the magnetic nanoparticles establish covalent connections. Usually, coupling agents like silanes, amines, carboxylic acids, or thiol groups are used to accomplish this. Due to their atomic thinness, high surface-to-volume ratio, and homogeneous surface chemical potential, 2D materials require covalent functionalization of the surface more than traditional bulk materials [92,93]. Covalent functionalization enables us to enhance or precisely adjust the electrical, mechanical, and chemical properties of 2D materials because they are made up of two surfaces without a dangling connection [94].

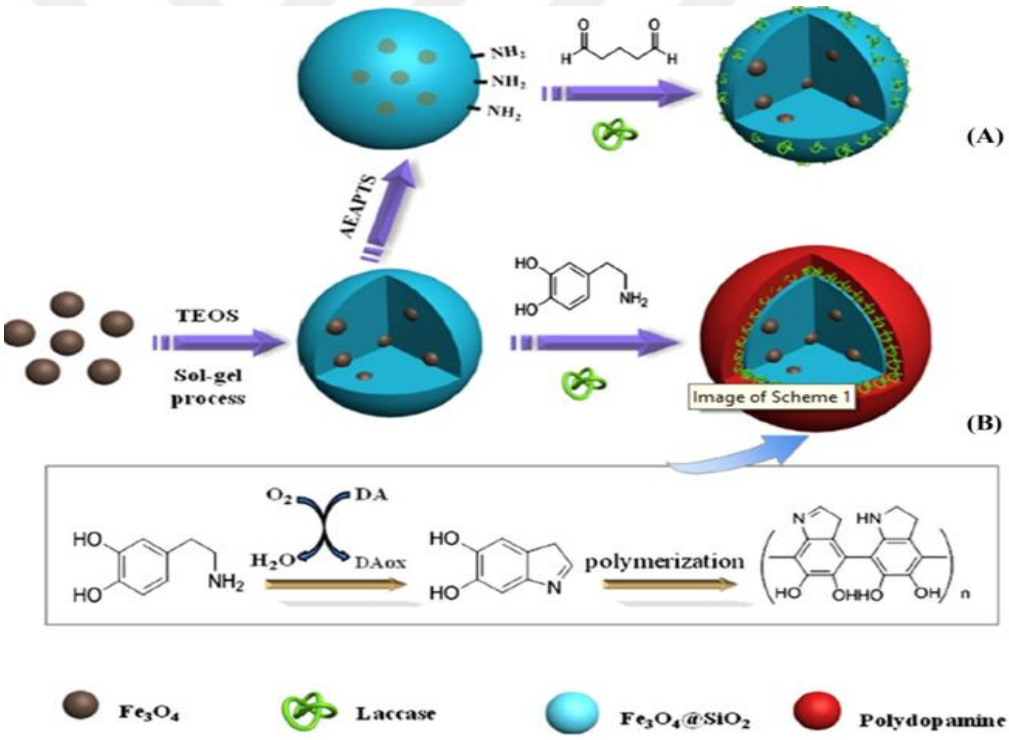

Figure 2.21: $Fe_3O_4@SiO_2$ NPs laccase stabilization illustration $Fe_3O_4@SiO_2$-GALac and $Fe_3O_4@SiO_2$-PDA-Lac are two examples of this compound—immobilized laccase's strong catalytic activity on core-shell magnetic nanoparticles produced by dopamine self-polymerization [95].

2.7.2 Non-covalent functionalization

Via weak physical interactions such as van der Waals forces, electrostatic contacts, or hydrophobic interactions, functional molecules are adsorbable to the surface of the

magnetic nanoparticles using this technique. Covalent and non-covalent surface modification of CNTs using microchemical and polymers is a common practice to increase their solubility and processability. Depending on the nature of the grafted polymer and even at low levels of functionalization, polymer grafting has the advantage of improving the affinity of the CNTs-g-polymer in polymer matrices while also making CNTs soluble in several solvents [96]. Surface-initiated polymerization, commonly known as "grafting from" or "grafting to," are two methods for covalent modification. On the other hand, weak interactions between the polymer and the carbon nanotubes' sp^2 hybridized network might result in the non-covalent grafting of polymers. As covalent functionalization breaks the typical graphene-type structure, it frequently changes the intrinsic attributes of CNTs, including conductivity and mechanical strength. The tubes can be effectively dispersed in aqueous and non-aqueous liquids by non-covalent functionalizing CNTs with polymers, preserving their intrinsic properties without compromising their distinctive structure [97,98].

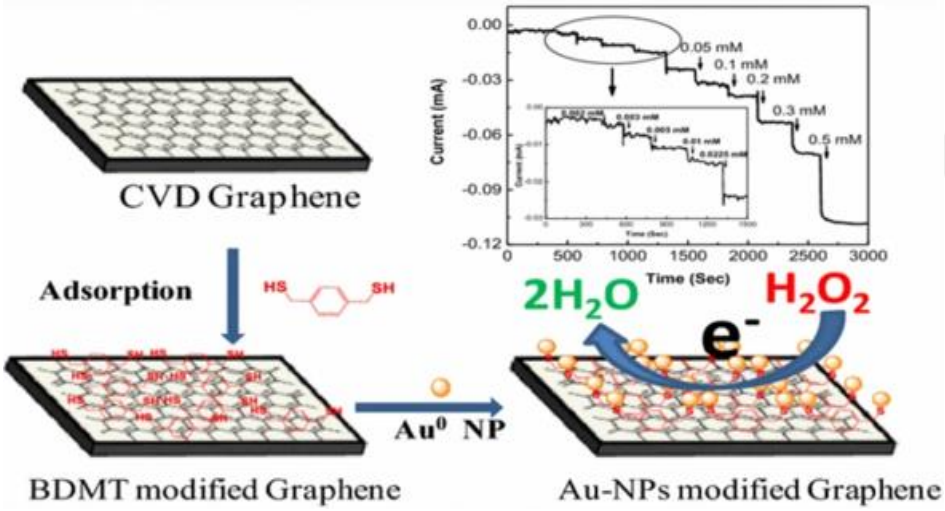

Figure 2.22: Diagrammatic description of the functionalization procedures for non-covalently bonded graphene produced by the CVD approach (self-assemble monolayer creation with AuNPs) [99].

2.7.3 Layer-by-layer (LbL) assembly

This process involves coating the magnetic nanoparticles' surface with successive layers of alternatingly charged polymers or monomers. This causes the creation of a multilayered shell that can give the nanoparticles certain features. Several polyelectrolytes and other particles were self-assembled using the layer-by-layer (LBL) method to develop hybrid multifunctional carriers for dyes, sensors, and

enzymes, medicines, numerous components, and cells [100]. A surface platform that can be used to bind specific molecules, like antibodies against folic acid, or a variety of surface functional groups, like hydroxyl, carboxyl, and thiol groups, is also made available by nanocoated substrates. Moreover, adding responsive materials to LbL constructions could result in the introduction of stimuli-sensitive characteristics. The robustness of LbL self-assembly is discussed in the following sections to produce adaptable carrier systems that combine oppositely charged materials onto a substrate to produce a PEM-coated system. Compared to other surface modification techniques, the production of nanocoatings utilizing the LbL self-assembly process stands out for its simplicity [101,102].

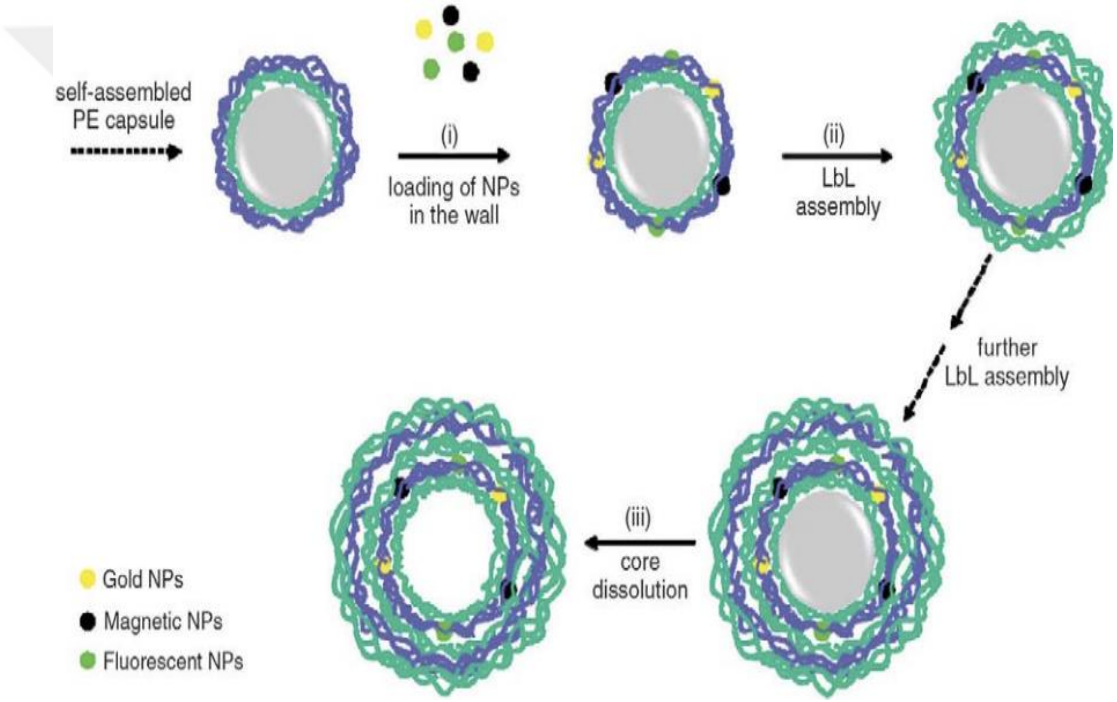

Figure 2.23: Diagram demonstrating the integration of several capabilities within the polyelectrolyte (PE) capsules' walls. (i) Inserting charged nanoparticles (NPs) such as metal (yellow), magnetic (black), and fluorescent (green) NPs into the PE wall. Because the NPs in the example are negatively charged, they adhere to the positively charged polymer layers. (ii) Capsule stabilization following LbL assembly [103].

2.7.4 Click chemistry

This technique entails attaching functional groups or molecules to the surface of the magnetic nanoparticles by applying highly specialized chemical processes, such as azide-alkyne cycloaddition or thiol-ene coupling. A strict set of criteria were used to identify the reactions, simple reaction conditions, excellent reaction efficiency, regio- and stereoselectivity, and reaction appropriateness in safe conditions. These reactions

move along quickly and are frequently very selective [104]. The latter trait is crucial for applications, including in vivo, where a wide range of functioning is present. The classic Huisgen cycloaddition with a copper catalyst saw a significant boost in reaction rate in 2002, according to reports from the Sharpless and Meldal laboratories. The copper-catalyzed alkyne-azide cycloaddition (CuAAC), a novel reaction, has emerged as the most prominent instance of click chemistry. Since 2004, this process has been used to create novel materials, ranging from complicated dendrimers to self-assembled materials to block copolymers [105,106].

2.7.5 DNA functionalization

Functionalizing the magnetic nanoparticles' surface with complementary DNA strands enables selective binding to additional DNA strands or molecules [107]. In 1996, Mirkin et al. published the first report on DNA-functionalized NPs (DNA-NPs), describing a synthetic method that made it possible to create nucleic acidNP nanostructures heavily functionalized materials and strongly orientated gold nanoparticles (AuNPs) have DNA bonded to their core surface covalently. In contrast to free DNA molecules, the AuNP surface was grafted with DNA molecules with a thiol end. Giving rise to distinct features like cooperative binding, fast melting transitions, and resistance to nuclease destruction. Then, inorganic and polymeric substances with unique optical, catalytic, and physicochemical capabilities, containing silver, palladium, iron oxide, quantum dots, nanoshells, proteins, and polymers, were used to fill the core's position. Methods to extract the core material and create a hollow structure encased in an ss-DNA shell was devised to increase biocompatibility [108]. Recently, sophisticated methods for attaching DNA to nanoparticles with metal-organic frameworks have been developed, an incredibly straightforward method for attaching DNA to nanoparticles for up-conversion doped with lanthanides. Spherical metal-DNA nanostructures were produced for medication and gene delivery via directly interacting metal ions with DNA like Fe^{2+}. Parallel to this, In DNA-lipid/polymer amphiphiles, self-assembled nanostructures of diverse forms have been studied. Using DNA hybridization-based methods, it has also been possible to combine DNA-NSs and DNA-NPs structures into a single nanoscale structure with superior/tunable optical properties and distinctive capabilities [107,109].

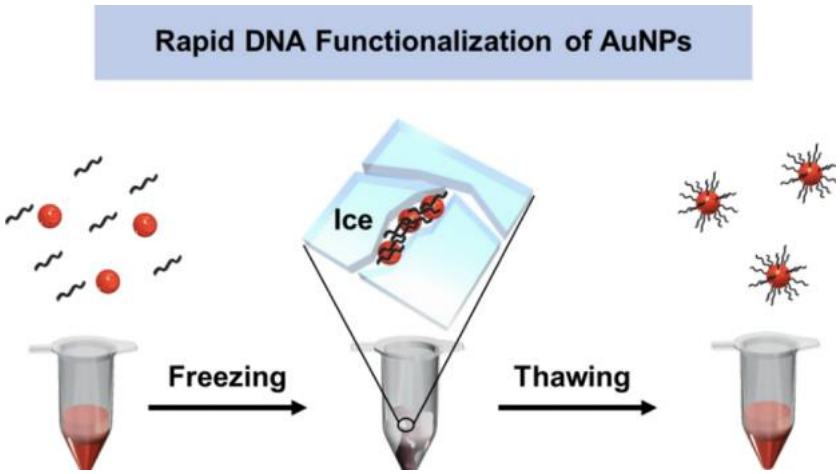

Figure 2.24: Illustration of a scheme for the freezing-based synthesis of DNA-AuNPs [108].

3. EXPERIMENTAL PROCEDURE

The experimental procedure of this study consisted of four main steps. First, solvothermal synthesis of Fe_3O_4 and Fe_3O_4@rGO nanoparticles was performed, and after the calcination processes, synthesized Fe_3O_4@rGO nanoparticles were coated with graphene by chemical vapor deposition. Finally, optimization studies on polymer coating and injecting into the cell lines were investigated to measure their cytotoxicity and biocompatibility. Their detailed microstructural and magnetic characterization studies were conducted for each route.

3.1 Solvothermal synthesis of Fe_3O_4 and Fe_3O_4@rGO nanoparticles

3.1.1 Raw materials used for the solvothermal synthesis of Fe_3O_4 and Fe_3O_4@rGO

($FeC_{10}H_{10}$) from ABCR) and **(**GO, from AEROFEN) powders were used for this study. Bruker D8 Advanced X-ray diffractometer (XRD) located at I.T.U. Particulate Materials Laboratory (PML) was used for phase identifications of these raw materials. The XRD patterns in Figure 3.1a show that only $FeC_{10}H_{10}$ phases were confirmed. Also, the Raman spectrometry analysis of GO is presented in Figure 3.1b.

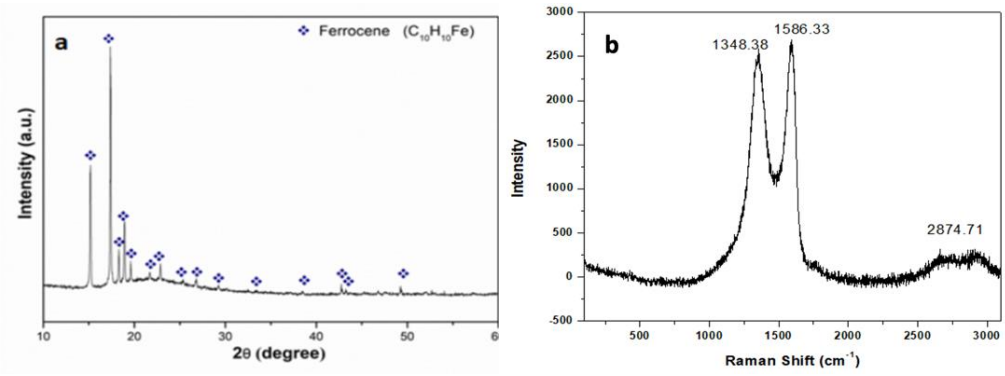

Figure 3.1: a) The XRD patterns for raw material $FeC_{10}H_{10}$, b) The Raman analysis of raw material.

3.1.2 Solvothermal synthesis of Fe_3O_4 nanoparticles

($FeC_{10}H_{10}$) powder was the starting material for synthesizing magnetic Fe_3O_4 powder. The KERN PLJ precision balance device was used for weighing powder, shown in Figure 3.2a.

In the beginning, we mixed 0.7 g ($FeC_{10}H_{10}$) in the 15 mL acetone and 15 mL distilled water and put it inside the ultrasonic shown in Figure 3.2b for 15 min, adding H_2O_2 and stirring them for 30 min.

After 30 min of mixing, we put our solution into the Teflon cup inside the stainless-steel chamber and put it in the autoclave for 26 h at 196 °C, as shown in Figure 3.2c. Repeated centrifugation was used to separate the residue from the leaching solution. Repeated centrifugation at 4000 rpm for 10 min with decantation and rinsing stages was carried out using a Hettich Rotofix 32A, as seen in Figure 3.2d.

The remnant had dried in GALLENKAMP Hotbox Oven, shown in Figure 3.2e, at 60 °C for 18 h in air. Leached powders were the new name given to the leftover material.

The residues, which are obtained were calcinated under the argon (Ar, Linde, 99.99% purity) gases by a Protherm tube furnace system that includes a vacuum pump, a mass flow controlling system, and a split furnace with a quartz reactor was picked. These boats were placed in the quartz reactor, which has an exterior diameter of 2.54 cm and a length of 80 cm, located at the horizontal tube furnace (Protherm ASP series, dual heating zone). The heater was first ramped to the reaction temperature over 60 min and maintained there for a predetermined time. The system received Argon gas at a constant flow rate of 100 mL/min for 1 h at 500 °C. The plane was then cooled to 300 °C over a 60 min cooling period using the same gas conditions as illustrated in **Figure 3.3**.

3.1.3 Solvothermal synthesis of Fe_3O_4@rGO nanoparticles

($FeC_{10}H_{10}$) and GO powders were the starting materials for producing magnetic Fe_3O_4 powder. Initial reactants 0.7 g ($FeC_{10}H_{10}$) and 0.1g GO were used.

For weighing powders, the KERN PLJ precision balance device was used, which is shown in Figure 3.2a. Then we mixed 0.1g of the GO in the 15 mL distilled water and stirred it for 10 min. Then we mix 0.7 g ($FeC_{10}H_{10}$) in the 15 mL acetone and put it

inside the ultrasonic shown in Figure 3.2b for 15 min. In the end, we mix two solutions by adding H_2O_2 and stirring them for 30 min.

Our solution was mixed for 30 min, then placed in a Teflon cup inside a stainless-steel chamber before being autoclaved for 26 h at 196°C, as shown in Figure 3.2c,e. Repeated centrifugation was used to separate the residue from the leaching solution. Repeated centrifugation at 4000 rpm for 10 min with decantation and rinsing stages was carried out using a Hettich Rotofix 32A, as seen in Figure 3.2d.

The residues were calcined using argon (Ar, Linde, 99.99% purity) gases using a Protherm tube furnace system comprising a vacuum pump, a mass flow control system, and an independent oven containing a quartz reactor. Various times were used to collect the leftovers. These boats were placed in the horizontal tube furnace's quartz reactor (Protherm ASP series, dual heating zone), with an outer diameter of 2.54 cm and a length of 80 cm. The furnace was ramped up to the reaction temperature over 60 min and maintained there. The system was subjected to argon gas for 1 h at a temperature of 500 °C, flowing continuously at a rate of 100 mL/min. The plane was reduced to 300 °C for 60 min using the same gas circumstances shown in **Figure 3.3**.

Figure 3.2: a) The KERN PLJ precision balance device, b) ultrasonic, c) Stainless steel Teflon cup, d) Hettich Rotofix 32A, e) GALLENKAMP Hotbox Oven.

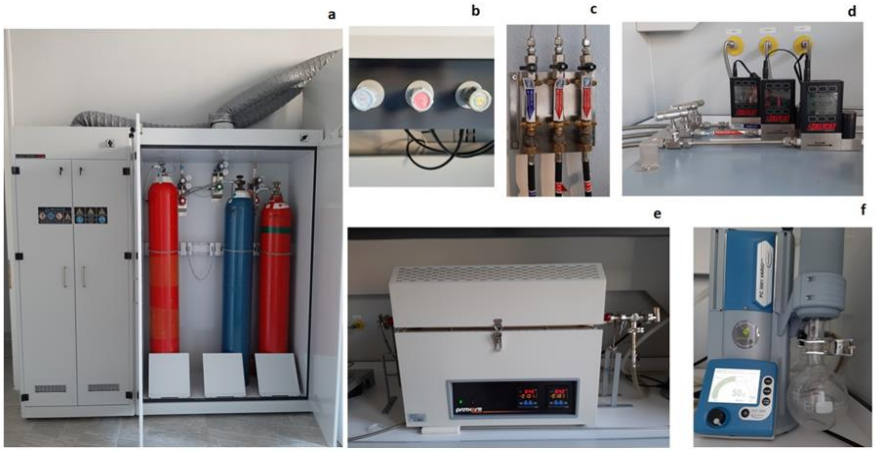

Figure 3.3: a) H_2, CH_4 and Ar gases, b, c) gas flow valves, d) gas flow controllers, e) tube furnace (CVD reactor), f) Vacuum pump.

3.2 Coating Fe_3O_4@rGO nanoparticles

Fe_3O_4@rGO@graphene core/shell nanoparticles were synthesized by methane (CH_4, 99.99% purity, Linde), and hydrogen (H_2, 99.99% purity, Linde) were the gases utilized in the CVD process. Over 60 min, the reaction temperature was first reached with the furnace turned up and kept there for a predetermined period. H_2 gas entered the system at a steady 100 mL/min flow rate. 100 or 200 mL/min of Once the furnace reached 500 °C, CH_4 gas was injected. Alicat Scientific flowmeters calibrated for the H_2 and CH_4 gases up to 1 L/min were used to regulate the gas flow rates. The system was also managed using a VacuuBrand vacuum pump that could purge the outlet pressure to 10 bar. The pressure was held constant throughout the CVD process. The system was cooled using the same gas conditions for over 60 min to 300 °C. The process parameters for the CVD experiment are (950°C reaction temperature, 90 min holding time, 50 mbar outlet pressure, 100 mL/min H_2 flow rate, and 500 mL/min CH_4 flow rate).

The CH_4 dissociation and carbon deposition on the Fe_3O_4@rGO positioned to create two heating zones, using two quartz boats, are shown schematically in Figure 3.4, for the quartz reactor utilized in the CVD system. To speed up the decomposition of the precursor and enable the production of C-C, H_2 gas was continually supplied to the reactor while CH_4 gas flowed through it. A vacuum pump system transferred residual Hx, CxHy, and possible effluent gases to a laboratory-scale gas scrubber. It has been suggested that using carbon sources in the gas form helps create enclosed particles. H_2 was also added to CH_4 gas to control unwanted gas products containing carbon.

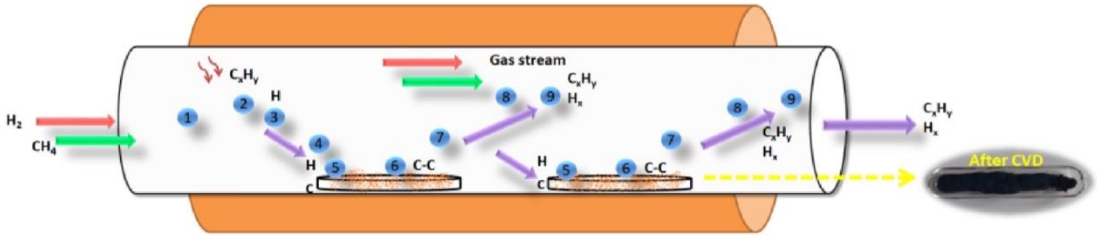

Figure 3.4: The quartz reactor used in the CVD system is shown schematically in this image [91].

3.2.1 Purification

Magnetic Fe_3O_4@rGO particles that were encapsulated in graphene underwent two phases of purification. First, after the CVD procedure, the non-encapsulated likely Fe_3O_4@rGO content of the produced powders was removed using a hydrofluoric acid (HF) solution. Fe_3O_4@rGO@graphene nanoparticles were considered insoluble in an HF solution at that time. Due to this, a 2 M HF solution (48% concentrated, Merck) was used, with a solids-to-liquid concentration of 8 mg/mL to the post-CVD powders. After being leached with HF solution for 1 h and swirled with an ultrasonic device (Bandelin Sonorex), the acidic solution material was left at room temperature for the remainder of the day. To get powders free of contaminants, the subsequent stages of centrifugation (Hettich Rotofix 32A centrifuge, at 3500 rpm, 15 min), decantation, and filtration were carried out three times.

Subsequently, non-encapsulated Fe_3O_4 nanoparticles were removed using a 37% concentrated hydrochloric acid (HCl) solution from Merck. The HCl leaching procedure was crucial for determining the encapsulated nanoparticles' chemical stability. The 2 M HCl solution was used for the HCl leaching process, and it was stirred using ultrasonic technology for 1 h before being left at room temperature overnight. The supernatant liquid was decanted, the remaining solids were centrifuged to precipitate the solids, and the solids were then cleaned three times with distilled water. Lastly, Fe_3O_4@rGO@graphene nanoparticles were produced by drying the resulting powders in a furnace overnight at 100 °C in the air.

3.3 Functionalized Fe_3O_4@rGO@graphene nanoparticles

3.3.1 Raw materials used for synthesizing PMA-POEGMA Polymer

POEGMA was passed through a neutral alumina column to remove the inhibitor before use. α-Bromoisobutyryl bromide (BIBB), triethylamine (TEA), 1-pyrenemethylamine

hydrochloride (PMA), *N,N,N′,N′,N″*-pentamethyldiethylenetriamine (PMDETA), poly(ethylene glycol) methyl ether methacrylate (average Mn 300) (POEGMA) and copper(I) bromide (Cu(I)Br) were purchased from Sigma-Aldrich.

3.3.2 Synthesis of PMA-POEGMA Polymer

Graphene cannot dissolve in water, so to make our particles disperse in water homogeneously and functionalize them, we started to synthesize PMA-POEGMA. First, Pyrene Initiator (PyrI) was synthesized. 1-Pyrenemethylamine hydrochloride (PMA) (116 mg, 4.33×10^{-4} mol) was put into a flask with a round bottom and three necks, which was repeatedly degassed and filled back up with N_2 gas three times. Using a syringe, TEA was (362 µL, 2.6×10^{-3} mol) at 0 ºC added to the flask first, then tetrahydrofuran (THF, 10 mL), BIBB (267.8 µL, 2.17×10^{-3} mol) was next slowly injected into the flask using a syringe, and the temperature was raised to room temperature gradually. 24 h were allowed for the reaction under stirring Figure 3.5. The solution was filtered, and the crude product was purified by recrystallizing from CH_2Cl_2/ethanol. The product was filtered, washed with cold ethanol, and dried under vacuum (Yield: 86.5%) [110].

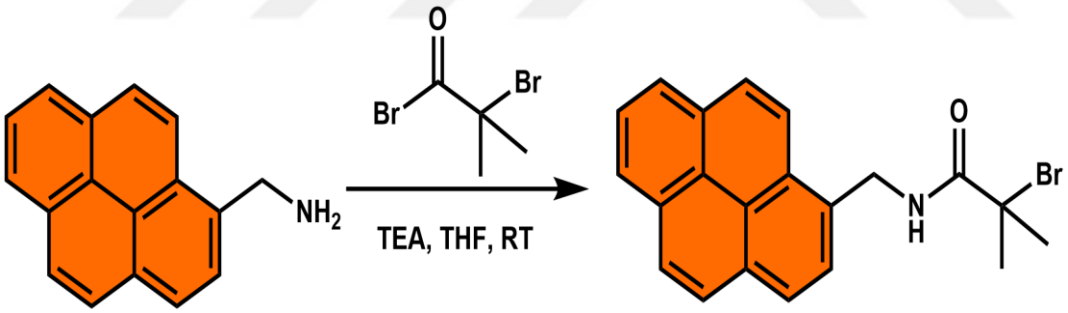

Figure 3.5: Synthesis of Pyrene Initiator (PyrI).

The next step is the synthesis of PMA-POEGMA Polymer by Atom Transfer Radical Polymerization (ATRP). Monomer (POEGMA, 2.00 g, 6.67×10^{-4} mol, 30 eq.), ligand (PMDETA, 77 mg, 2.22×10^{-4} mol, 2 eq.), catalyst (CuBr, 38 mg, 2.67×10^{-4} mol, 1.2 eq.), the initiator (PyrI, 84.5 mg 2.22×10^{-4} mol, 1 eq.) and dimethylsulfoxide (DMSO) were added, consecutively, into a Schlenk tube with a magnetic stirring bar. The tube was vacuum-sealed for three freeze-pump-thaw cycles to degas it, then placed in a thermostated oil bath (90 ºC) for 1 h. Polymerization after 24 h, as shown in Figure 3.6, the solution was dialyzed against H_2O for 48 h in a dialysis membrane (MWCO 1

kDa) to remove excess Cu ions and further purification. The polymer was dried via lyophilization.

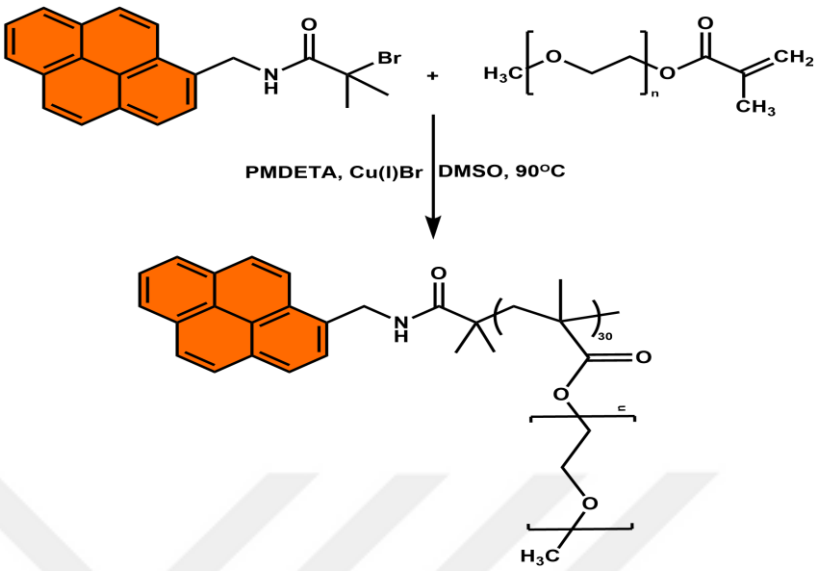

Figure 3.6: Synthesis of PMA-POEGMA Polymer by ATRP

After synthesizing PMA-POEGMA for coating our nanoparticles, we dissolve 5mg graphene-encapsulated iron oxide with 5 mL distilled water, and at the same time, we dissolve 5 mg PMA-POEGMA with 5 mL dilute water. After dissolving, mix them in ultrasonic for 10 min and then put them in the Vortex (Dragon Lab MX-F Light Microscope Olympus CH30) for 24 h.

3.4 Cell Culture and Preparation for Cytotoxicity Test in the breast cell lines

3.4.1 Raw materials used for measuring cytotoxicity in the breast cell lines

Gibco Thermo Fisher (DMEM, high glucose, pyruvate, 500 mL, 41966029), Gibco (FBS, qualified, heat-inactivated, Brazil 500 mL, 10500064), and Gibco Thermo FisherPenicillin-Streptomycin (10,000 U/mL), 15140122), and (GENAXXON DMSO, Cell culture grade 100m, M6323.0100), and (BIOMATIK, Thiazolyl Blue Tetrazolium Bromide [MTT]. Ultra Pure 250mg, A3338-250MG) were used in this experiment.

3.4.2 Cytotoxicity test of MNPs in the breast cell lines

DMEM high glucose medium supplemented with 10% FBS was used to cultivate MCF-7 cells in a humid incubator at 37 °C and 5% CO_2, as shown in Figure 3.7a.

Upon reaching 80-90% confluency, measured by the cell counting device (EVE) as shown in Figure 3.7b, cells were harvested by trypsinization, and 5x103 cells were seeded to 96-well plates in 100 µl media, as shown in Figure 3.7c. The next day, nanoparticles were resuspended in cell culture grade DMSO, and the stock solution was prepared as 25 mg/mL, as shown in Figure 3.7d. Cells were treated with a specific concentration of nanoparticles ranging from 5x10-5 µg/mL to 5x102 µg/mL. DMSO was used as the negative control, and its concentration was kept at 2% in each condition, which was determined as the maximum limit. Each condition was prepared as three replicates. MTT reagent was added upon 24 h and 48 h incubation Figure 3.7e, and plates were incubated for 3 h in the incubator for formazan crystals to be formed. Upon incubation, media was removed, and formazan crystals were dissolved in 100 µl DMSO. Absorbance measurement was performed at 570 nm by microplate spectrophotometer (BIO-RAD Benchmark Plus), as is shown in Figure 3.7f.

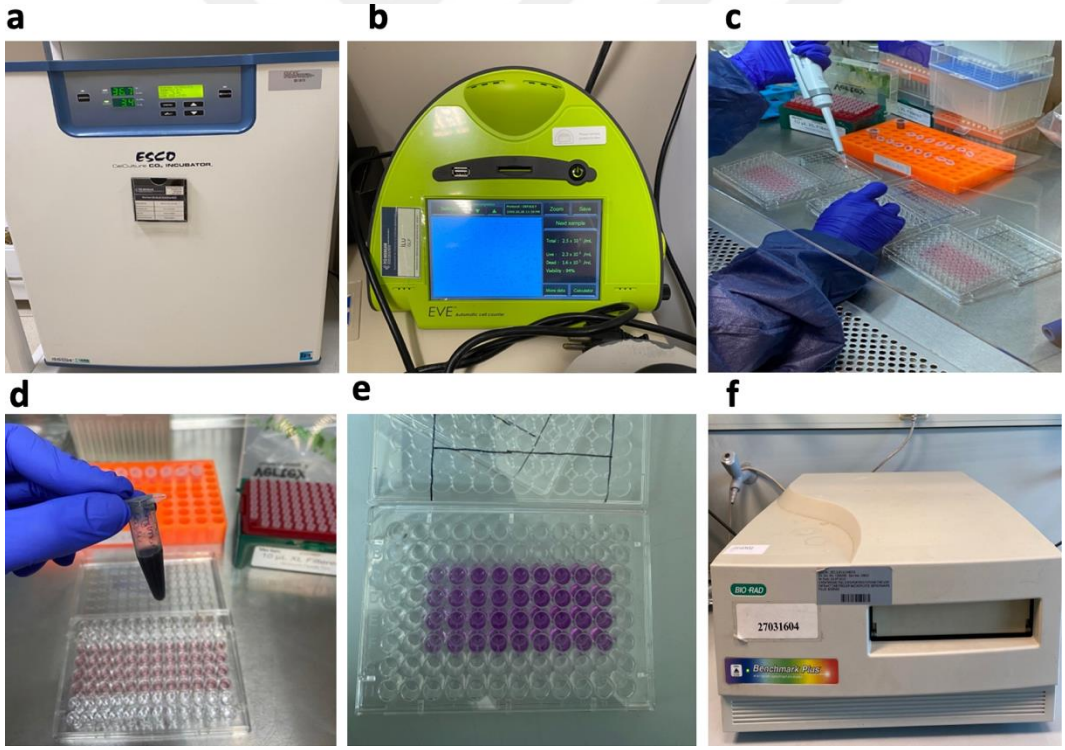

Figure 3.7: a) humidified incubator, b) cell counting device (EVE), c) cells were seeded to 96-well plates, d) prepared nanoparticles, e) MTT reagent, f) microplate spectrophotometer.

3.5 Characterization Investigations

THE Bruker D8, Advanced Series XRD equipment, shown in Figure 3.8 was used for phase analysis. Powder and bulk samples were scanned between 10-90° at a 2 °/min scan rate. The database of ICDD PDF -22016 was used to phase analysis.

The average particle sizes and distributions of the Fe_3O_4, Fe_3O_4@rGO, Fe_3O_4@rGO@graphene, and Fe_3O_4@rGO@graphene@PMA-POEGMA nanoparticles were measured by using a Malvern™ Mastersizer 2000 particle size analyzer shown in Figure 3.9a and determined as 5.069 µm, 7.271 µm, 385.994 µm, and 107.619 µm, respectively. Also, Bandelin Sonopuls ultrasonic stirring, shown in Figure 3.9b was used against particle agglomeration. Solution with particulates waited 10 min after ultrasonic stirring to provide Brownian behavior for particles.

Figure 3.8: Bruker D8 Advanced Series XRD equipment.

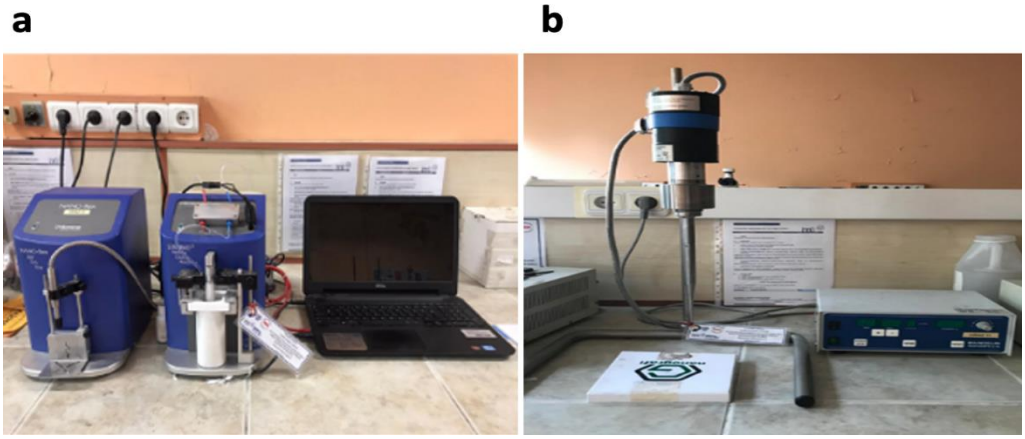

Figure 3.9: a) Malvern Mastersizer 2000, and b) Bandelin Sonopuls.

Also, purified Fe_3O_4@rGO nanoparticles were characterized by Raman spectroscopy (Renishaw Invia-Raman Microscope), as shown in Figure 3.10, utilizing a 532 nm room-temperature excitation laser source. The laser power was controlled between 0.5 and 1 mW to prevent local heating and phase transition by oxidation.

Figure 3.10: Renishaw Invia Raman Microscope.

Thermoscientific Quattro S scanning electron microscope (SEM) equipped with energy dispersive spectroscopy (EDS), shown in Figure 3.11, was used to analyze the microstructure of the samples. SEM analyses were performed under a high-vacuum atmosphere and before SEM analyses. Colorful and point EDS analyses were performed using the EDS equipment to determine elemental distribution. The powders were dispersed in ethanol to prevent powder agglomeration before being individually put onto the aluminum foil. After drying, we can analyze each component.

Figure 3.11: Electron scanning microscope (SEM)

The magnetic behavior of the Fe_3O_4, Fe_3O_4@rGO, Fe_3O_4@rGO@graphene, and Fe_3O_4@rGO@graphene@PMA-POEGMA nanoparticles was examined using a Lake Shore 7407 vibrating sample magnetometer (VSM, Kel-F non-magnetic sample kit), as shown in Figure 3.12. Measurements were made at the room's temperature with an ideal induced field of 10000 Oe.

Figure 3.12: Vibrating sample magnetometer, Lake Shore 7407.

Agilent VNMRS 500 MHz nuclear magnetic resonance spectrometry, shown in Figure 3.13, was utilized to establish the atomic composition of the molecular structure of a PMA-POEGMA and PyrI.

Figure 3.13: Agilent VNMRS 500 MHz nuclear magnetic resonance spectrometry.

Fourier transform infrared (FT-IR) spectra were taken on PerkinElmer Spectrum One spectrometer with ATR accessory shown in Figure 3.14 to identify materials.

Figure 3.14: Illustration of Fourier transform infrared (FT-IR).

4. RESULTS AND DISCUSSION

This part of this dissertation comprises the results of magnetic nanoparticle synthesis using the solvothermal method, the calcination process of these magnetic nanoparticles and graphene-encapsulated magnetic nanoparticles using the CVD method, and the functionalization of graphene-encapsulated magnetic nanoparticles using a specific polymer. To demonstrate the potential of several nanoparticles for biomedical applications, cytotoxicity studies were carried out on these particles.

4.1 Characterization of the solvothermal synthesized powders

4.1.1 Characterization and cytotoxicity tests of Fe_3O_4 nanoparticles

The XRD pattern of the solvothermal synthesized powders is shown in Figure 4.1a. The existence of Fe_3O_4 was seen at 36°, but the initial phase intensity is low. However, the intensity and crystallinity of phases improve after the calcination process, which shows the XRD pattern in Figure 4.1b. Similarly, the study by Vasiljevic et al. demonstrates how a rise in calcination temperature causes an increase in crystallite size. During longer calcination at lower temperatures, smaller crystallites were generated, measuring 24 nm, while shorter calcination, lasting 4 h at 550 °C, produced slightly better crystallites, measuring 30 nm [111]. Also, the carbon peak is visible before calcination at 27°; however, due to the detection limits of the XRD instrument (1-2 wt%), we cannot discern the carbon peak after calcination.

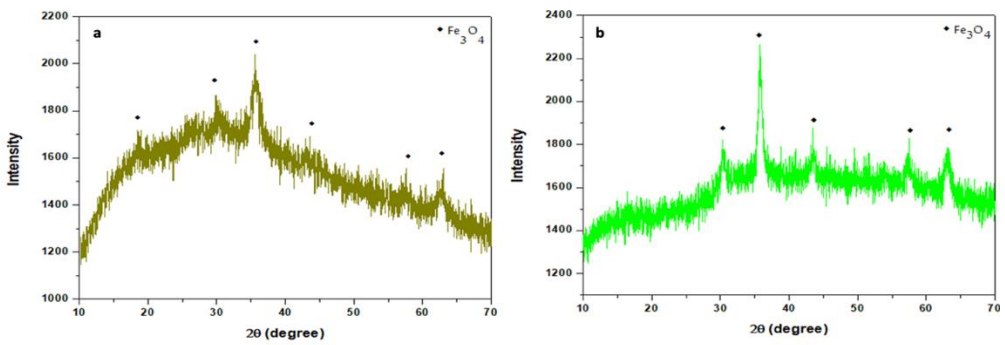

Figure 4.1: XRD patterns a) before the calcination process and b) after the calcination process.

Raman spectra of the solvothermally synthesized Fe_3O_4 are illustrated in Figure 4.2. The Raman spectra of the sp^2 carbon materials (amorphous carbon, graphite, single-layer nanotube, graphene, etc.) can be used to identify various peak intensities corresponding to minor structural differences [112–114]. The D band, linked to amorphous carbon and structural flaws in carbon, is represented by the high peak at 1345.07 cm^{-1}. The other sharp peak, located at approximately 1603.02 cm^{-1}, displays the graphitic/graphene structures and denotes a G band brought on sp^2 carbon has been stretched. Additionally, the peak near 2871.40 cm^{-1} is a member of the 2D band, and this lists the number of graphene layers [112–114] before the calcination. After calcination, the 2D, G, and D bands are signified by 1390.01, 1589.04, and 2800.53 cm^{-1} peaks. The samples' intensity ratio between the D and G bands can be used to determine the extent of graphitization. The I_D/I_G ratios of the samples for the before- and after-calcination powders were 0.75 and 0.74, respectively, according to calculations based on the Raman spectra. Also, I_{2D}/I_G ratios indicate the quantity of graphene shell layers [114]. The powders' I_{2D}/I_G ratios were discovered to be 0.28 and 0.29. Figure 4.2 depicts the Raman shift after calcination.

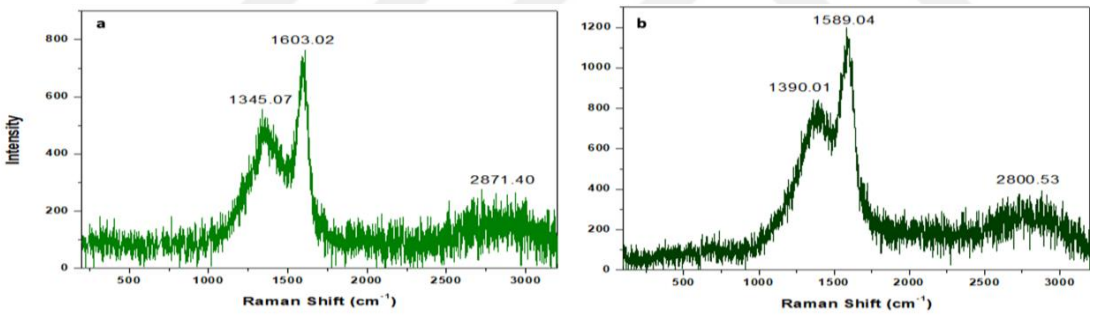

Figure 4.2: a) Raman spectra of Fe_3O_4 before calcination, b) Fe_3O_4 after calcination.

Also, Figure 4.3 which displays stable dispersions with average particle sizes of 35.5 nm, illustrates the average particle size distribution of Fe_3O_4 nanoparticles. Similar to the work of Behera et al., iron oxide distribution is more stable, and the average particle size is 66 nm. [115].

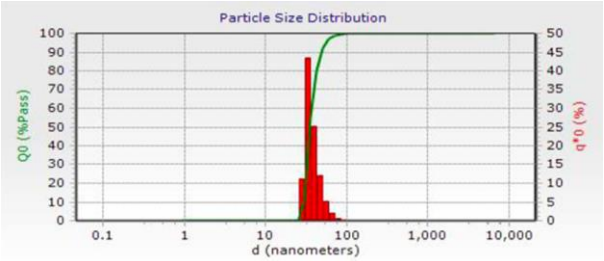

Figure 4.3: Particle size distributions of the Fe_3O_4.

SEM images and mappings (for Fe, C, and O elements) were obtained from Solvothermal synthesized Fe_3O_4 is presented in Figure 4.4. As a result, the distribution of Fe, C, and O is homogenous, and NPs have particles smaller than 90 nm. However, we have agglomeration in this analysis.

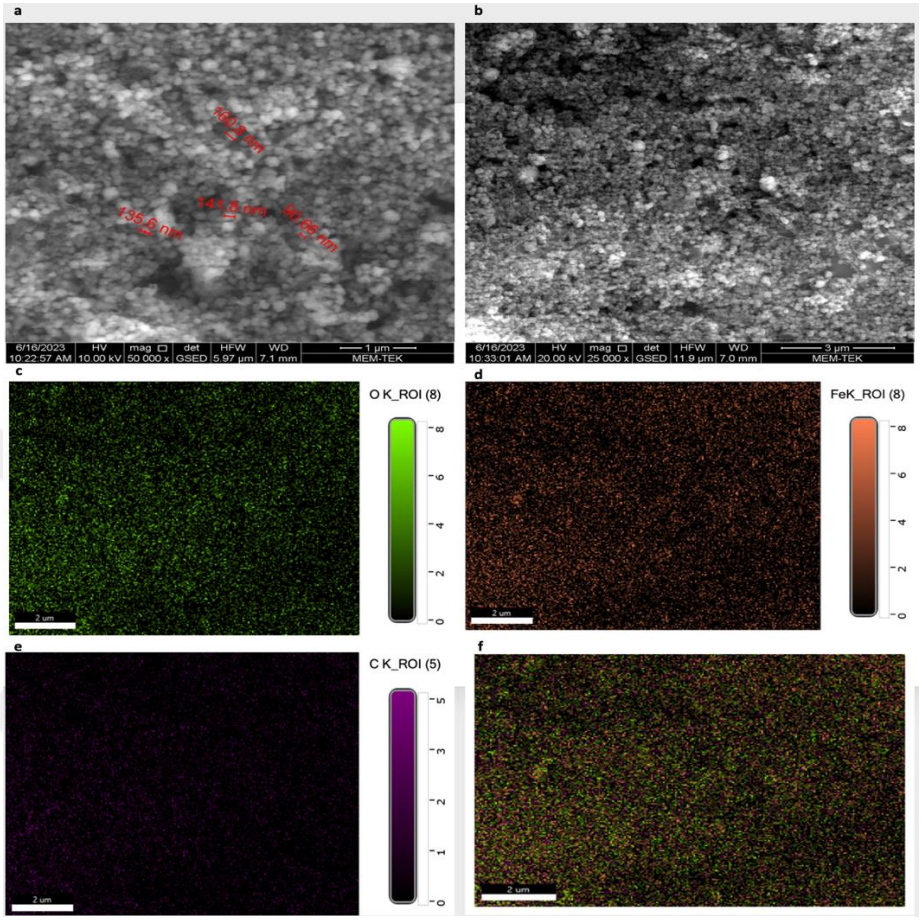

Element	Weight %	Atomic %	Net Int.	Error %	Kratio	Z	R	A	F
C K	20.31	35.92	147.20	11.69	0.0715	1.1328	0.9222	0.3107	1.0000
O K	35.64	47.32	512.63	9.06	0.1321	1.0873	0.9454	0.3407	1.0000
FeK	44.05	16.76	481.72	3.76	0.3883	0.8420	1.0581	1.0146	1.0318

Figure 4.4: a) and b) SEM images of Fe_3O_4 and c), d), e), and f) elemental mapping results (for C, Fe, O)**.**

Magnetization versus magnetic field curves of Fe_3O_4 nanoparticles before the calcination is presented in Figure 4.5a. A magnified version of VSM curves is also presented in Figure 4.5b. The magnetization value (M_s) is 41.90 emu/g, and the coercivity value (H_c) is 13.16 Oe which shows high ferromagnetic properties. Also, the retentivity value (M_r) is 2.65 emu/g. Compared to after the calcination process, Figure 4.6a,b, the magnetization value (M_s) is 60.95 emu/g, and the coercivity value

(H_c) is 13.58 Oe. Also, the retentivity value (M_r) is 3.73 emu/g which means that the magnetization of Fe_3O_4 is increased. Based on the study by Esmaeili et al., nanoparticles' magnetization can be changed by different factors, such as the particle size, volume, and presence of adsorbed oxygen [116].

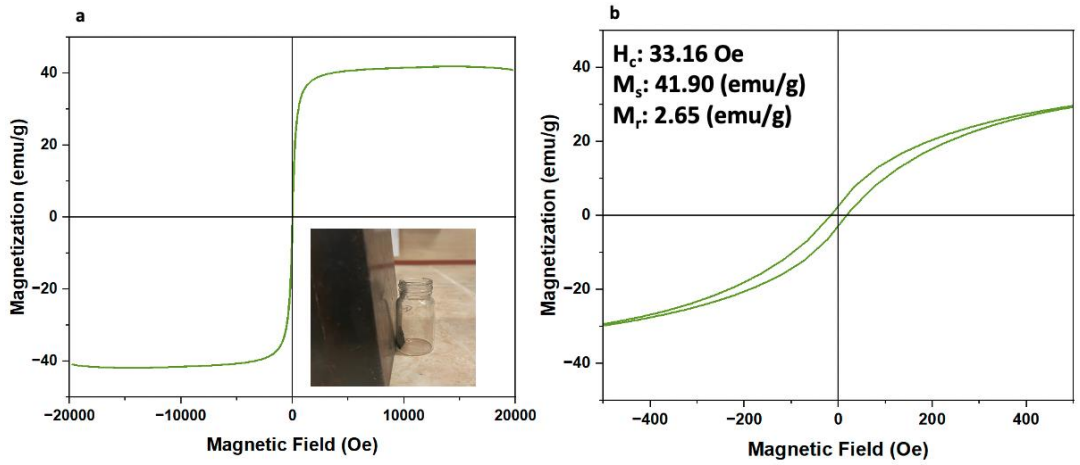

Figure 4.5: a) VSM curve of the synthesized Fe_3O_4 before calcination, b) zoom-in version of the curve.

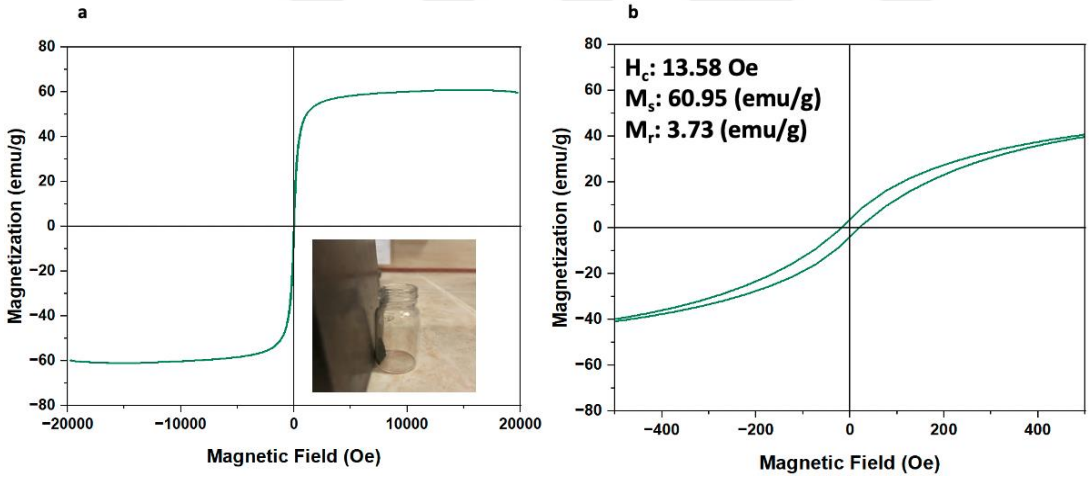

Figure 4.6: a) VSM curve of the synthesized Fe_3O_4 after calcination, b) zoom-in version of the curve.

Cytotoxicity test results on MCF7 cell lines demonstrate that there is not significant toxicity upon Fe_3O_4 treatment of cells for 24 h to higher dosages of 48 h of treatment, as shown in Figure 4.7.

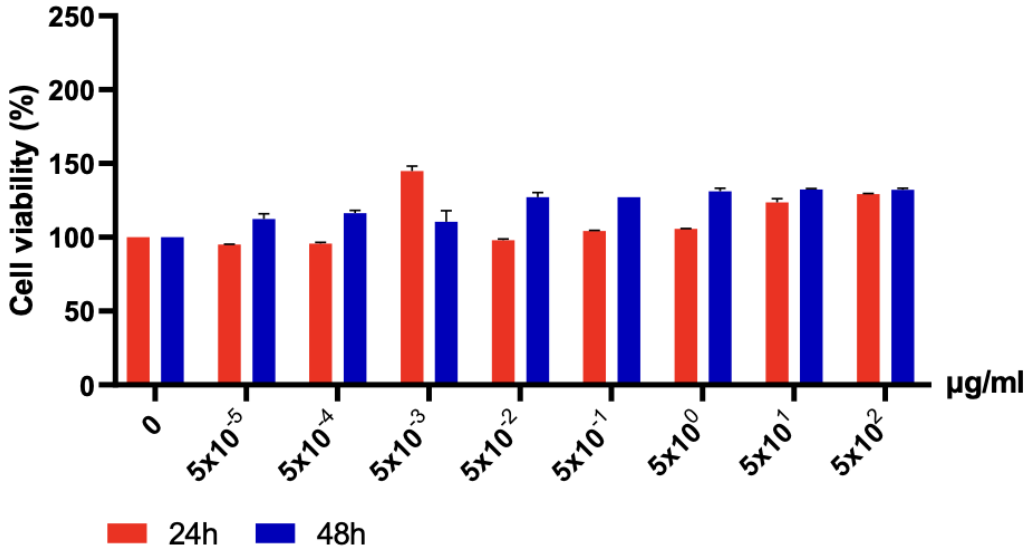

Figure 4.7: Cell viability of Fe_3O_4 nanoparticles on MCF7 cells.

4.1.2 Microstructural characterization of Fe_3O_4@rGo

Figure 4.8a depicts the XRD pattern of the powders produced during solvothermal synthesis. Fe_3O_4 was detected at 36°. However, the strength of the early phase is weak. The XRD pattern in Figure 4.8b demonstrates how the intensity and crystallinity of phases improve during the calcination process. The carbon peak is also visible at 27° better after the calcination.

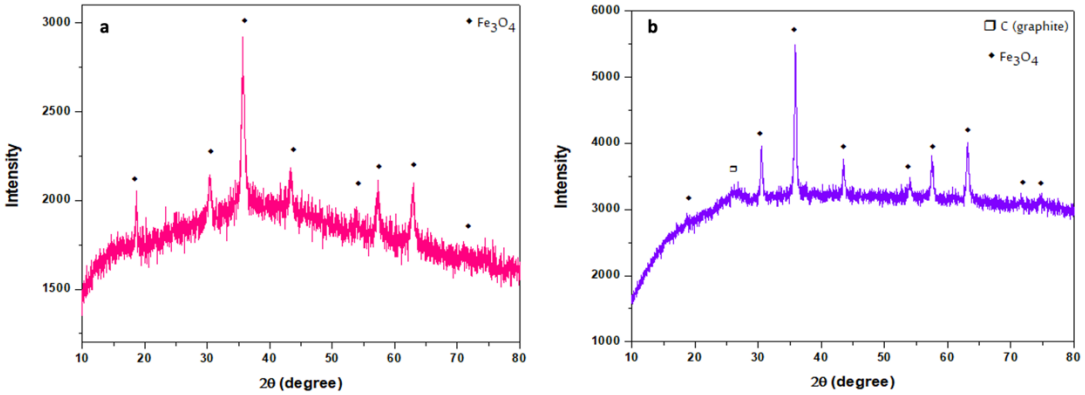

Figure 4.8: XRD patterns a) before calcination. b) after the calcination process.

The Raman spectra of synthetic powders of Fe_3O_4@rGo are illustrated in Figure 4.9a,b. Before the calcination, the D, G, and 2D bands are represented by 1336.26, 1595.33, and 2840.47 cm^{-1} peaks. After calcination, the 2D, G, and D bands are signified by 1356.25, 1602.82, and 2827.39 cm^{-1} peaks. Between 2500 and 3000 cm^{-1}, reduced graphene oxide peaks are shown. Therefore, peaks become more intense after the calcination process. The I_D/I_G ratios of the samples for the before- and after-

calcination powders were 0.73 and 0.29, respectively; the powders' I_{2D}/I_G ratios were discovered to be 0.74 and 0.27.

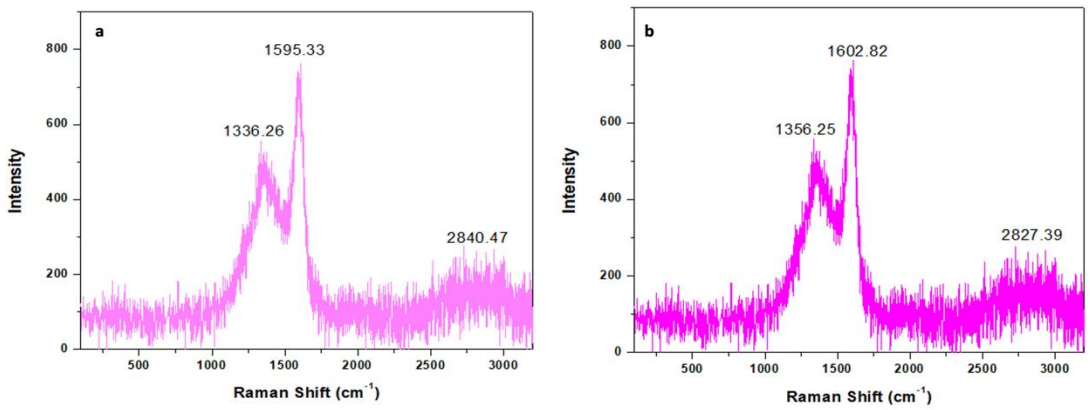

Figure 4.9: a) Raman spectra of Fe_3O_4@rGo before calcination, b) Fe_3O_4@rGo after calcination.

TEM images which are shown in Figure 4.10, demonstrate that carbon is partially coated on magnetic iron oxide and embedded inside them. Also, Solvothermal synthesized SEM pictures and mappings (for Fe, C, and O elements) were obtained, and Figure 4.11 display Fe_3O_4@rGo. As a result, there is homogeneity in the distribution of Fe, C, and O.

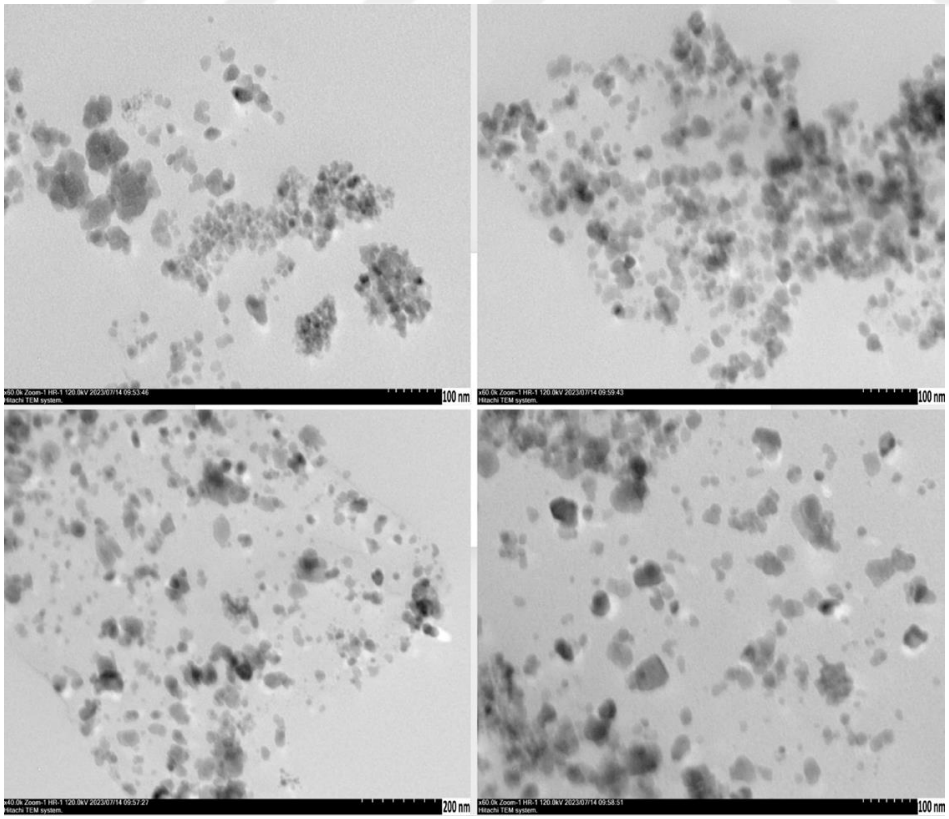

Figure 4.10: TEM images of Fe_3O_4@rGo.

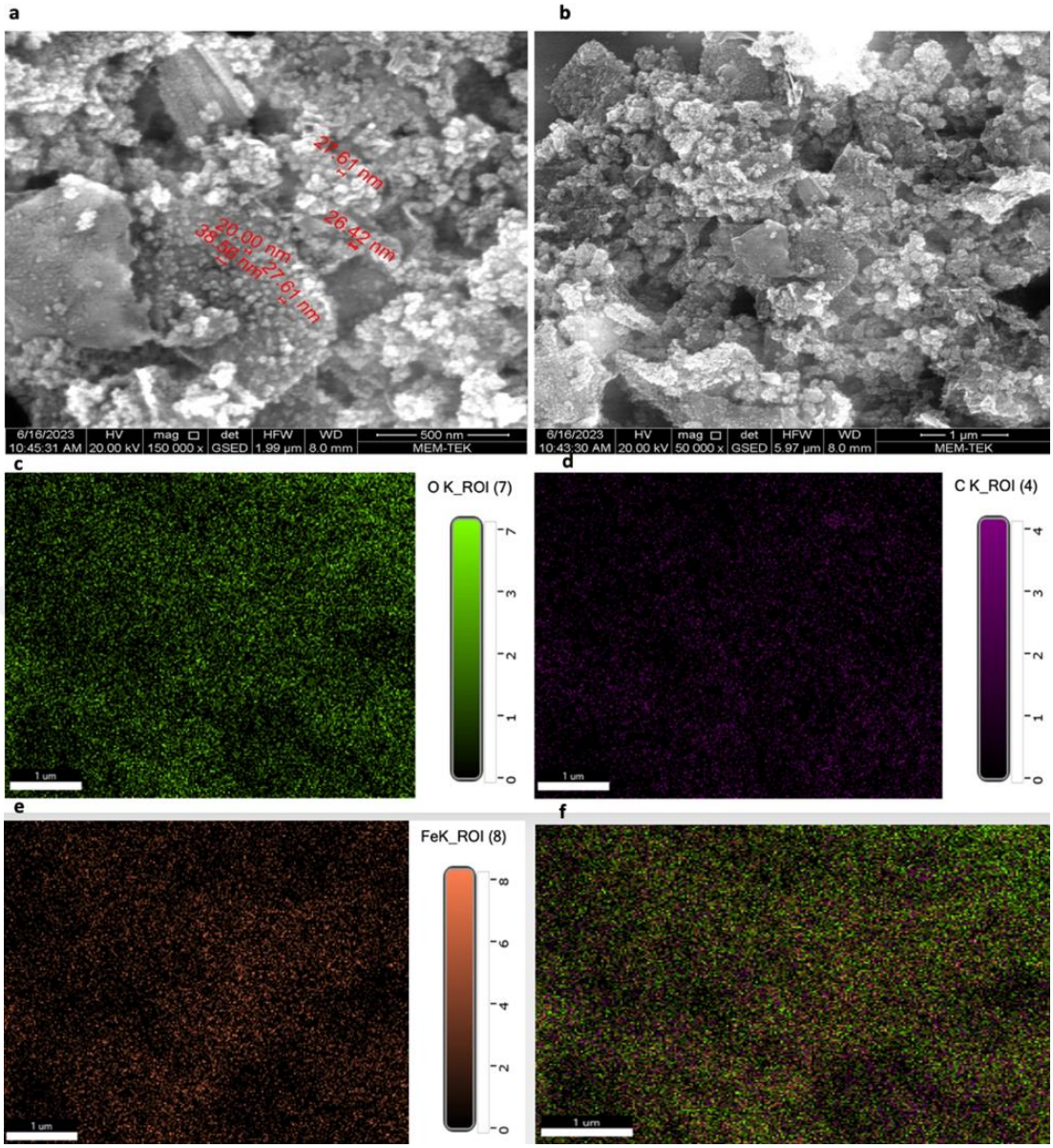

Element	Weight %	Atomic %	Net Int.	Error %	Kratio	Z	R	A	F
C K	48.32	62.05	252.50	7.89	0.2361	1.0561	0.9660	0.4627	1.0000
O K	34.43	33.19	138.79	11.31	0.0685	1.0111	0.9866	0.1968	1.0000
FeK	17.24	4.76	93.68	6.11	0.1435	0.7750	1.0800	1.0231	1.0500

Figure 4.11: a) and b) SEM images of Fe_3O_4@rGo and c), d), e), and f) elemental mapping results (for C, Fe, O)**.**

Before calcination, the curves of Fe_3O_4@rGo nanoparticle magnetization vs. magnetic field are shown in Figure 4.12a. A more detailed illustration of VSM curves can be found in Figure 4.12b. Indicating ferromagnetic properties are the coercivity value (H_c) of 16.82 Oe and the magnetization value (M_s) of 33.10 emu/g. The retentivity value (M_r) is 0.98 emu/g as well. The outcomes of the calcination process are compared in Figure 4.13a,b, 18.85 Oe is the coercivity value, and the magnetization value is 59.39

emu/g. Additionally, because the retentivity value (M_r) is 3.21 emu/g, Fe_3O_4@rGo is more magnetic. As a result, the magnetization of Fe_3O_4@rGo nanoparticles compared to Fe_3O_4 nanoparticles is reduced.

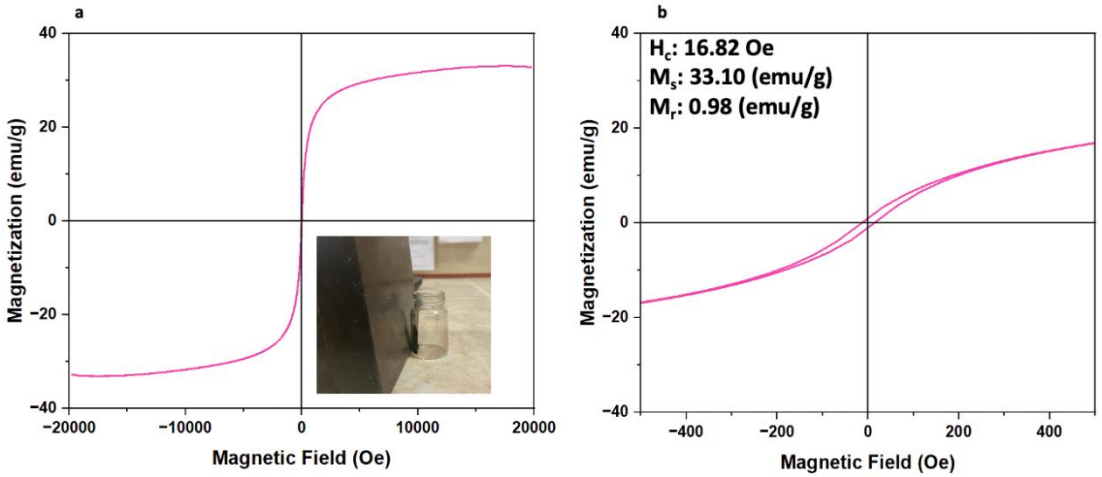

Figure 4.12: a) VSM curve of the synthesized Fe_3O_4 before calcination, b) zoom-in version of the curve.

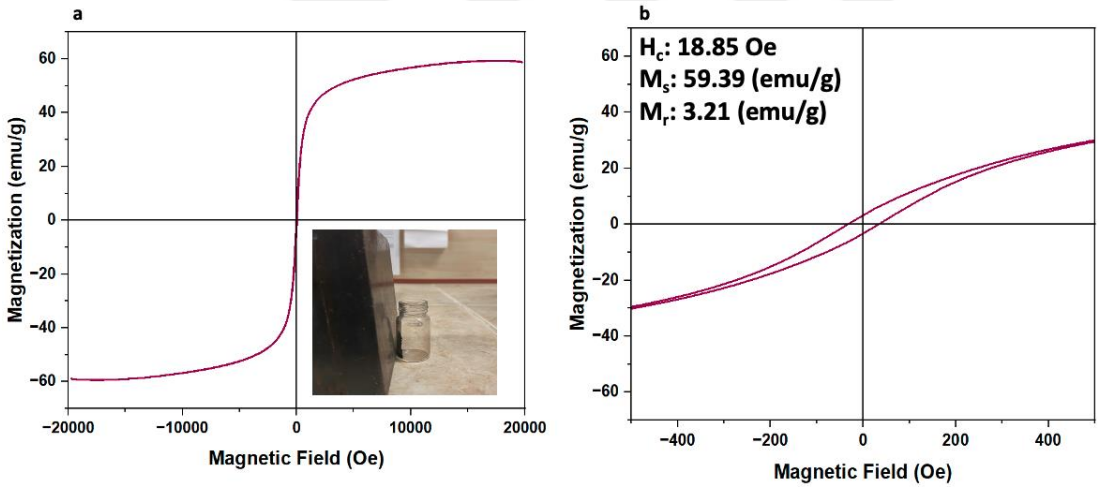

Figure 4.13: a) VSM curve of the synthesized Fe_3O_4 after calcination, b) zoom-in version of the curve.

Upon Fe_3O_4@rGo treatment of cells for 24 h, not observed significant toxicity, similar to higher dosages of 48 h of treatment. On the other hand, at low dosages of 48 h of treatment, except for the highest dosage, cell proliferation is observed after treatment with Fe_3O_4@rGo, as shown in Figure 4.14.

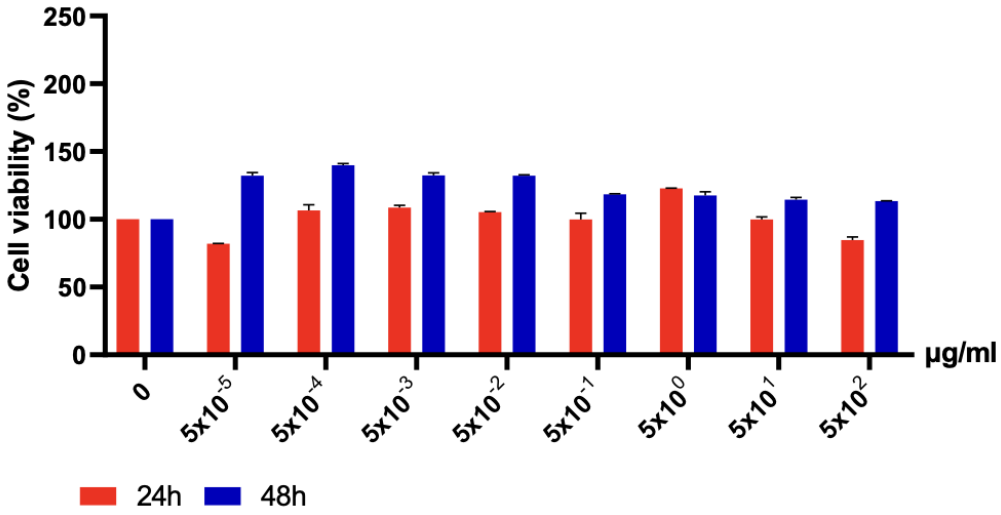

Figure 4.14: Cell viability of Fe_3O_4@rGo nanoparticles on MCF7 cells.

4.1.3 Microstructural characterization of Fe_3O_4@rGo@graphene

For microstructural analyses, Figure 4.15 displays the Fe_3O_4@rGo@graphene XRD pattern after leaching treatment by HF and HCl. The presence of the carbon peak is highly demonstrated at 27°. The furnace temperature was raised to 950 °C in around 60 min with a flow rate of 200 mL/min of CH_4 gas and 100 mL/min of H_2. The furnace's quartz tube, as well as the precursor powders at the boats, were both covered in a layer of carbon. These formations are linked to the high rate of CH_4 flow and high temperature-induced carbon deposition. The patterns of the powders reveal that they contain a significant quantity of C phase (graphite, ICDD card number: 01-075-2078). For the powders in Figure 4.15, the phases BCC Fe (ICDD card number: 00-01-1252), Fe_3O_4 (ICDD card number: 01-085-1436), and FCC (Fe, C) (00-052-0513), BCC Fe (ICDD card number: 00-01-1252) were also found.

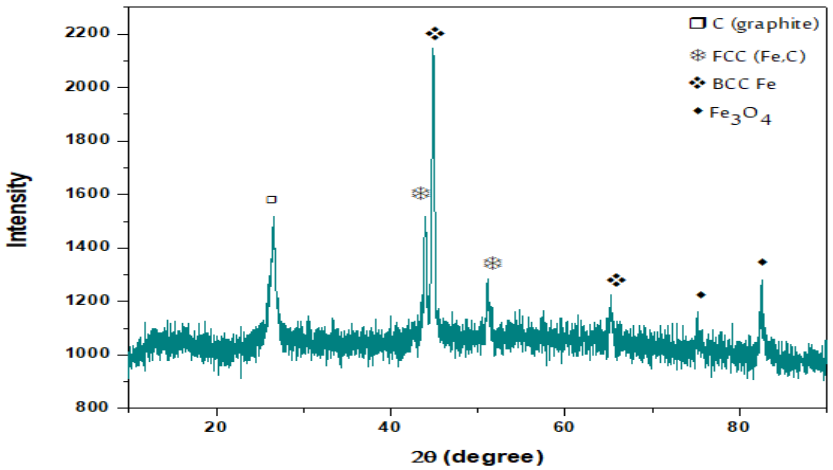

Figure 4.15: XRD pattern of powders after graphene coating.

The Raman spectra of synthesized powders of Fe_3O_4 @rGo@graphene are shown in Figure 4.16. The C phase's D, G, and 2D bands are represented by 1357.74, 1577.02, and 2710.77 cm^{-1} peaks. Since Compared to the G bond, the D bond is higher., it means amorphous carbon is present in the structure. Also, comparatively, the 2D peak's intensity with Fe_3O_4@rGo and Fe_3O_4 increases. The I_D/I_G ratio of the samples is 1.07. An I_D/I_G ratio of 1.07 indicates some defects or disorders in the graphene lattice, but it's not excessively high. This could be due to various factors, such as impurities, lattice distortions, or other structural imperfections in the graphene sample. Generally, lower I_D/I_G ratios (closer to 1) are associated with higher-quality graphene, as they indicate fewer defects. However, a ratio of 1.07 is still relatively close to 1, suggesting that the graphene may not be severely compromised in quality. The powders' I_{2D}/I_G ratios were discovered to be 0.81. An I_{2D}/I_G ratio of 0.81 suggests that the graphene sample is likely composed of a small number of layers. In particular, the value is consistent with few-layer graphene.

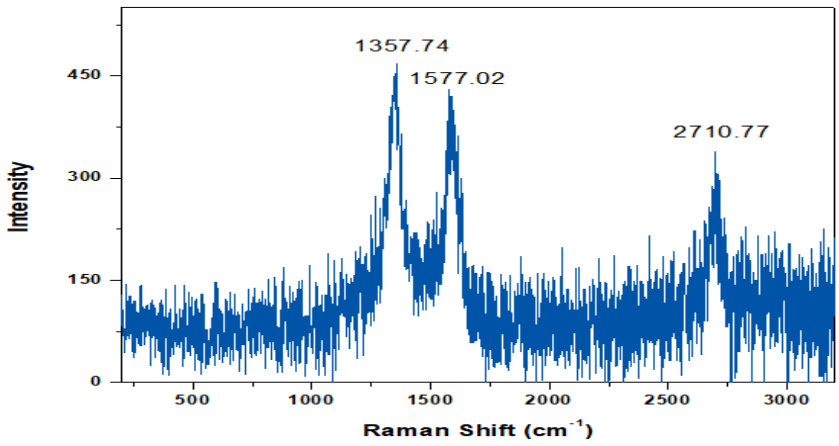

Figure 4.16: Raman spectra of Fe_3O_4@rGo@graphene.

For the elements Fe, C, and O, synthesized SEM images and mappings were obtained. Fe_3O_4@rGo@graphene is shown in Figure 4.17. As a result, graphene-coated on Fe_3O_4@rGo homogenously as the carbon elements increase compared to Fe_3O_4@rGo and Fe_3O_4. Also, in TEM images of Fe_3O_4@rGo@graphene, as demonstrated in Figure 4.18, we can see the multi-graphene layers that coated our particles.

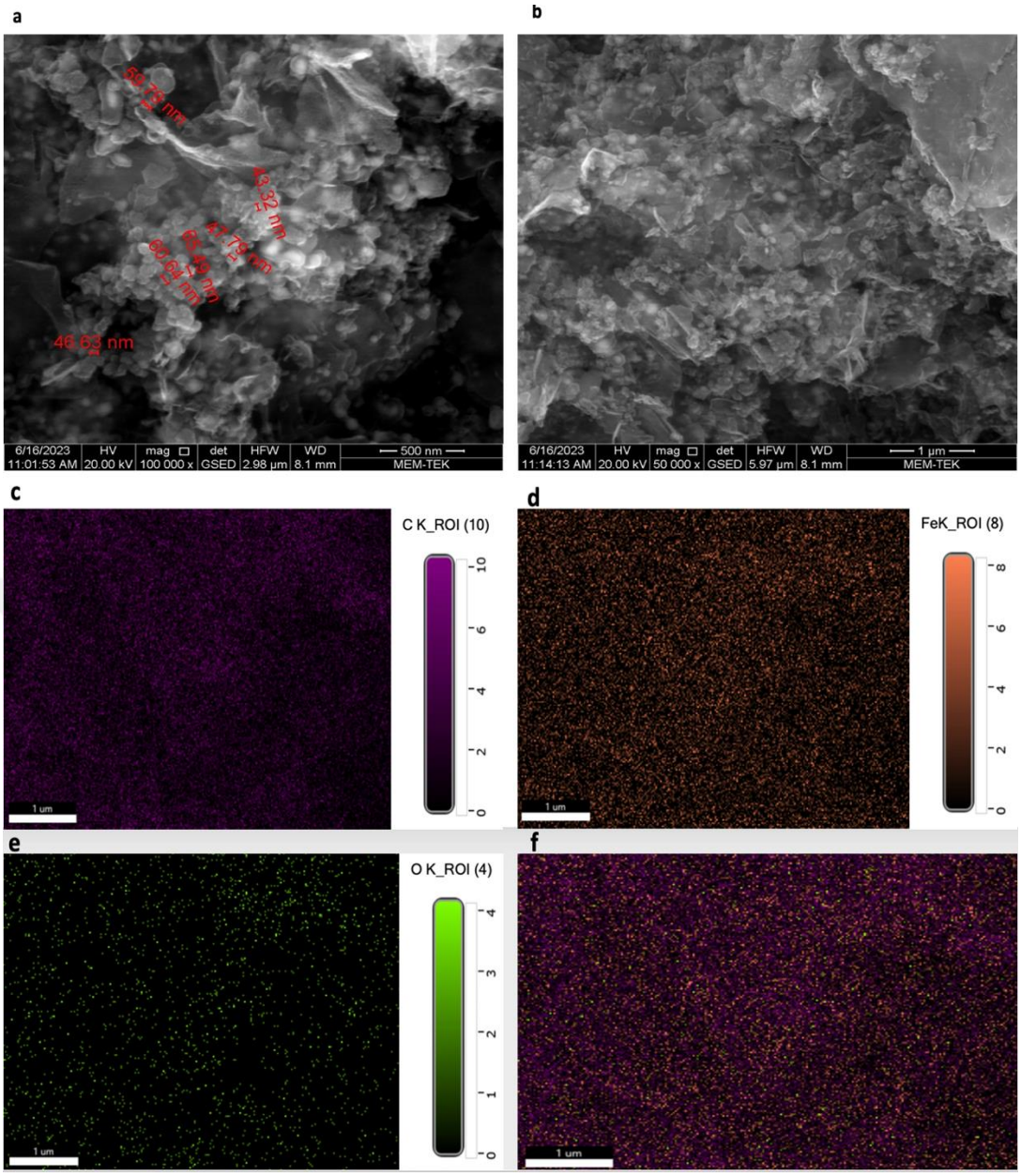

Element	Weight %	Auto MDL	Atomic %	Net Int.	Error %	R	A	F
C K	85.4	0.04	94.9	873.3	9.5	0.9264	0.1697	1.0000
O K	2.7	0.17	2.3	22.8	14.9	0.9353	0.0544	1.0000
Fe K	11.9	0.12	2.8	395.9	2.5	0.9778	0.9928	1.0546

Figure 4.17: a) and b) SEM images of Fe_3O_4@rGo@graphene and c), d), e,) and f) elemental mapping results (for C, Fe, O)**.**

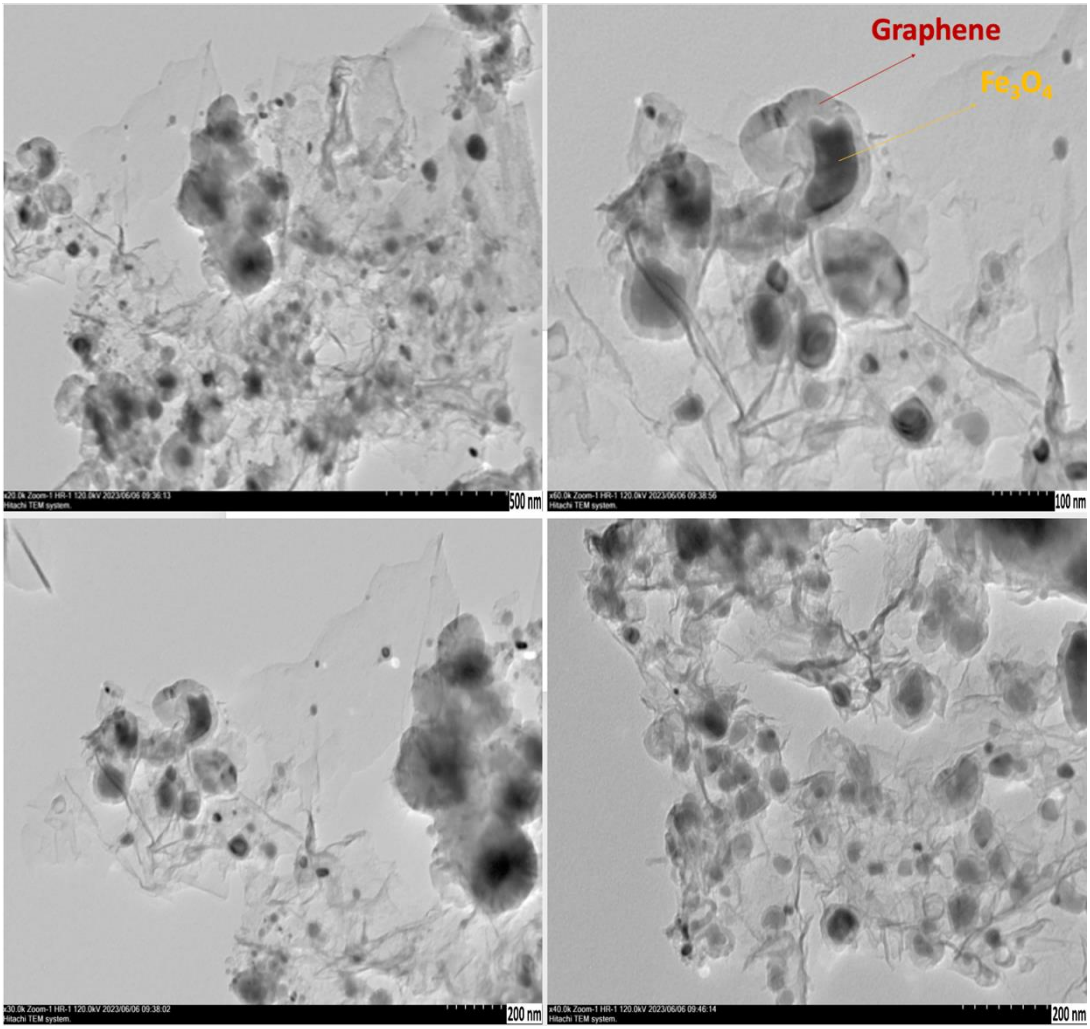

Figure 4.18: TEM images of Fe_3O_4@rGo@graphene.

Figure 4.19 illustrates the average distribution of the particle sizes of Fe_3O_4@rGo@graphene nanoparticles and displays stable dispersions with average particle sizes of 255 nm. Consequently, the agglomeration of nanoparticles is high.

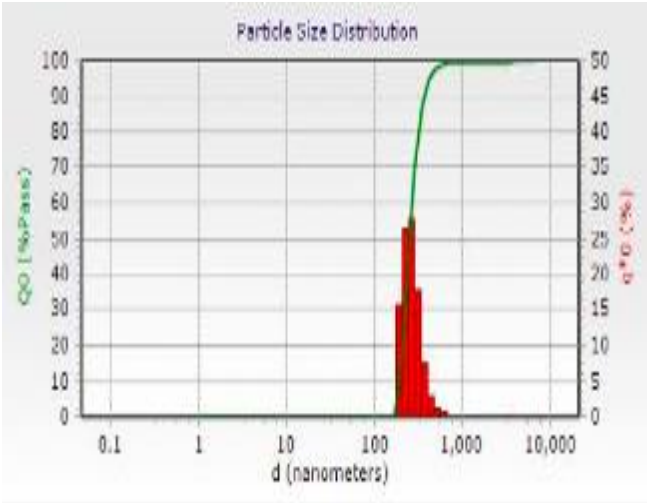

Figure 4.19: Particle size distributions of the Fe_3O_4@rGo@graphene.

Figure 4.20a shows the curves of Fe_3O_4@rGo@graphene nanoparticle magnetization vs. the magnetic field. Figure 4.20b also includes an enlarged representation of VSM curves. The coercivity value (H_c) is 402.12 Oe, the magnetization value (M_s) is 139.48 emu/g, and the retentivity value (M_r) is 37.73 emu/g as well, indicating soft magnetic characteristics which are used in biomedical applications. The magnetization of these nanoparticles compared to Fe_3O_4@rGo and Fe_3O_4 is high because of the reduction of Fe_3O_4@rGo nanoparticles at a high temperature of 950°C in CVD, which we obtained Fe nanoparticles, and as a characteristic, it has a high magnetization.

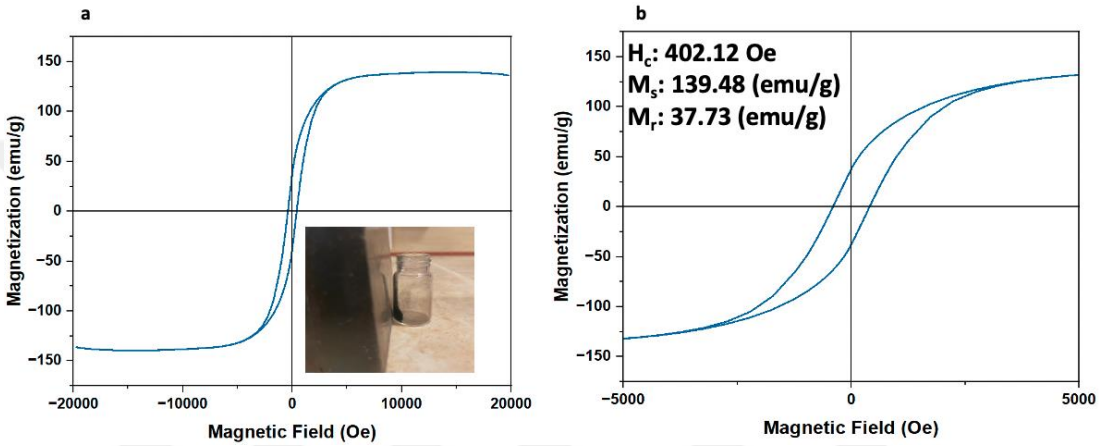

Figure 4.20: a) VSM curve of the synthesized Fe_3O_4@rGo@graphene, b) zoom-in version of the curve.

4.2 Microstructural characterization polymer coating Fe_3O_4@rGo@graphene

Firstly, as a pyrene initiator (PyrI) synthesized, it is characterized by a ^{1}H-NMR spectrum shown in Figure 4.21. ^{1}H-NMR analysis in $CDCl_3$ validated PyrI's structural details. As seen from the NMR spectrum, the signals around 7.9 to 8.3 ppm belonged to protons in the characteristic pyrene ring. Other protons in the structure of PyrI are -NH at 7-7.1 ppm, -CH_2 (a) at 5.2 ppm, and -CH_3 (b) around 1.9-2.1 ppm, respectively.

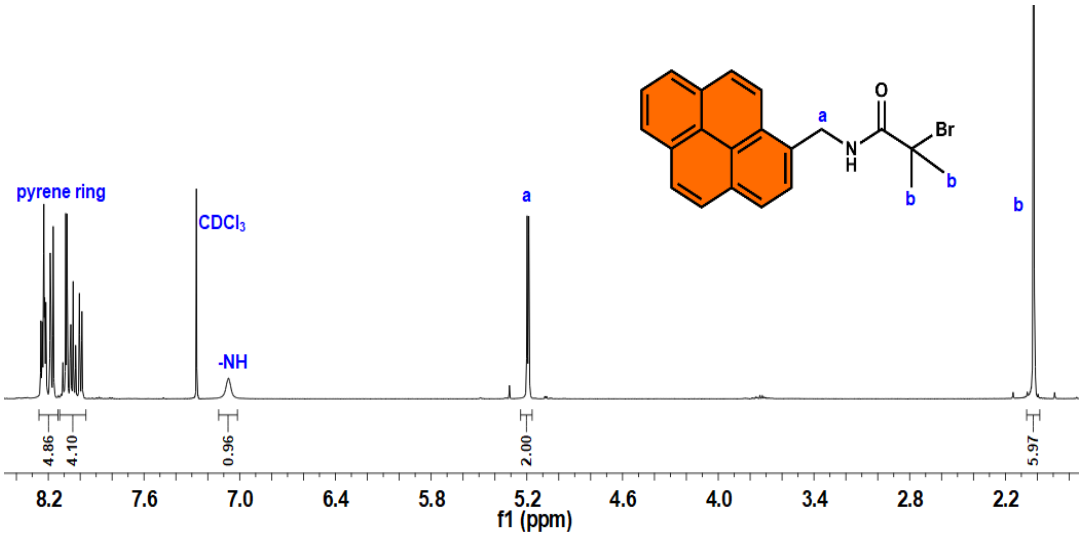

Figure 4.21: Pyrene Initiator (PyrI) ^{1}H-NMR spectrum.

In addition, after synthesizing the PMA-POEGMA, it was characterized by a ^{1}H-NMR spectrum, shown in Figure 4.22. The structure of PMA-POEGMA was confirmed by ^{1}H-NMR analysis in $CDCl_3$, as seen from the NMR spectrum. The signals around 8.0 to 8.2 ppm are attributed to aromatic protons of the pyrene moiety. All other typical proton signals in the structure of PMA-POEGMA were observed around 5 to 5.3 ppm (a), 3.6 to 3.8 ppm (b and c), 3.3 to 3.4 ppm (d), 1.6 to 2 ppm (e) and 0.7 to 1.1 ppm (g and f), respectively.

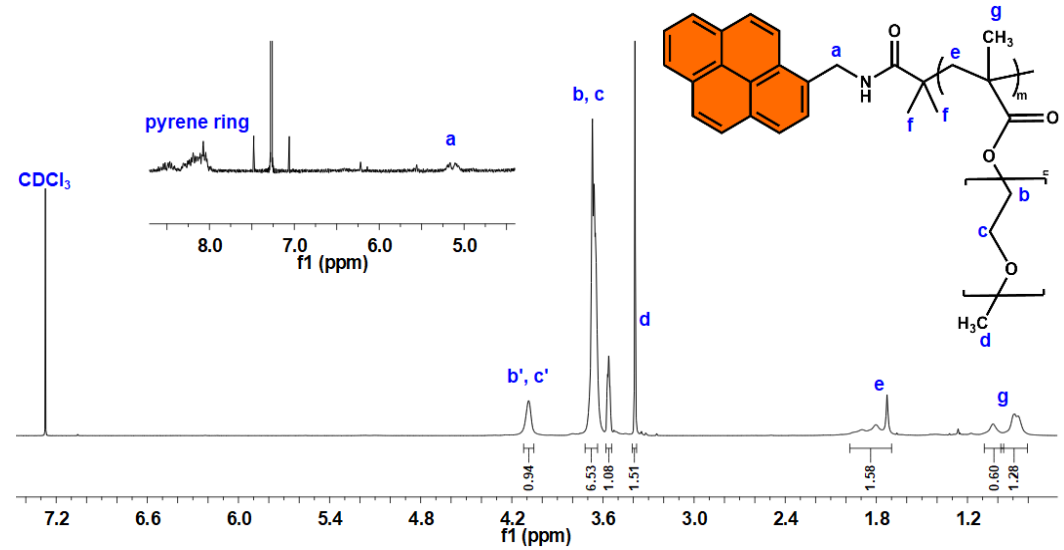

Figure 4.22: PMA-POEGMA ^{1}H-NMR spectrum.

FTIR results of Fe_3O_4@rGo@graphene@PMA-POEGMA with different concentrations of polymer (5mg,10mg, 50mg) are shown in Figure 4.23. As a result,

three characteristic absorption bands were observed in FTIR spectra of graphene-encapsulated iron oxides at 1109 cm^{-1} (C-O stretching), 1725 cm^{-1} (C=O stretching), and 2870 cm^{-1} (C-H stretching) [117]. Considering the feed ratio of PMA-POEGMA for coating (5 mg to 50 mg), the peak intensities were directly increased with increasing amounts of PMA-POEGMA. These results confirmed that graphene-encapsulated iron oxides were successfully coated with PMA-POEGMA.

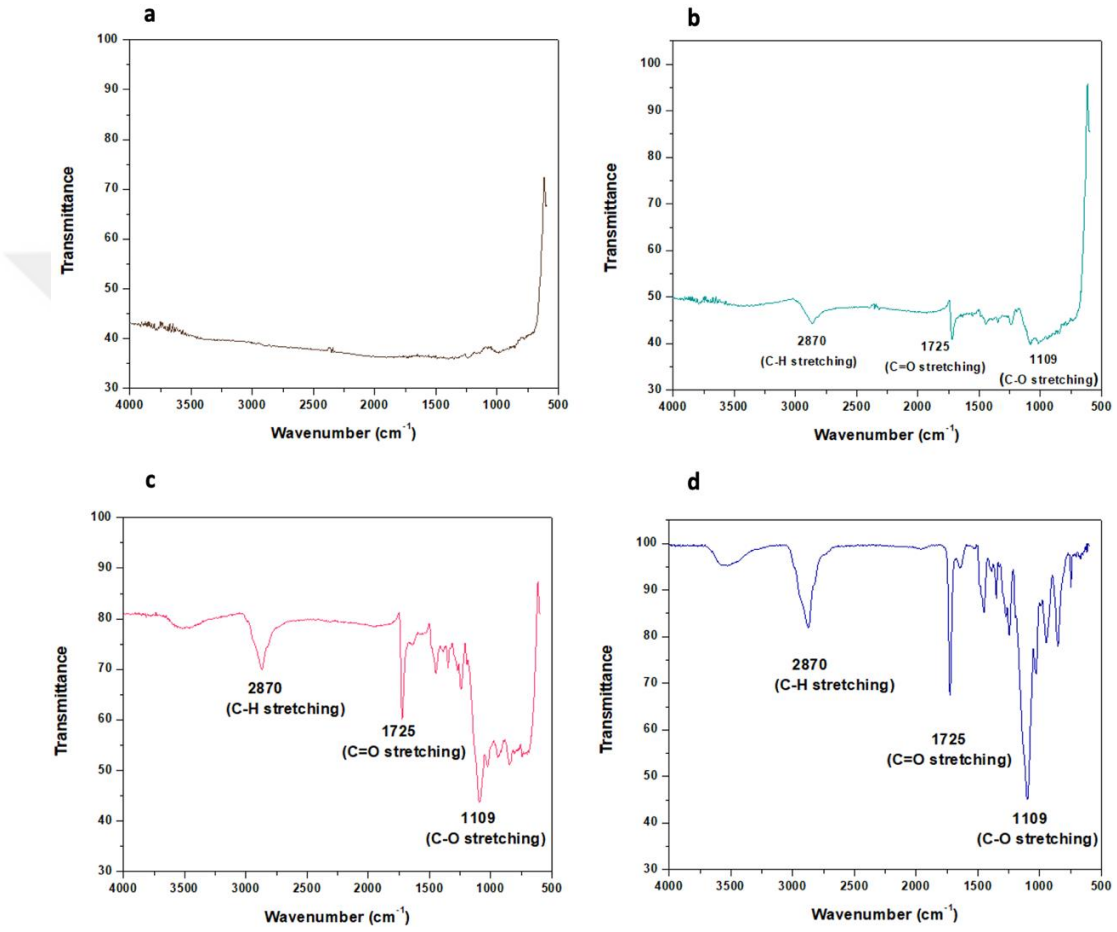

Figure 4.23: FTIR results of a) 0mg b) 5 mg c) 10 mg d) 50 mg PMA-POEGMA.

The precipitation rate of these nanoparticles with different concentrations is represented in Figure 4.24. As shown, the precipitation of our nanoparticles can be reduced over time by raising the polymer concentration. So obviously, we can disperse our graphene-coated MNPs homogeneously in water.

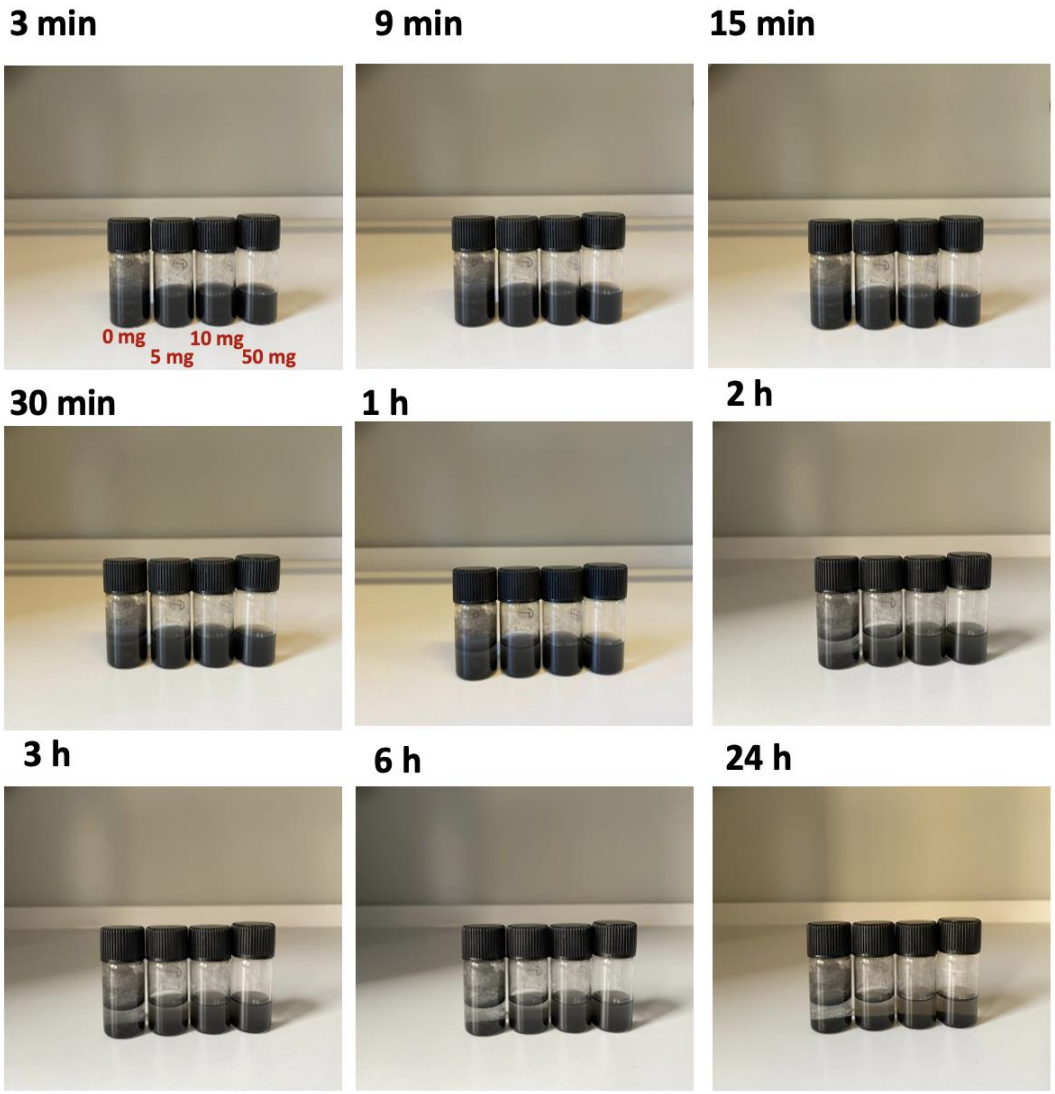

Figure 4.24: Precipitation rate of Fe_3O_4@rGo@graphene@PMA-POEGMA by passing time.

The Raman spectra of synthetic powders of Fe_3O_4@rGo@graphene@PMA-POEGMA are shown in Figure 4.25. The D, G, and 2D bands are represented by 1346.25, 1607.99, and 2688.31 cm^{-1} peaks. As the D bond, in comparison with the G bond, is more highly increased after coating with polymer, it can be represented that polymer carbon peaks are amorphous. The I_D/I_G ratio of the samples is 1.2, and the powders' I_{2D}/I_G ratios were discovered to be 0.6.

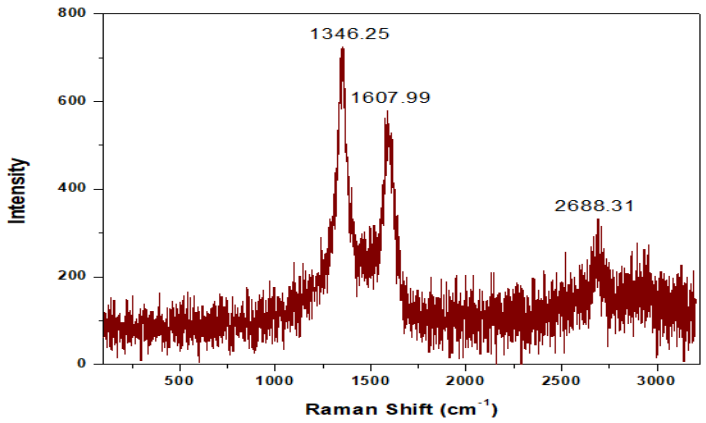

Figure 4.25: Raman spectroscopy of Fe_3O_4@rGo@graphene@PMA-POEGMA.

Also, the average particle size analysis result of Fe_3O_4@rGo@graphene@PMA-POEGMA is shown in Figure 4.26. The homogenous dispersion of our particles results is 84.5nm, and by functionalizing graphene, we can avoid agglomeration of magnetic NPs.

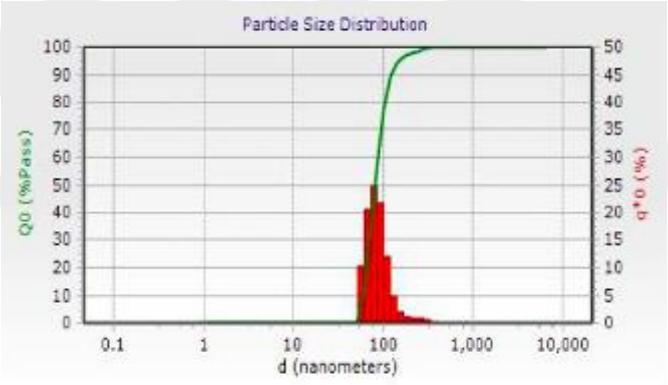

Figure 4.26: Particle size distributions of the Fe_3O_4@rGo@graphene@ PMA-POEGMA.

The relationships between the magnetization of Fe_3O_4@rGo@graphene@PMA-POEGMA nanoparticles and the magnetic field are shown in Figure 4.27a. A more detailed illustration of VSM curves can be found in Figure 4.27b. The coercivity value (H_c) of 363.77 Oe and the magnetization value (M_s) of 84.06 emu/g, and the retentivity value (M_r) is 16.64 emu/g as well indicate the soft magnetic properties used in biomedical applications. The magnetization of these nanoparticles, as compared to Fe_3O_4@rGo@graphene is reduced.

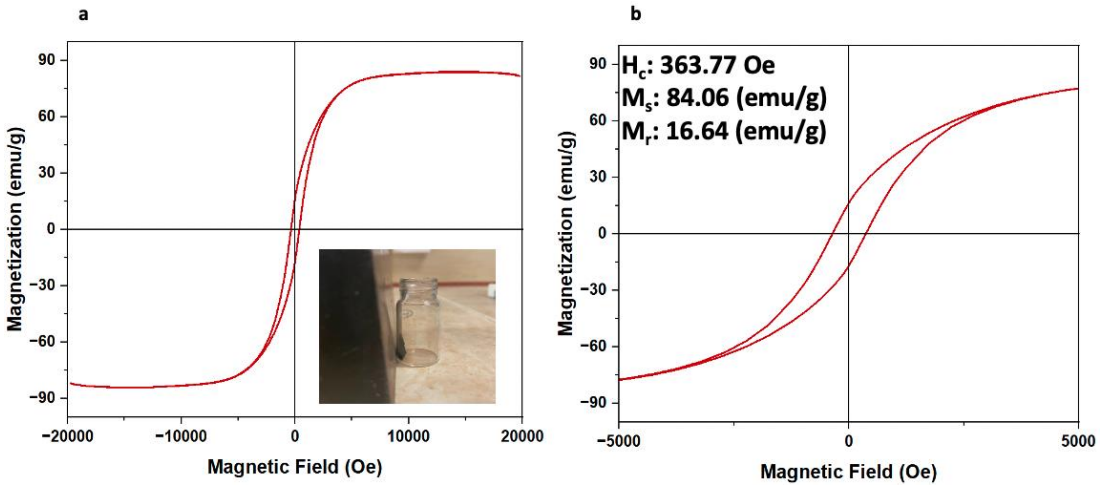

Figure 4.27: a) VSM curve of the synthesized Fe_3O_4@rGo@graphene@ PMA-POEGMA, b) zoom-in version of the curve.

Then cytotoxicity of the polymer without any nanoparticles is done, as demonstrated in Figure 4.28. Significant alteration in cell number was not observed in the cells treated with pyrene for 24 h. However, cell number was slightly increased in the low dosages upon treatment for 48 h.

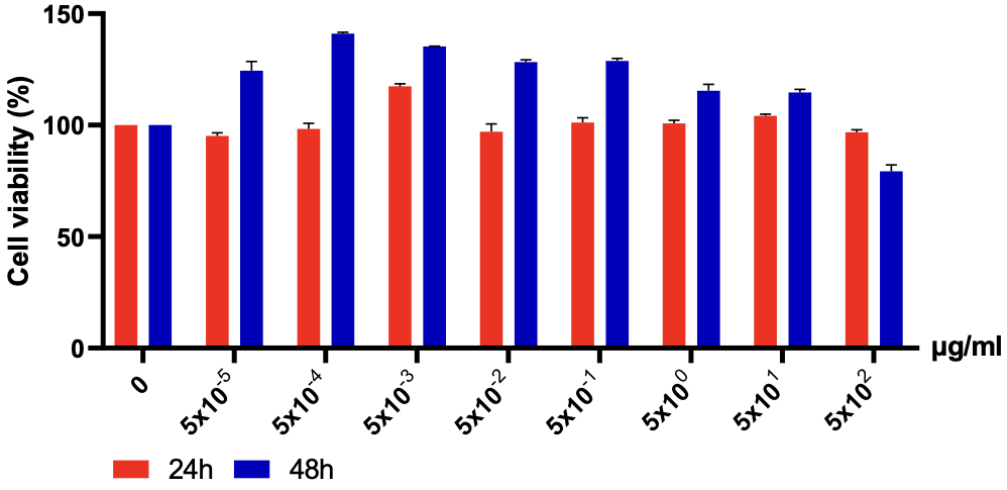

Figure 4.28: Cell viability of PMA-POEGMA on MCF7 cells.

After that, the cytotoxicity test of Fe_3O_4@rGo@graphene@ PMA-POEGMA is done as shown in Figure 4.29, and as a result, In the cells treated with graphene for 24 h, it showed a toxic effect when the concentration is higher than 5x10 µg/mL. Treatment for 48 h resulted in low toxic effects only in the highest dose.

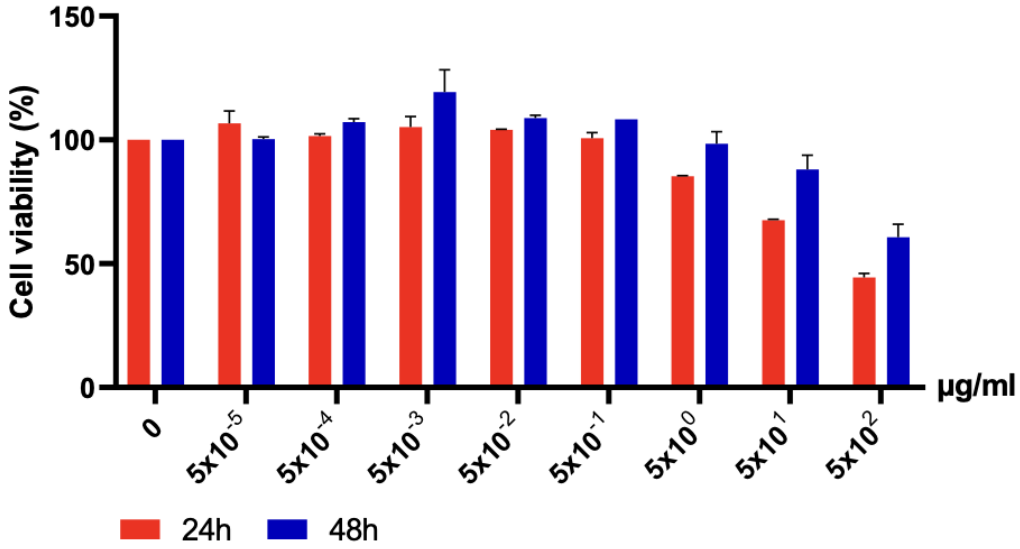

Figure 4.29: Cell viability of Fe_3O_4@rGo@graphene@ PMA-POEGMA nanoparticles on MCF7 cells.

To summarize, the schematic of Fe_3O_4, Fe_3O_4@rgo, Fe_3O_4@rgo@graphene, and Fe_3O_4@rgo@graphene@PMA-POEGMA nanoparticles are briefly explained in Figure 4.30.

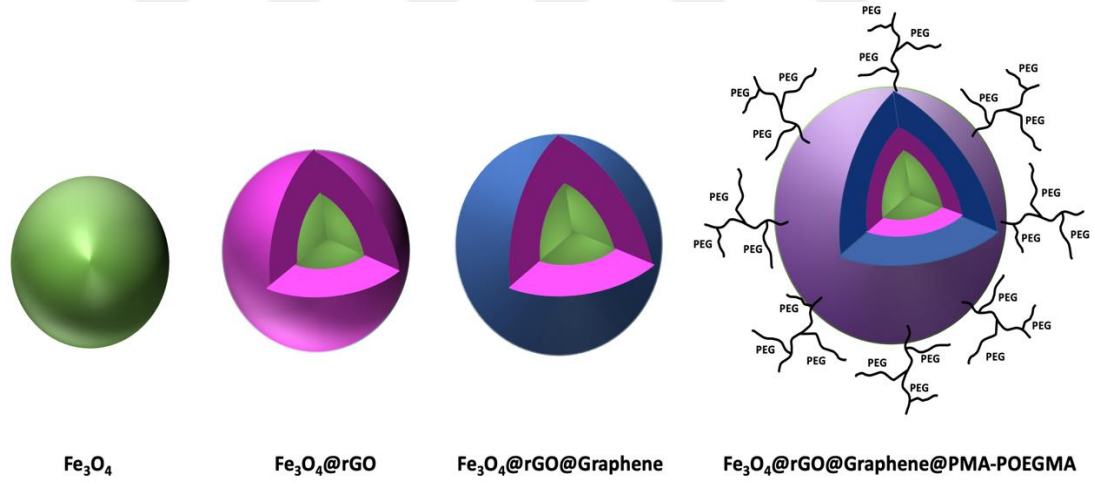

Figure 4.30: Schematic of all utilized steps in the synthesis of nanoparticles.

5. CONCLUSIONS

This dissertation utilized an integrative approach to synthesize graphene shells encapsulated on magnetic iron oxide nanoparticles for potential applications in electronics, biomedicine, and the environment. They were coated with graphene layers to improve the surface properties of magnetic iron oxide nanoparticles. Four steps were used to obtain functionalized graphene-encapsulated magnetic iron oxide nanoparticles. These novel studies focus on optimizing synthesis conditions and detailed characterization of nanoparticles to show their potential applications, especially in biomedicine.

As mentioned in the results and discussion sections, the synthesis of Fe_3O_4 and Fe_3O_4@rGO and graphene encapsulation of Fe_3O_4@rGO nanoparticles and their functionalization steps were summarized.

- Solvothermal synthesis of Fe_3O_4 and Fe_3O_4@rGO succeeded after 26 h and 196°C. After synthesizing the Fe_3O_4 and Fe_3O_4@rGO nanoparticles, calcination processes were done to improve crystallinity and remove organic compounds. The particle size of the Fe_3O_4 powders was measured as 35.5 nm. A mixed morphology was observed in the Fe_3O_4 system, and spherical and coaxial nanoparticles were obtained. Before and after calcination, Fe_3O_4 nanoparticles, the H_c value was respectively 13.16 and 33.16 Oe, the M_s value was 41.90 and 60.95 emu/g, and the M_r value was 2.65 and 3.73 emu/g. Also, before and after calcination, Fe_3O_4@rGO nanoparticles, the H_c value was respectively 16.82 and 18.85 Oe, the M_s value was 33.10 and 59.39 emu/g, and the M_r value was 0.98 and 3.21 emu/g
- Multilayer graphene encapsulated Fe_3O_4@rGO nanoparticles were achieved using the CVD method in which synthesis conditions are 950 °C, 60 min, 50 MPa pressure, 100 mL/min CH_4 and 100 mL/min H_2 gas flows. Purification processes were done by leaching Fe_3O_4@rGO@graphene with HF and HCl acid solutions. The particle size of the Fe_3O_4@rGO@graphene powders was measured at 255 nm, revealing an agglomerated microstructure. Synthesized

core/shell nanoparticles have soft magnetic properties. The H_c value was 402.12 Oe, the M_s value was 139.48 emu/g, and the M_r value was 37.73 emu/g.

- XRD patterns of purified Fe_3O_4@rGO@graphene nanoparticles showed C (graphite), BCC Fe, FCC (Fe, C), and Fe_3O_4 phases, and Raman spectra revealed the multilayer graphene encapsulation with I_D/I_G (1.07) and I_{2D}/I_G (1.81) values.

- Polymer coated on graphene encapsulated nanoparticles to dissolve them easily in water and reduce the precipitation rate and agglomeration of MNPs, so designing and utilizing PMA-POEGMA Polymer is done, and Absorption bands were observed in FTIR spectra of graphene-encapsulated iron oxides at 1109 cm^{-1} (C-O stretching), 1725 cm^{-1} (C=O stretching), and 2870 cm^{-1} (C-H stretching). Also, the average particle size of Fe_3O_4@rGO@graphe is reduced to 84.5 nm. These particles are soft magnetic, which the H_c value was 363.77 Oe, the M_s value was 84.06 emu/g, and the M_r value was 16.64 emu/g.

- Cytotoxicity tests were performed on cells purchased in kits from commercial companies. Biocompatibility tests were applied to five different products (Fe_3O_4 and Fe_3O_4@rGO and Fe_3O_4@rGO@graphene and PMA-POEGMA and Fe_3O_4@rGO@graphene@PMA-POEGMA) obtained by solvothermal and chemical vapor deposition methods. In the project, the breast cancer cell line MCF7 was used. It was determined that the particles showed a time and dose-dependent toxicity. Toxicity is very low at the highest dose and incubation period of 24 h and 48 h.

For further research studies, cytotoxicity measurements of these nanoparticles can be done on different cell lines, such as HeLa, MDA-MB-23, and Vero E6 cells. Also, other tests, such as SAR and Phototoxicity tests, can be done.

REFERENCES

[1] **L. Wu, A. Mendoza-Garcia, Q. Li, S. Sun,** (2016), Organic Phase Syntheses of Magnetic Nanoparticles and Their Applications, *Chem Rev, 116,* 10473–10512.

[2] **P.M. Martins, A.C. Lima, S. Ribeiro, S. Lanceros-Mendez, P. Martins,** (2021), Magnetic Nanoparticles for Biomedical Applications: From the Soul of the Earth to the Deep History of Ourselves, *ACS Appl Bio Mater, 4*, 5839–5870.

[3] **R.H. Kodama,** Magnetic nanoparticles, (1999).

[4] **L.L. Vatta, R.D. Sanderson, K.R. Koch,** (2006), Magnetic nanoparticles: Properties and potential applications*, *Pure Appl. Chem. 78,* 1793–1801.

[5] **B. Skóra, K.A. Szychowski, J. Gmiński,** (2020), A concise review of metallic nanoparticles encapsulation methods and their potential use in anticancer therapy and medicine, *European Journal of Pharmaceutics and Biopharmaceutics. 154,* 153–165.

[6] **A.M. Abu-Dief, S.M. Abdel-Fatah,** (2018), Development and functionalization of magnetic nanoparticles as powerful and green catalysts for organic synthesis, *Beni Suef Univ J Basic Appl Sci. 7,* 55–67.

[7] **S. Nakashima, K. Sugioka, K. Tanaka, M. Shimizu, Y. Shimotsuma, K. Miura, ... M. Inoue,** (1975), Enhanced magnetooptical response in dumbbell-like Ag-CoFe2O4 nanoparticle pairs. https://doi.org/10.1364/OE.20.028191

[8] **A.H. Lu, E.L. Salabas, F. Schüth,** (2007), Magnetic nanoparticles: Synthesis, protection, functionalization, and application, *Angewandte Chemie - International Edition. 46,* 1222–1244.

[9] **V. V. Boldyrev,** (2006), Thermal decomposition of ammonium perchlorate, *Thermochim Acta. 443,* 1–36.

[10] **A. Juríková, K. Csach, J. Mi²kuf, M. Koneracká, V. Závi²ová, M. Kubov£íková, P. Kop£anský,** (2012), Thermal Analysis of Magnetic Nanoparticles Modied with Dextran. https://doi.org/10.12693/aphyspola.121.1296

[11] **G. Huang, C.H. Lu, H.H. Yang,** (2019), Magnetic Nanomaterials for Magnetic Bioanalysis, in: Novel Nanomaterials for Biomedical, *Environmental and Energy Applications, Elsevier: pp*. 89–109.

[12] **R.J. Acheson, P.W.M. Jacobs,** Thermal Decomposition op Magnesium Perchlorate the Thermal Decomposition of Magnesium Perchlorate and of Ammonium Perchlorate and Magnesium Perchlorate Mixtures, n.d. https://pubs.acs.org/sharingguidelines.

[13] **S.J. Shin, Y.H. Kim, C.W. Kim, H.G. Cha, Y.J. Kim, Y.S. Kang,** (2007), Preparation of magnetic FeCo nanoparticles by coprecipitation route, Current *Applied Physics. 7,* 404–408.

[14] **L. Yang, P. Zou, J. Cao, Y. Sun, D. Han, S. Yang, ... J. Yang,** (2014), Facile synthesis and paramagnetic properties of Fe3O4@SiO2 core-shell nanoparticles, Superlattices Microstruct. *76*, 205–212. https://doi.org/10.1016/j.spmi.2014.10.011

[15] **J.C. De Freitas, R.M. Branco, I.G.O. Lisboa, T.P. Da Costa, M.G.N. Campos, M.J. Júnior, R.F.C. Marques,** (2015), Magnetic nanoparticles obtained by homogeneous coprecipitation sonochemically assisted, in: *Materials Research, Universidade Federal de Sao Carlos: pp.* 220–224. https://doi.org/10.1590/1516-1439.366114

[16] **M.R.Z. Kouhpanji, B.J.H. Stadler,** (2020), A guideline for effectively synthesizing and characterizing magnetic nanoparticles for advancing nanobiotechnology: *A review, Sensors (Switzerland). 20*.

[17] **F. Ozel, H. Kockar,** (2017), A Simple Method of Synthesis and Characterizations of Oleate-Coated Iron Oxide Nanoparticles, *J Supercond Nov Magn. 30*, 2023–2027.

[18] **V. Cabuil, V. Dupuis, D. Talbot, S. Neveu,** (2011), Ionic magnetic fluid based on cobalt ferrite nanoparticles: Influence of hydrothermal treatment on the nanoparticle size, in: *J Magn Magn Mater: pp*. 1238–1241.

[19] **M. Bustamante-Torres, D. Romero-Fierro, J. Estrella-Nuñez, B. Arcentales-Vera, E. Chichande-Proaño, E. Bucio, ... P. Yachay,** (2022), Polymeric Composite of Magnetite Iron Oxide Nanoparticles and Their Application in Biomedicine: A Review. https://doi.org/10.3390/polym14040752

[20] **H.D.T. Duong, D.T. Nguyen, K.S. Kim,** (2021), Effects of process variables on properties of CoFe2O4 nanoparticles prepared by solvothermal process, Nanomaterials. 11.

[21] **H. Shen, J. Hou, Z. Gao, B. Chen, T. Tan,** (2014), Solvothermal synthesis of functional magnetic nanoparticles for biocatalyst, *Appl Biochem Biotechnol. 173*, 2279–2286.

[22] **D.L. Andrews, G.D. Scholes, G.P. Wiederrecht,** Editors-in-Chief, n.d.

[23] **Y.Y. Zheng, Q. Sun, Y.H. Duan, J. Zhai, L.L. Zhang, J.X. Wang,** (2020), Controllable synthesis of monodispersed iron oxide nanoparticles by an oxidation-precipitation combined with solvothermal process, *Mater Chem Phys. 252.*

[24] **S. Veintemillas-Verdaguer, O. Bomat I I-Miguel, M.P. Morales,** Effect of the process conditions on the structural and magnetic properties of c-Fe 2 O 3 nanoparticles produced by laser pyrolysis, n.d. www.actamat-journals.com.

[25] **S. Wang, L. Gao,** (2019), Laser-driven nanomaterials and laser-enabled nanofabrication for industrial applications, in: *Industrial Applications of Nanomaterials, Elsevier: pp.* 181–203.

[26] **I. Morjan, R. Alexandrescu, F. Dumitrache, C. Fleaca, R. Birjega, I. Soare, ... D. Wang,** (2010), Development of magnetic Fe@C nanocomposites obtained via the laser pyrolysis: Structural and disaggregation properties, in: *AIP Conf Proc: pp.* 17–21. https://doi.org/10.1063/1.3505074

[27] **L. Carvajal, R. Buitrago-Sierra, A. Santamaría, S. Angel, H. Wiggers, J. Gallego,** (2020), Effect of Spray Parameters in a Spray Flame Reactor During FexOy Nanoparticles Synthesis, *Journal of Thermal Spray Technology. 29*, 368–383.

[28] **W.Y. Teoh,** (2013), A perspective on the flame spray synthesis of photocatalyst nanoparticles, *Materials. 6*, 3194–3212.

[29] **R. Strobel, S.E. Pratsinis,** (2009), Direct synthesis of maghemite, magnetite and wustite nanoparticles by flame spray pyrolysis, *Advanced Powder Technology. 20*, 190–194.

[30] **Y. Li, Y. Hu, G. Huang, C. Li,** (2013), Metallic iron nanoparticles: Flame synthesis, characterization and magnetic properties, *Particuology. 11*, 460–467.

[31] **W. Li, P. Xu, H. Zhou, L. Yang, H. Liu,** (2012), Advanced functional nanomaterials with microemulsion phase, *Sci China Technol Sci. 55*, 387–416.

[32] **A.K. Ganguli, A. Ganguly, S. Vaidya,** (2010), Microemulsion-based synthesis of nanocrystalline materials, *Chem Soc Rev. 39*, 474–485.

[33] **M. Salvador, G. Gutiérrez, S. Noriega, A. Moyano, M.C. Blanco-López, M. Matos,** (2021), Microemulsion synthesis of superparamagnetic nanoparticles for bioapplications, *Int J Mol Sci. 22*, 1–17.

[34] **C.C. Berry,** (2009), Progress in functionalization of magnetic nanoparticles for applications in biomedicine, *J Phys D Appl Phys. 42.*

[35] **H. Fatima, T. Charinpanitkul, K.S. Kim,** (2021), Fundamentals to apply magnetic nanoparticles for hyperthermia therapy, *Nanomaterials. 11.*

[36] **M. Peiravi, H. Eslami, M. Ansari, H. Zare-Zardini,** (2022), Magnetic hyperthermia: Potentials and limitations, *Journal of the Indian Chemical Society. 99.*

[37] **E. Baco, O. Ukimura, E. Rud, L. Vlatkovic, A. Svindland, M. Aron, ... I.S. Gill,** (2015), Magnetic resonance imaging-transectal ultrasound image-fusion biopsies accurately characterize the index tumor: Correlation with step-sectioned radical prostatectomy specimens in 135 patients, *Eur Urol. 67*, 787–794. https://doi.org/10.1016/j.eururo.2014.08.077

[38] **M. Arruebo, R. Fernández-Pacheco, M.R. Ibarra, J. Santamaría,** (2007), Magnetic nanoparticles for drug delivery The potential of magnetic NPs stems from the intrinsic properties of their magnetic cores combined with their drug loading capability and the biochemical properties that can be bestowed on them by means of a suitable coating.

[39] **A. Rastogi, K. Yadav, A. Mishra, M.S. Singh, S. Chaudhary, R. Manohar, A.S. Parmar,** (2022), Early diagnosis of lung cancer using magnetic nanoparticles-integrated systems, *Nanotechnol Rev. 11*, 544–574. https://doi.org/10.1515/ntrev-2022-0032

[40] **A. Rajan, N.K. Sahu,** (2020), Review on magnetic nanoparticle-mediated hyperthermia for cancer therapy, *Journal of Nanoparticle Research. 22.*

[41] **S. Thangudu, C.C. Yu, C.L. Lee, M.C. Liao, C.H. Su,** (2022), Magnetic, biocompatible FeCO3 nanoparticles for T2-weighted magnetic resonance imaging of in vivo lung tumors, *J Nanobiotechnology. 20*.

[42] **S. Roth, M. Margulis, A. Danielli,** (2022), Recent Advances in Rapid and Highly Sensitive Detection of Proteins and Specific DNA Sequences Using a Magnetic Modulation Biosensing System, *Sensors. 22*.

[43] **K. Yasuda, Y. Kitamoto,** (2018), Fabrication of Fe3O4 nanorods designed for liquid-phase magnetic biosensing, in: *AIP Conf Proc, American Institute of Physics Inc*.

[44] **H. Chen, F. Liu, Z. Lei, L. Ma, Z. Wang,** (2015), Fe2O3@Au core@shell nanoparticle-graphene nanocomposites as theranostic agents for bioimaging and chemo-photothermal synergistic therapy, *RSC Adv. 5*, 84980–84987.

[45] **X. Ke, X. Song, N. Qin, Y. Cai, F. Ke,** (2019), Rational synthesis of magnetic Fe 3 O 4 @MOF nanoparticles for sustained drug delivery, *Journal of Porous Materials. 26*, 813–818.

[46] **Y.L. Liu, D. Chen, P. Shang, D.C. Yin,** (2019), A review of magnet systems for targeted drug delivery, *Journal of Controlled Release. 302*, 90–104.

[47] **Y.H. Deng, C.C. Wang, J.H. Hu, W.L. Yang, S.K. Fu,** (2005), Investigation of formation of silica-coated magnetite nanoparticles via sol-gel approach, *Colloids Surf A Physicochem Eng Asp. 262*, 87–93.

[48] **J. Pan, L. Xu, J. Dai, X. Li, H. Hang, P. Huo, ... Y. Yan,** (2011), Magnetic molecularly imprinted polymers based on attapulgite/Fe3O4 particles for the selective recognition of 2,4-dichlorophenol, *Chemical Engineering Journal. 174*, 68–75. https://doi.org/10.1016/j.cej.2011.08.046

[49] **L. Wang, H.Y. Park, S.I.I. Lim, M.J. Schadt, D. Mott, J. Luo, ... C.J. Zhong,** (2008), Core@shell nanomaterials: Gold-coated magnetic oxide nanoparticles, *J Mater Chem. 18*, 2629–2635. https://doi.org/10.1039/b719096d

[50] **P. Nikolaidis,** (2020), Analysis of Green Methods to Synthesize Nanomaterials, in: *Green Synthesis of Nanomaterials for Bioenergy Applications, Wiley: pp.* 125–144.

[51] **B. Fotovvati, N. Namdari, A. Dehghanghadikolaei,** (2019), On coating techniques for surface protection: *A review, Journal of Manufacturing and Materials Processing. 3.*

[52] **N. Wang, Z. Yang, F. Xu, K. Thummavichai, H. Chen, Y. Xia, Y. Zhu,** (2017), A generic method to synthesise graphitic carbon coated nanoparticles in large scale and their derivative polymer nanocomposites, *Sci Rep. 7*. https://doi.org/10.1038/s41598-017-12200-1

[53] **S. Wu, L. Cheng, W. Yang, Y. Liu, L. Zhang, Y. Xu,** (2006), Oxidation protective multilayer CVD SiC coatings modified by a graphitic B-C interlayer for 3D C/SiC composite, *Applied Composite Materials. 13*, 397–406.

[54] **O.H. Kessler, F.T. Hoffmann, P. Mayr,** (1999), Microstructure and property changes caused by diffusion during CVD coating of steels. www.elsevier.nl/locate/surfcoat.

[55] **M. Saeed, Y. Alshammari, S.A. Majeed, E. Al-Nasrallah,** (2020), Chemical Vapour Deposition of Graphene—Synthesis, Characterisation, and Applications: *A Review, Molecules*.

[56] **J. Liu, X. Fang, C. Zhu, X. Xing, G. Cui, Z. Li,** (2020), Fabrication of superhydrophobic coatings for corrosion protection by electrodeposition: *A comprehensive review, Colloids Surf a Physicochem Eng Asp. 607*.

[57] **Q. Li, (**2013), Sol-gel coatings to improve the corrosion resistance of magnesium (Mg) alloys, in: Corrosion Prevention of Magnesium Alloys: *A Volume in Woodhead Publishing Series in Metals and Surface Engineering, Elsevier Ltd: pp.* 469–485.

[58] **H. Li, Y. Luo, F. Yu, L. Peng,** (2022), Simple and scalable preparation of robust and magnetic superhydrophobic papers by one-step spray-coating for efficient oil-water separation, *Colloids Surf a Physicochem Eng Asp. 640*.

[59] **M.N. Islam, M. Abbas, B. Sinha, J.R. Joeng, C.G. Kim,** (2013), Silica encapsulation of sonochemically synthesized iron oxide nanoparticles, *Electronic Materials Letters. 9,* 817–820.

[60] **L. Khanna, N.K. Verma,** (2013), Synthesis and characterization of silica coated potassium ferrite nanoparticles, in: *AIP Conf Proc: pp*. 71–72.

[61] **K. Ashtari, K. Khajeh, J. Fasihi, P. Ashtari, A. Ramazani, H. Vali,** (2012), Silica-encapsulated magnetic nanoparticles: Enzyme immobilization and cytotoxic study, *Int J Biol Macromol. 50,* 1063–1069.

[62] **L. Tonthat, M. Kimura, T. Ogawa, N. Kitamura, Y. Kobayashi, K. Gonda, S. Yabukami,** (2023), Development of gold-coated magnetic nanoparticles as a theranostic agent for magnetic hyperthermia and CT imaging applications, *AIP Adv. 13.* https://doi.org/10.1063/9.0000592

[63] **M. Tintoré, S. Mazzini, L. Polito, M. Marelli, A. Latorre, Á. Somoza, ... R. Eritja,** (2015), Gold-coated superparamagnetic nanoparticles for single methyl discrimination in DNA aptamers, *Int J Mol Sci. 16,* 27625–27639. https://doi.org/10.3390/ijms161126046

[64] **S. Moraes Silva, R. Tavallaie, L. Sandiford, R.D. Tilley, J.J. Gooding,** (2016), Gold coated magnetic nanoparticles: From preparation to surface modification for analytical and biomedical applications, *Chemical Communications. 52,* 7528–7540.

[65] **A.N. Subba Rao, V.T. Venkatarangaiah,** (2014), Metal oxide-coated anodes in wastewater treatment, *Environmental Science and Pollution Research. 21*, 3197–3217.

[66] **G. Cao, Z. Jin, J. Zhu, Y. Li, B. Xu, Y. Xiong, J. Yang,** (2020), A green Al2O3 metal oxide coating method for LiNi0.5Co0.2Mn0.3O2 cathode material to improve the high voltage performance, *J Alloys Compd. 832*. https://doi.org/10.1016/j.jallcom.2020.153788

[67] **D. Li, Y. Kato, K. Kobayakawa, H. Noguchi, Y. Sato,** (2006), Preparation and electrochemical characteristics of LiNi1/3Mn1/3Co1/3O2 coated with metal oxides coating, *J Power Sources. 160,* 1342–1348.

[68] **S. Liu, M.D. Regulacio, S.Y. Tee, Y.W. Khin, C.P. Teng, L.D. Koh, ... M.Y. Han,** (2016), Preparation, Functionality, and Application of Metal Oxide-coated Noble Metal Nanoparticles, *Chemical Record.* 1965–1990. https://doi.org/10.1002/tcr.201600028

[69] **A. Razaq, F. Bibi, X. Zheng, R. Papadakis, S.H.M. Jafri, H. Li,** (2022), Review on Graphene-, Graphene Oxide-, Reduced Graphene Oxide-Based Flexible Composites: From Fabrication to Applications, *Materials. 15.*

[70] **S. Deng, V. Berry, Wrinkled,** (2016), rippled and crumpled graphene: *An overview of formation mechanism, electronic properties, and applications, Materials Today. 19,* 197–212.

[71] **A.R. Urade, I. Lahiri, K.S. Suresh,** (2023), Graphene Properties, Synthesis and Applications: *A Review, JOM. 75,* 614–630.

[72] **M. Farokhnezhad, M. Esmaeilzadeh,** (2019), Graphene coated gold nanoparticles: An emerging class of nanoagents for photothermal therapy applications, *Physical Chemistry Chemical Physics. 21,* 18352–18362.

[73] **D. Choi, Y. Pyo, S.B. Jung, Y. Kim, E.H. Yoon, C.S. Lee,** (2016), Application of the Taguchi method to optimize graphene coatings on copper nanoparticles formed using a solid carbon source, *Mater Trans. 57,* 1177–1182.

[74] **K.Z. Donato, H.L. Tan, V.S. Marangoni, M.V.S. Martins, P.R. Ng, M.C.F. Costa, ... A.H. Castro Neto,** (2023), Graphene oxide classification and standardization, *Sci Rep. 13,* 6064. https://doi.org/10.1038/s41598-023-33350-5

[75] **J. Wu, H. Lin, D.J. Moss, K.P. Loh, B. Jia,** (2023), Graphene oxide for photonics, electronics and optoelectronics, *Nat Rev Chem. 7,* 162–183.

[76] **K. Cao, Z. Tian, X. Zhang, Y. Wang, Q. Zhu,** (2023), Green preparation of graphene oxide nanosheets as adsorbent, *Sci Rep. 13,* 9314.

[77] **M. Bilal, H.M.N. Iqbal, S.F. Adil, M.R. Shaik, A. Abdelgawad, M.R. Hatshan, M. Khan,** (2022), Surface-coated magnetic nanostructured materials for robust bio-catalysis and biomedical applications-*A review, J Adv Res. 38,* 157–177. https://doi.org/10.1016/j.jare.2021.09.013

[78] **S. Pei, H.M. Cheng,** (2012), The reduction of graphene oxide, *Carbon N Y. 50,* 3210–3228.

[79] **V. Agarwal, P.B. Zetterlund,** (2021), Strategies for reduction of graphene oxide – A comprehensive review, *Chemical Engineering Journal. 405.*

[80] **S. Azizighannad, S. Mitra,** (2018), Stepwise reduction of Graphene Oxide (GO) and its effects on chemical and colloidal properties, *Sci Rep. 8.*

[81] **S. Soleimani, M. Yousefzadi, A. Jannesari, A. Ghaderi, A. Shahdadi,** (2023), Green synthesis of graphene oxide-based nanocomposite by Polycladia myrica: antibacterial, anti-algae, and acute zooplanktonic responses, *J Appl Phycol.*

[82] **M. Yari, M.M. Larijani, A. Afshar, M. Eshghabadi, A. Shokouhy,** (2012), Physical properties of sputtered amorphous carbon coating, *J Alloys Compd. 513,* 135–138.

[83] **T. Krumpiegl, H. Meerkamm, W. Fruth, C. Schaufler, G. Erkens, H. Bö Hner,** (1999), Amorphous carbon coatings and their tribological behavior at high temperatures and in high vacuum. www.elsevier.nl/locate/surfcoat.

[84] **M. Zawischa, S. Makowski, M. Kuczyk, V. Weihnacht,** (2022), Comparison of fracture properties of different amorphous carbon coatings using the scratch test and indentation failure method, *Surf Coat Technol. 435*.

[85] **S. Wang, K. Komvopoulos,** (2020), Structure evolution during deposition and thermal annealing of amorphous carbon ultrathin films investigated by molecular dynamics simulations, *Sci Rep. 10*.

[86] **J.C. Tristão, A.A.S. Oliveira, J.D. Ardisson, A. Dias, R.M. Lago,** (2011), Facile preparation of carbon coated magnetic Fe3O4 particles by a combined reduction/CVD process, *Mater Res Bull. 46,* 748–754.

[87] **J. Chen, B. Duncan, Z. Wang, L.S. Wang, V.M. Rotello, S.R. Nugen,** (2015), Bacteriophage-based nanoprobes for rapid bacteria separation, *Nanoscale. 7,* 16230–16236.

[88] **C.W. Lin, J.M. Chen, Y.J. Lin, L.W. Chao, S.Y. Wei, C.H. Wu, ... K.L. Chen,** (2019), Magneto-Optical Characteristics of Streptavidin-Coated Fe3O4@Au Core-Shell Nanoparticles for Potential Applications on Biomedical Assays, *Sci Rep. 9*. https://doi.org/10.1038/s41598-019-52773-7

[89] **I. Covarrubias-García, G. Quijano, A. Aizpuru, J.L. Sánchez-García, J.L. Rodríguez-López, S. Arriaga,** (2020), Reduced graphene oxide decorated with magnetite nanoparticles enhance biomethane enrichment, *J Hazard Mater. 397*.

[90] **D. Li, M. Deng, Z. Yu, W. Liu, G. Zhou, W. Li, ... W. Zhang,** (2018), Biocompatible and Stable GO-Coated Fe3O4 Nanocomposite: A Robust Drug Delivery Carrier for Simultaneous Tumor MR Imaging and Targeted Therapy, *ACS Biomater Sci Eng. 4,* 2143–2154. https://doi.org/10.1021/acsbiomaterials.8b00029

[91] **S. Mertdinç-Ülküseven, U. Savaci, K. Onbasli, Ö. Balci-Çagiran, H.Y. Acar, M.L. Öveçoglu, D. Agaogullari,** (2022), In-situ synthesis of graphene encapsulated Fe/Fe2O3nanoparticles for possible biomedical applications, *Journal of Materials Research and Technology. 20*, 2558–2577. https://doi.org/10.1016/j.jmrt.2022.08.059

[92] **J.H. Jeong, S. Kang, N. Kim, R. Joshi, G.H. Lee,** (2022), Recent trends in covalent functionalization of 2D materials, *Physical Chemistry Chemical Physics.*

[93] **J.H. Jeong, S. Kang, N. Kim, R. Joshi, G.H. Lee,** (2022), Recent trends in covalent functionalization of 2D materials, *Physical Chemistry Chemical Physics.*

[94] **J.H. Jeong, S. Kang, N. Kim, R. Joshi, G.H. Lee,** (2022), Recent trends in covalent functionalization of 2D materials, *Physical Chemistry Chemical Physics.*

[95] **S. Sadjadi, S. Sadjadi,** (2022), Covalent functionalized silica-coated magnetic nanoparticles: classification, synthetic methods and their applications, in: *Fundamentals and Industrial Applications of Magnetic Nanoparticles, Elsevier: pp.* 117–152.

[96] **V. Georgakilas, M. Otyepka, A.B. Bourlinos, V. Chandra, N. Kim, K.C. Kemp, ... K.S. Kim,** (2012), Functionalization of graphene: Covalent and non-covalent approaches, derivatives and applications, *Chem Rev. 112*, 6156–6214. https://doi.org/10.1021/cr3000412

[97] **P. Bilalis, D. Katsigiannopoulos, A. Avgeropoulos, G. Sakellariou,** (2014), non-covalent functionalization of carbon nanotubes with polymers, *RSC Adv. 4*, 2911–2934.

[98] **J. Zhan, Z. Lei, Y. Zhang,** (2022), non-covalent interactions of graphene surface: Mechanisms and applications, *Chem. 8*, 947–979.

[99] **I. Shown, A. Ganguly,** (2016), non-covalent functionalization of CVD-grown graphene with Au nanoparticles for electrochemical sensing application, *J Nanostructure Chem. 6*, 281–288.

[100] **S. Srivastava, N.A. Kotov,** (2008), Composite Layer-by-Layer (LBL) assembly with inorganic nanoparticles and nanowires, *Acc Chem Res. 41*, 1831–1841.

[101] **M.M. De Villiers, D.P. Otto, S.J. Strydom, Y.M. Lvov,** (2011), Introduction to nanocoatings produced by layer-by-layer (LbL) self-assembly, *Adv Drug Deliv Rev. 63*, 701–715.

[102] **X. Pang, Y. Tao, Y. Xu, J. Pan, J. Shen, C. Gao,** (2020), Enhanced monovalent selectivity of cation exchange membranes via adjustable charge density on functional layers, *J Memb Sci. 595*.

[103] **P.R. Gil, L.L. del Mercato, P. del Pino, A. Muñoz-Javier, W.J. Parak,** (2008), Nanoparticle-modified polyelectrolyte capsules, *Nano Today. 3*, 12–21.

[104] **A.K. Agrahari, P. Bose, M.K. Jaiswal, S. Rajkhowa, A.S. Singh, S. Hotha, ... V.K. Tiwari,** (2021), Cu(I)-Catalyzed Click Chemistry in Glycoscience and Their Diverse Applications, *Chem Rev. 121*, 7638–7956. https://doi.org/10.1021/acs.chemrev.0c00920

[105] **G.K. Such, A.P.R. Johnston, K. Liang, F. Caruso,** (2012), Synthesis and functionalization of nanoengineered materials using click chemistry, *Prog Polym Sci. 37*, 985–1003.

[106] **A.K. Agrahari, P. Bose, M.K. Jaiswal, S. Rajkhowa, A.S. Singh, S. Hotha, ... V.K. Tiwari,** (2021), Cu(I)-Catalyzed Click Chemistry in Glycoscience and Their Diverse Applications, *Chem Rev. 121*, 7638–7956. https://doi.org/10.1021/acs.chemrev.0c00920

[107] **S. Ishizawa, M. Tumurkhuu, E.J. Gross, J. Ohata,** (2022), Site-specific DNA functionalization through the tetrazene-forming reaction in ionic liquids, *Chem Sci. 13*, 1780–1788.

[108] **F. Liu, H. Wu, Q. Chen, J. Gao, G. Wang,** (2023), Demonstration of a Magic Reaction: Accelerating DNA Functionalization of Gold Nanoparticles by Freezing, *J Chem Educ.*

[109] **F. Nicolson, A. Ali, M.F. Kircher, S. Pal,** (2020), DNA Nanostructures and DNA-Functionalized Nanoparticles for Cancer Theranostics, *Advanced Science. 7*.

[110] **S.W. Hong, K.H. Kim, J. Huh, C.H. Ahn, W.H. Jo,** (2005), Design and synthesis of a new pH sensitive polymeric sensor using fluorescence resonance energy transfer, *Chemistry of Materials. 17,* 6213–6215.

[111] **Z. Vasiljević, M.P. Dojčinović, J.D. Vujančević, M. Spreitzer, J. Kovač, D. Bartolić, ... M.V. Nikolić,** (2021), Exploring the impact of calcination parameters on the crystal structure, morphology, and optical properties of electrospun Fe2TiO5nanofibers, *RSC Adv. 11*, 32358–32368. https://doi.org/10.1039/d1ra05748k

[112] **R. Kumar, B. Sahoo,** (2018), Investigation of disorder in carbon encapsulated core-shell Fe/Fe3C nanoparticles synthesized by one-step pyrolysis, *Diam Relat Mater. 90*, 62–71.

[113] **L. Ning, L. Xiaojie, W. Xiaohong, Y. Honghao, M. Fei, S. Wei,** (2009), Preparation and magnetic behavior of carbon-encapsulated iron nanoparticles by detonation method, *Compos Sci Technol. 69*, 2554–2558.

[114] **W. Konicki, A. Hełminiak, W. Arabczyk, E. Mijowska,** (2017), Removal of anionic dyes using magnetic Fe@graphite core-shell nanocomposite as an adsorbent from aqueous solutions, *J Colloid Interface Sci. 497,* 155–164.

[115] **S.S. Behera, J.K. Patra, K. Pramanik, N. Panda, H. Thatoi,** (2012), Characterization and Evaluation of Antibacterial Activities of Chemically Synthesized Iron Oxide Nanoparticles, *World Journal of Nano Science and Engineering. 02*, 196–200.

[116] **H. Esmaeili, S. Tamjidi,** Ultrasonic-assisted synthesis of natural clay/Fe 3 O 4 /graphene oxide for enhance removal of Cr (VI) from aqueous media, (n.d.).

[117] **A. Wang, M. Qiao, J. Xu, Y. Pan, Q. Ran, S. Wu, Q. Chen,** (2016), POEGMA-b-PAA comb-like polymer dispersant for Al2 suspensions, *J Appl Polym Sci. 133*. https://doi.org/10.1002/app.43352

CURRICULUM VITAE

Name Surname **:** Aysa AZMOUDEH

EDUCATION **:**

- **Bachelor's Degree** **:** 2017. Islamic Azad University of Tabriz Faculty of Biomedical Engineering. Biomedical Engineering Programme
- **Master's Degree** **:** Istanbul Technical University. Department of Materials Science and Engineering. Ceramic Engineering Programme

PROFESSIONAL EXPERIENCE AND REWARDS:

- 2020-2023 Istanbul Technical University at the Particulate Materials Laboratory (PML)
- 2020-2023 Istanbul Technical University at Scientific Research Projects (ITU BAP, M.Sc. Thesis Projects), the project number MYL-2022-44189.
- 2022-2023 Istanbul Technical University at Prof. Dr. Adnan Tekin Materials Science and Production Technologies Applied Research Center (ATARC)

PUBLICATIONS. PRESENTATIONS AND PATENTS ON THE THESIS:

- **Azmoudeh A.,** Moral S., Turk M., Doganay G., Ağaoğulları. D. 2022: Synthesis of graphene-encapsulated iron oxide nanoparticles using the solvothermal method and cytotoxicity test International Graduate Research Symposium. June 1-3. 2022 Istanbul. Turkey.